MOLECULAR MECHANISMS UNDERLYING THE FUNCTION OF THE TYROSINE PHOSPHATASE PTPRD IN CANCER

by

Berenice Ortiz Thompson

A Dissertation

Presented to the Faculty of the Louis V. Gerstner, Jr.

Graduate School of Biomedical Sciences,

Memorial Sloan Kettering Cancer Center

in Partial Fulfillment of the Requirements for the Degree of

Doctor of Philosophy

New York, NY

May, 2014

_____ _____

Timothy A. Chan, MD, PhD
Dissertation Mentor

Date

To my parents Carmen and Claudio Ortiz and my husband Colin Thompson.

Their unceasing love, support, and patience made this work possible.

ABSTRACT

PTPRD, which encodes the protein tyrosine phosphatase receptor delta, is a frequently inactivated gene in several human cancers, including glioblastoma multiforme (GBM). However, it is still unknown whether loss of *PTPRD* can promote tumorigenesis *in vivo,* and the mechanistic basis of PTPRD function in tumors is unclear. This thesis addresses these important questions. In Chapter Two, using genomic analysis and a glioma mouse model, we demonstrate that loss of *Ptprd* accelerates tumor formation and define the oncogenic context in which *Ptprd* loss acts. Specifically we show that heterozygous loss of *PTPRD* is the predominant type of lesion and that *PTPRD* and *CDKN2A*, a cell cycle inhibitor, are frequently co-deleted in human GBM. Accordingly, heterozygous loss of *Ptprd* cooperated with *Cdkn2a* deletion to promote gliomagenesis. Moreover, loss of the *Ptprd* phosphatase resulted in phospho-Stat3 accumulation and altered pathways governing the macrophage response. Since PTPRD is inactivated in several other cancers, we also examine the role of PTPRD in a spontaneous tumorigenesis mouse model in Chapter Three. While loss of *Ptprd* alone did not form tumors, loss of *Ptprd* and *Cdkn2a* cooperated to promote tumorigenesis. The loss of *Ptprd* resulted in changes to tumor spectrum in mice and increased incidence of lymphomas. Altogether, our results from the glioma and spontaneous tumorigenesis mouse models show that loss of *Ptprd* and *Cdkn2a* accelerate tumorigenesis. Since other substrates of PTPRD may mediate its tumor suppressive function, in Chapter Four we present a preliminary identification of proteins that interact with PTPRD. We validated that PTPRD and Prohibitin interact, and future work will confirm that PTPRD de-phosphorylates Prohibitin and reveal the biological significance of that PTPRD substrate. Altogether, we establish PTPRD as a

bona fide tumor suppressor and identify a potential substrate that mediates the tumor suppressive role of PTPRD. Further studies can provide the field with possible molecular targets for therapeutic intervention or diagnostics.

BIOGRAPHICAL SKETCH

Berenice Ortiz first became interested in the biological sciences after learning about the Human Genome Project in her high school biology class. Following graduation, Berenice pursued her undergraduate studies at Rutgers University in New Brunswick, New Jersey. In order to learn first hand what research science was like, Berenice conducted research under the guidance of Dr. Loredana Quadro in the Nutritional Sciences Department at Rutgers University. There she worked on her undergraduate thesis studying the effects of conjugated linoleic acid, a dietary supplement component, on vitamin metabolism. While at Rutgers, Berenice also worked as an academic tutor for the Tutoring and Learning Center. She realized that she really enjoyed helping students understand difficult science concepts, and as a result, Berenice completed a Master's biology teacher education program. As part of the program, she taught biology and forensics at Freehold High School in New Jersey. In 2008, Berenice graduated from the teacher education program and matriculated in a PhD program at Gerstner Sloan-Kettering Graduate School of Biomedical Studies. Berenice joined the laboratory of Timothy Chan in the Human Oncology and Pathogenesis Program for her thesis project, which focused on understanding the role of the PTPRD phosphatase in cancer. In 2012, Berenice was awarded a Ruth L. Kirschstein National Research Service Award to Promote Diversity in Health-Related Research from the NIH. Upon completion of her degree, Berenice would like to start a career in medical education. In this way, she can continue her love of teaching and communicating science in a creative way.

ACKNOWLEDGMENTS

I would first like to thank my mentor, Dr. Timothy Chan, for the opportunity to be his first graduate student. His support and training throughout the years made this dissertation possible. I would like to thank the members of my thesis advisory committee, Drs. David Solit and Jacqueline Bromberg, for their insightful comments and feedback at every committee meeting. I would also like to acknowledge my thesis committee chair Dr. Sarat Chandarlapaty and my external examining committee member Dr. Nancy Du for their time and support.

Throughout the years, I was fortunate to have worked with a wonderful group of scientists who supported me both professionally and personally. In particular, I am very grateful for the unceasing support and feedback from my friends and lab mates Armida Fabius, Sevin Turcan, Alexandra Snyder-Charen, and Stephanie Eng. I also greatly appreciate the help of Armida Fabius and Wei Wu with the enormous amount of mouse work that was needed for this project. I would like to thank all the members of the Chan lab, both past and present, for their assistance and guidance with all my projects.

Several collaborators provided valuable expertise, protocols, and reagents that were critical for the success of this dissertation. I would like to thank Nikolaus Schultz for performing bioinformatics analysis of human GBM tumors. I am very appreciative of the many hours Dr. Jason Huse spent with me to grade all of my glioma mouse tumors. The expertise of Dr. Julie White was essential for the pathology analysis of the spontaneous tumorigenesis mouse model, thank you. I would like to thank Alicia Pedraza and Dr. Cameron Brennan for performing the western blot analysis of p-Stat3 in human GBM

tumors. Lastly, I am very grateful for the patience and support of both Ken Pitter and Daniel Ciznadija. Both were crucial for the success of the RCAS PDGF mouse experiments by teaching me many protocols and sharing necessary reagents.

The core facilities at MSKCC provided outstanding technical assistance. I would like to thank Afsar Barlas, Dmitry Yarilin, Sho Fujisawa, Ke Xu, Ning Fan, and Mesruh Turkekul of the Molecular Cytology core facility for their remarkable help with the immunohistochemistry staining and analysis. Maria Jiao, Jackie Candelier, and Sheena Morales of the Comparative Pathology core facility were exceptionally helpful in providing technical assistance with the pathology analysis. Other core facilities that provided crucial technical assistance include the Research Animal Resource Center, the Small Imaging core facility, the Genomics core facility, the Flow Cytometry Sorting core facility, and the Microchemistry and Proteomics core facility.

I would like to give a special thank you to the GSK staff (Maria Torres, Iwona Abramek, Ivan Gerena, Katherine Gentile, Linda Burnley, and Ken Marians) for all of their efforts to help students with a smile and to ensure that the program runs smoothly.

I am the most lucky to have met my classmates and best friends, Neha Bhagwat, Armine Matevossian, and Jessica Rios. No matter where we end up, the memories we have made will always stay with me. Last, but not least, I am most indebted to my family and husband. Their patience, encouragement, and support made what seemed impossible at times possible.

TABLE OF CONTENTS

LIST OF FIGURES

LIST OF TABLES

LIST OF ABBREVIATIONS

CCL2	Chemokine C-C motif ligand 2
CCL6	Chemokine C-C motif ligand 6
CD34	Cluster of differentiation marker 34
CDKN2A	Cyclin dependent kinase inhibitor 2A
cDNA	Complementary DNA
CXCL14	C-X-C motif chemokine 12
DMEM	Dulbecco's Modified Eagle Medium
EGFR	Epidermal growth factor receptor
GAPDH	Glyceraldehyde 3-phosphate dehydrogenase
GBM	Glioblastoma multiforme
GFAP	Glial fibrillary acidic protein
GFP	Green fluorescent protein
GST	Glutathione S-transferase
IBA1	Ionized calcium-binding adapter molecule 1
IHC	Immunohistochemistry
MRI	Magnetic resonance imaging
mRNA	Messenger RNA
OLIG2	Oligodendrocyte transcription factor
P-STAT3	Phosphorylated form of Stat3
PCA	Principal component analysis
PDGFB	Platelet-derived growth factor subunit B
PHB	Prohibitin
PTP	Protein tyrosine phosphatase
PTPRD	Protein Tyrosine Phosphatase Receptor Delta
PTPRT	Protein tyrosine phosphatase receptor T
qPCR	Quantitative polymerase chain reaction
RCAS	Replication competent ASLV long terminal repeat with a Splice acceptor
SILAC	Stable isotope labeling of amino acids in cell culture
STAT3	Signal transducer and activator of transcription 3
TRAP	Substrate-trapping mutant
tv-A	Avian tumor virus receptor A

CHAPTER ONE

Thesis Introduction

Mechanisms of cancer development

Human bodies are made up of billions of cells that work together to form tissues and organs. Within each cell, DNA encodes detailed instructions for producing proteins that regulate whether a cell will divide, migrate, and/or signal to other cells. When new cells are generated during cell division, DNA proofreading and repair mechanisms ensure that genetic material remains unchanged and complete. However upon exposure to carcinogens, un-repairable alterations to DNA can occur. Some DNA alterations can alter protein abundance or structure, and consequently promote cell processes that lead to cancer. Cells with alterations that promote cancer growth will survive and divide forming a tumor.

Molecular alterations in the genome can be genetic or epigenetic. Genetic alterations are changes in the DNA nucleotide sequence and include point mutations, deletions, and insertions. Epigenetic alterations modify the DNA structure via DNA methylation and/or histone modification. Both types of alterations can alter the expression of genes and proteins to ultimately change a cell's processes. Genes that are commonly altered in cancer are classified as either tumor suppressor genes or oncogenes. The inactivation of tumor suppressor genes and/or the activation of oncogenes result in cell processes that promote cancer.

Cell processes that promote cancer

A number of biological processes are altered in tumors. Douglas Hanahan and Robert Weinberg summarized the complexity of cancer to changes in a distinct set of cell processes called the "Hallmarks of Cancer" (Hanahan and Weinberg 2000 and 2011). Hanahan and Weinberg describe cell processes that promote cancer as ones that ultimately enable tumor growth and/or activate metastasis. Several mechanisms for increased tumor growth exist. Enhanced tumor growth can occur via amplified expression of growth oncogenes or reduced expression of growth suppressors and/or apoptosis genes. Tumor cells can also obtain alterations that allow limitless replicative potential or adjust energy metabolism pathways to fuel cell growth and division. Lastly, the expression of pro-angiogenic factors can increase blood vessel formation that provides tumors with nutrients and oxygen to sustain tumor growth. Tumor metastasis, or the dissemination of tumor cells, can be caused by alterations that allow cell contact inhibition, migration, invasion, and extravasation of tumor cells.

In addition to describing cell processes inherent of tumors, Hanahan and Weinberg describe genomic instability and inflammation as characteristics that further enable tumor formation. Genomic instability occurs when cells acquire alterations to genes that repair defects and/or maintain the genome. As a result, more mutations that promote tumor growth are generated. Tumor-associated inflammation that consists of macrophages, mast cells, neutrophils, and T- and B-lymphocytes can help tumor cells acquire cell processes that promote tumorigenesis. More specifically, immune cells can supply tumors with growth factors that promotes proliferation, survival factors that limit cell death, pro-

angiogenic factors, and extracellular matrix modifying enzymes that lead to angiogenesis, invasion, and metastasis (Hanahan and Weinberg 2011).

Efforts in cancer research involve determining the molecular mechanisms underlying cell processes that promote tumor growth and/or metastasis. The genomic analysis of cancer cells has allowed for the identification of novel tumor suppressors and oncogenes. However the challenge remains to determine in what way these molecular alterations drive tumorigenesis. Ultimately, answering this important question will provide insight into the development of targeted therapies that inhibit cancer-specific cell processes.

PTPRD **is a tumor suppressor inactivated in many human cancers**

We and others have identified that the *Protein Tyrosine Phosphatase Receptor Delta* (*PTPRD*) is a frequently inactivated tumor suppressor gene on Chromosome 9p in a number of cancer types including: colorectal, esophageal adenocarcinoma, neuroblastoma, renal cell carcinoma, Ewing sarcoma, chronic myeloid leukemia, squamous cell carcinoma of the vulva, breast, lung cancer, melanoma, and glioblastoma (Brim et al. 2014, Frankel et al. 2014, Boeva et al. 2013, Du et al. 2013, Jiang et al 2013, Gerber et al. 2013, Micci et al. 2013, TCGA 2012, Kohno et al. 2010, Solomon et al. 2009 and Veeriah et al. 2009). Figure 1.1 illustrates the frequency of PTPRD deletion and mutation among a variety of cancers. Although PTPRD is frequently inactivated in many cancers, its function in tumors remains unclear.

PTPRD structure, function, and regulation

A total of 107 protein tyrosine phosphatases (PTP) are encoded by the human genome with 38 of these belonging to the 'classical PTP' subgroup that shows specificity for phospho-tyrosine (Ostman et al. 2006). Classical PTP are broadly separated into receptor-like forms and non-transmembrane / non-receptor-like forms (Figure 1.2). PTPRD is a receptor-like PTP that has a single transmembrane domain and variable extracellular domains made up of fibronectin type III domains. The intracellular portion of PTPRD consists of two tandem PTP domains (D1 and D2) with most of its catalytic activity present in D1 (Ostman et al. 2006). Non-transmembrane PTP are structurally diverse and often contain sequences that target them to specific locations or enable their binding to specific proteins (Mauro et al. 1994).

PTPRD is a tyrosine phosphatase. Within cells, phosphatases bind to and remove phosphorylation from proteins (a process called de-phosphorylation). In contrast, protein kinases add phosphorylation to proteins. The presence or absence of protein phosphorylation determines the activation of signaling pathways, including ones that control cell proliferation, adhesion, and migration. Currently, it is known that PTPRD can de-phosphorylate two proteins. Veeriah et al. (2009) demonstrated that PTPRD can de-phosphorylate p-STAT3 in glioblastoma. More recently, Meehan et al. (2012) demonstrated that PTPRD dephosphorylates aurora kinase A, which causes downstream destabilization of MYCN within Neuroblastoma. *In vitro* studies have suggested that the expression of the PTPRD phosphatase can suppress growth, induce apoptosis, and/or reduce migration (Veeriah et al. 2009, Solomon et al. 2009 and Funato et al. 2009).

Regulation of receptor-type PTP has been known to occur via dimerization of the receptor, ligand binding, and reversible oxidation (Tonks et al. 2006). Wallace et al. (1998) demonstrated that the D2 domain of PTPRD interacts with and inhibits the D1 catalytic domain of PTPRS. The D2 intracellular domain of PTPRD has been shown to interact with the D1 and D2 domains of PTPRA, PTPRE, or LAR, however the regulation of PTPRD via these interactions has only been suggested (Blanchetot et al. 2002). The ligand(s) of PTPRD are currently unknown.

Significance of Thesis

PTPRD is a frequently inactivated gene in many human cancers, however it is unknown whether loss of *PTPRD* promotes tumorigenesis *in vivo*. In addition, the mechanistic basis of PTPRD function in tumors is unclear. This thesis addresses these important questions. Using genomic analysis, a glioma mouse model, and a spontaneous tumorigenesis mouse model, we demonstrate that loss of *Ptprd* accelerates tumorigenesis and define the oncogenic context in which *Ptprd* loss acts. We also identified a novel substrate of PTPRD, for which future work will determine its biological significance. Our work establishes PTPRD as a *bona fide* tumor suppressor and identifies a possible molecular basis for PTPRD function in cancer. Ultimately, this work provides the field with a better understanding of the molecular mechanisms underlying the suppression of growth by a tumor suppressor that is inactivated in several cancers.

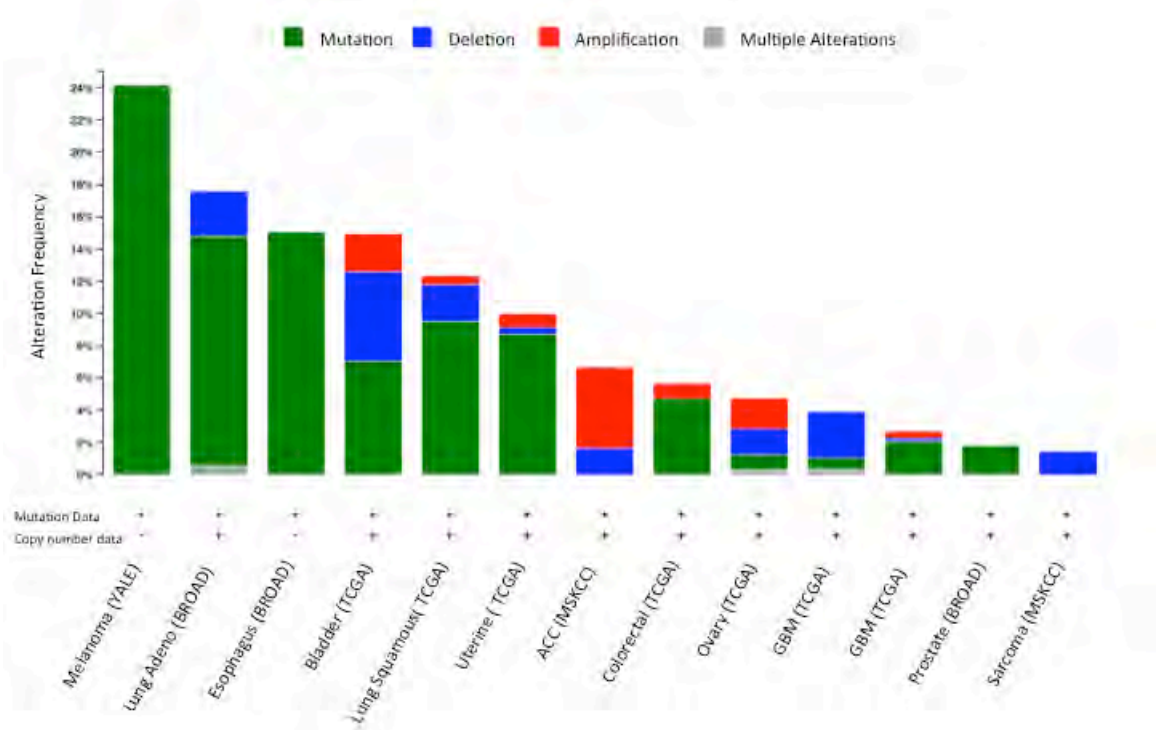

Figure 1.1 *PTPRD* alterations across several cancers. CBio portal illustration with data from Skin Cutaneous Melanoma (n=91, Krauthammer et al. 2012); Lung Adenocarcinoma (n=183, Imielinski et al. 2012); Esophageal Adenocarcinoma (n=149, Dulak et al. 2013); Bladder Urothelial Carcinoma (n=131, TCGA 2014); Lung Squamous Cell Carcinoma (n=178, TCGA 2012); Uterine Corpus Endometrioid Carcinoma (n=373, TCGA 2013); Adenoid Cystic Carcinoma (n=60, Ho et al. 2013); Colon and Rectum Adenocarcinoma (n=276, TCGA 2012); Ovarian Serous Cystadenocarcinoma (n=489, TCGA 2011); Glioblastoma (n=578, TCGA 2013); Breast Invasive Carcinoma (n=825, TCGA 2012); Prostate Adenocarcinoma (n=112, Barbieri et al. 2012); Sarcoma (n=207, Barretina et al. 2010). Color of the bars are as listed in the figure legend.

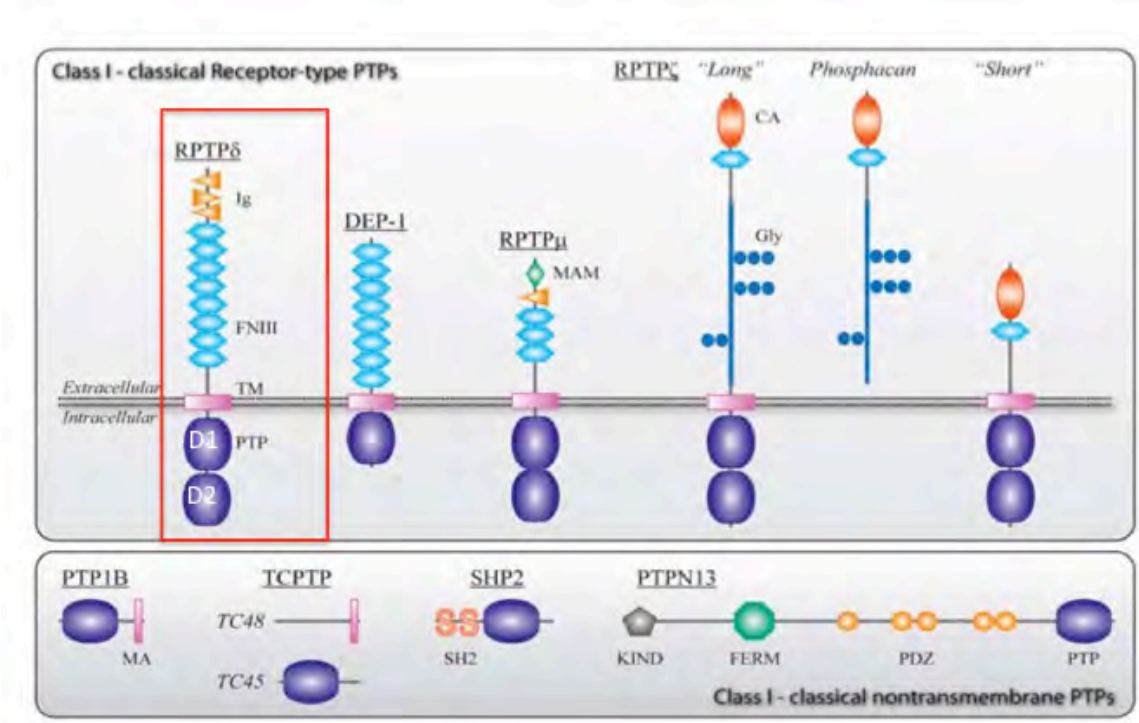

Figure 1.2 Domain structures of protein tyrosine phosphatases implicated in glioma biology. PTPRD is a receptor-type PTP with fibronectin and IgG extracellular domains and two intracellular phosphatase domain. PTPRD is highlighted by a red box.
Springer and Acta Neuropathol. 119, 2010, 157-75, Protein tyrosine phosphatases in glioma biology, Navis AC, van den Eijnden M, Schepens JT, Hooft van Huijsduijnen R, Wesseling P, Hendriks WJ., Figure 3, with kind permission from Springer Science and Business Media.

CHAPTER TWO

Loss of the Tyrosine Phosphatase PTPRD Leads to Aberrant STAT3 Activation and Promotes Gliomagenesis

ABSTRACT

PTPRD, which encodes the protein tyrosine phosphatase receptor delta, is a frequently inactivated gene across human cancers, including glioblastoma. *PTPRD* undergoes both deletion and mutation in cancers, with copy number loss comprising the primary mode of inactivation in glioblastoma multiforme (GBM). However it is unknown whether loss of *PTPRD* promotes tumorigenesis *in vivo*, and the mechanistic basis of PTPRD function in tumors is unclear. Here, using genomic analysis and a glioma mouse model, we demonstrate that loss of *Ptprd* accelerates tumor formation and define the oncogenic context in which *Ptprd* loss acts. Specifically, we show that in human GBMs, heterozygous loss of *PTPRD* is the predominant type of lesion and that loss of *PTPRD* and the *CDKN2A/p16*^{INK4A} tumor suppressor frequently co-occur. Accordingly, heterozygous loss of *Ptprd* cooperates with *p16* deletion to drive gliomagenesis in mice. Moreover, loss of the Ptprd phosphatase resulted in phospho-Stat3 accumulation and constitutive activation of Stat3-driven genetic programs. Surprisingly, the consequences of *Ptprd* loss are maximal in the heterozygous state, demonstrating a tight dependence on gene dosage. Ptprd loss did not increase cell proliferation but rather altered pathways governing the macrophage response. In total, we reveal that PTPRD is a *bona fide* tumor suppressor, pinpoint *PTPRD* loss as a cause of aberrant STAT3 activation in gliomas, and

establish *PTPRD* loss, in the setting of *CDKN2A/p16*^{INK4A} deletion, as a driver of glioma progression.

INTRODUCTION

Glioblastoma multiforme (GBM)

GBM is a devastating disease as it is the most common and aggressive type of primary brain tumor in adults. GBM tumors are classified as WHO grade IV, and are either de novo primary, or secondary tumors that have progressed from a lower grade II/III glioma. Current treatment, consisting of surgical resection followed by a combination of radiotherapy and the alkylating agent temazolomide, produces an overall median survival time of less than 15 months (Stupp et al. 2005). Poor response to current treatment has prompted efforts to generate an extensive genomic profile of GBM with the intention of creating therapies against molecular targets that drive tumorigenesis.

Genetic and epigenetic changes in GBM

The Cancer Genome Atlas (TCGA) Research Network has provided a detailed view of the mutations, changes in copy number, methylation, gene expression, and patient clinical information for GBM tumors (TCGA 2008 and Brennan et al. 2013). Genetic alterations/mutations in *TP53, PTEN, EGFR, RB1, CDKN2A, NF1, ERBB2, PIK3R1,* and *PIK3CA* were identified. In parallel to TCGA, Parsons et al. (2008) conducted a whole exome sequencing survey of GBM and identified similar somatic mutation profiles. In addition, they also found mutations in *IDH1* in 12% of GBM patients. As GBM is a highly heterogeneous tumor, a challenge remains to determine which molecular

alterations drive tumorigenesis and to understand their underlying mechanism(s) of action.

Inactivation of the *PTPRD* tumor suppressor in GBM

Recent work by our group and others have identified inactivation of protein tyrosine receptor phosphatase delta (*PTPRD*) as a frequent alteration in GBM and other tumors, and showed that *PTPRD* copy number loss correlates with poor prognosis (Veeriah et al. 2009, Solomon et al. 2008, Boeva et al. 2013, Du et al. 2013, Meehan et al. 2012, and TCGA 2012). Veeriah et al. (2009) examined the array comparative genomic hybridization (aCGH) TCGA data for 215 GBM tumors, and reported loss at the *PTPRD* loci (9p23-24) in 89 tumors (41%). Intragenic homozygous deletions were found in the *PTPRD* gene that removed *PTPRD* exons, but not surrounding genes, suggesting that there is a minimal common region of deletion at the *PTPRD* locus. Moreover, both heterozygous and homozygous loss of *PTPRD* was observed. Solomon et al. (2008) examined the *PTPRD* locus in 58 GBM tumors and reported focal deletions of *PTPRD* in 14% of GBM tumors and large-scale loss occurred in 33% of tumors. In addition to deletion of *PTPRD*, Veeriah et al. (2009) reported that epigenetic silencing occurs at the *PTPRD* promoter. Hypermethylation of *PTPRD* was found in 37% of GBM tumors that do not have deletions in *PTPRD*. Moreover, hypermethylation of the *PTPRD* promoter was associated with loss of gene expression in both cell lines and GBM tumors. Both groups found that inactivation of *PTPRD* can also occur via somatic mutations. For example, mutation Q1481X is predicted to result in a truncated protein product lacking a functional C-terminal phosphatase domain. R1088C is a missense mutation in the

fibronectin domain and is predicted to be deleterious. These mutations resulted in a decreased ability of PTPRD to inhibit growth as compared with wild-type PTPRD (Veeriah et al. 2009). Solomon et al. (2008) identified three missense mutations (P459L, I1115T, and G1272V) and one nonsense mutation (R427Stop). The functional consequence of I1115T was tested, and this mutation destroyed the growth suppressive ability of PTPRD.

Veeriah et al. (2009) studied the tumor suppressive function of PTPRD *in vitro*. Knockdown of PTPRD enhanced cell growth and tumor growth of xenografts, while overexpression of PTPRD reduced cell growth. Furthermore, lower PTPRD expression correlated with higher-grade tumors and poor survival, suggesting PTPRD can predict poor prognosis. Solomon et al. (2008) also observed a growth suppressive effect and increased apoptosis with overexpression of wild-type PTPRD in cells.

Despite the high prevalence of *PTPRD* inactivation in human tumors, it is not known whether loss of *PTPRD* can promote tumorigenesis *in vivo*. Furthermore, the mechanism(s) of action and the oncogenic context in which PTPRD acts remains unclear. This thesis addresses these important questions.

Signal Transducer of and Activator of Transcription 3 (STAT3) and PTPRD

Previously our lab demonstrated that phosphorylated STAT3 (p-STAT3) is a substrate of PTPRD, and that cancer-specific mutations in *PTPRD* abrogate the ability of the phosphatase to dephosphorylate STAT3 (Veeriah et al. 2009). STAT3 has been described

as molecular hub for signaling pathways in glioma because of its roles in cell cycle progression, apoptosis, angiogenesis, differentiation, and immune invasion (Brantley et al. 2008). STAT3 is a transcription factor that is activated by tyrosine phosphorylation in response to cytokines and growth factors. More specifically, STAT3 is known the be activated by members of the interleukin 6 (Il-6) cytokine family, including IL-6 oncostatin, and leukemia, inhibitory factor, and by growth factors such as platelet-derived growth factor (PDGF), fibroblast growth factor (FGF), and epidermal growth factor (EGF). STAT3 is tyrosine phosphorylated by receptor tyrosine kinases such as EGFR, FGFR, PDGFR, or janus kinase (JAK), as well as by non-receptor tyrosine kinases such as Ret, Src, or the Bcl-Abl fusion protein (Brantley et al. 2008). STAT3 is tightly regulated by suppressors of cytokine signaling (SOCS) proteins that down-regulate the kinases responsible for STAT3 phosphorylation (Starr et al. 1999), and by protein inhibitors of activated STATs (PIAS) proteins (Chung et al. 1997). Protein tyrosine phosphatases target the STAT3 protein directly and include PTPRD (Veeriah et al 2009) and PTPRT (Zhang et al. 2007). Interestingly, accumulation of phosphorylated STAT3 and STAT3 hyperactivation are frequent events in solid tumors like GBM, yet the genetic basis of aberrant STAT3 activation is poorly understood. In this study, we show that allelic loss of *Ptprd* results in p-Stat3 accumulation and Stat3 hyperactivation, elucidating one genetic root cause for aberrant STAT3 activation in GBM.

PTPRD **and** ***CDKN2A*** **inactivation in GBM**

Chromosome 9p, a region frequently lost in gliomas, contains the genes encoding *PTPRD* and the cyclin dependent kinase inhibitor 2A (*CDKN2A*). Veeriah et al. (2009) examined

the frequency of copy number alterations (CNAs) at the *PTPRD* and *CDKN2A* loci in 215 TCGA GBM tumors. In 41% of the tumors, deletion was seen at both the *PTPRD* and *CDKN2A* loci. Of the tumors with deletion at both loci, 33% showed a distinct copy number decrease in each region with euploidy in the DNA between the genes. Additionally, in an independent panel of 35 tumors, 15 tumors (43%) showed inactivation of *PTPRD* and *CDKN2A* by methylation or loss. Altogether these results suggest that selective pressure exists for inactivation of both *PTPRD* and *CDKN2A*, on chromosome 9p. In order to determine if these genes cooperate in tumorigenesis, we developed a murine glioma tumor model in which we inactivate both genes and assess survival.

The *CDKN2A* locus produces $p16^{INK4A}$ and $p14^{ARF}$ alternative splicing products

The *CDKN2A* locus is located on chromosome 9p21 and consists of four exons (E1β, E1α, E2, and E3) that produce the $p16^{INK4A}$ and $p14/p19^{ARF}$ tumor suppressors by alternate splicing (Sherr et al. 2001). The p16 (INK4A) variant is made up of E1β and E2, while the p14 (ARF) variant is made up of E1α, E2, and E3. Both products ultimately inhibit cellular proliferation (Sherr et al. 2001). $p16^{INK4A}$ is a cyclin-dependent kinase inhibitor that binds to and inhibits cyclinD/cdk4 from phosphorylating Rb. As a result, progression through G1 phase does not occur. The $p14^{ARF}$ product inhibits Mdm2 causing an accumulation of p53. Induction of p53 inhibits the cell cycle via the p21 cell cycle inhibitor. Knockout mice have been generated with deletion of exon 1B (Arf KO), exon 1a (Ink4a KO), and exons 2 and 3 (Ink4aArf KO) (Sharpless et al. 2004, Kamijo et al. 1997, and Serrano et al. 1996 respectively).

RCAS PDGFB / *Nestin*-TvA glioma mouse model

Several glioma mouse models exist with latencies that range from 2-52 weeks (reviewed by Chen et al. 2012). For reasons that follow, we chose to study the cooperative effects of *Ptprd* and *Cdkn2a* in the RCAS PDGFB / *Nestin*-tvA glioma mouse model. In the RCAS/tvA system, genes of interest are introduced into the chromosomes of target cells using the RCAS retroviral vector (replication competent avian sarcoma-leukosis virus long terminal repeat with splice acceptor). RCAS viruses can only infect avian cells that express the tvA cell surface receptor. Introduction of a gene of interest into a specific mouse cell or tissue type is possible by generating transgenic mice with expression of tvA under a cell- or tissue- specific promoter. As opposed to traditional genetically engineered mouse models, genes can be introduced into specific adult somatic cells of mice, and thus the RCAS-tvA mouse model is more consistent with human cancer formation (Orsulic et al. 2002).

Two tvA transgenic mouse lines have been generated to study glioma tumorigenesis using the RCAS-tvA system. *Nestin*-tvA mice express the tvA receptor from a *Nestin* promoter. As a result, *Nestin* expressing glial progenitors are infected with RCAS. A *GFAP*-tvA transgenic mouse is also available, in which gene transfer occurs in differentiated astrocytes, however tumor incidence is significantly less in these mice (Tchougounova et al. 2007).

A variety of glioma relevant oncogenes have been inserted into the RCAS vector and tested for their ability to induce gliomas. RCAS Akt, RCAS Kras, RCAS EGFR, and

RCAS PDGFB have all been shown to generate gliomas in *Nestin*-tva or *GFAP*-tva mice with different latencies and aggressiveness (Dai et al. 2005, Tchougounova et al. 2007, Dai et al. 2001, and Holland et al. 1998). RCAS PDGFB infection in *Nestin*-tva mice has been the most studied (Hambardumyan et al. 2009, Katz et al. 2012, Dai et al. 2001, Ciznadija et al. 2011, and Charles et al. 2010). Here, we show that *Ptprd* is a haploinsufficient tumor suppressor that cooperates with deletion of *Cdkn2a/p16*^{Ink4a} to promote tumor progression in the RCAS PDGFB/*Nestin*-tva glioma mouse model.

RESULTS

Genetic patterns of *PTPRD* loss in human GBM

Previously, we showed that the *CDKN2A* and *PTPRD* genes are both commonly inactivated regions on chromosome 9p with distinct focal deletions at each locus, indicating that each gene is a minimal commonly deleted region. Furthermore, both genes are subject to somatic mutation and/or hypermethylation, and are hypothesized to be cancer driver genes. We set out to define GBM alterations that co-occur most frequently with *PTPRD* loss. Figure 2.1A illustrates the co-occurrence of select GBM alterations with *PTPRD* loss in GBM tumors from the TCGA data set. *CDKN2A/CDKN2B* deletions co-occurred most frequently with *PTPRD* loss ($p<0.05$, Table 2.1). Importantly, the vast majority of tumors that lose *PTPRD* also lose *CDKN2A*. Interestingly, 87% of the tumors with *PTPRD* deletion only lost one copy (Figure 2.1B).

Heterozygous loss of *Ptprd* cooperates with *Cdkn2a/p16^{Ink4a}* deletion to promote gliomagenesis

In order to investigate the functional significance of concurrent *Ptprd* and *Cdkn2a* loss in tumorigenesis, we used the RCAS PDGFB/*Nestin*-tvA proneural glioma mouse model. As shown in Table 2.2, *PTPRD* loss occurs in tumors of all GBM subgroups, including the proneural transcriptional subclass, which is characterized by PDGF activity. We crossed *Ptprd* knockout mice with *p16^{Ink4a}* knockout; *Nestin*-tvA (N-tvA) mice to generate *Ptprd*+/+*p16*-/-;N-tvA, *Ptprd*+/-*p16*-/-;N-tvA, and *Ptprd*-/-*p16*-/- ;N-tvA mice. We then injected neonatal mice intracranially with DF-1 chicken cells expressing RCAS PDGFB virus. Since our glioma tumor model is dependent on Nestin expression, we first measured Nestin expression in un-injected neonatal mice by flow cytometry analysis and confirmed that Nestin is unaltered by *Ptprd* loss (Figure 2.2). Symptom-free survival was measured by observing the mice for the onset of brain tumor symptoms, including hydrocephalus, seizure, or general malaise. Interestingly, *Ptprd*+/-*p16*-/- mice showed significantly worse survival than *Ptprd*+/+*p16*-/- mice ($p<0.05$, Figure 2.3A). In contrast, *Ptprd*-/-*p16*-/- mice only showed a trend toward worse survival (Figure 2.3A), consistent with a somewhat weaker phenotype. To our knowledge, this is the first data to show that *Ptprd* loss promotes tumorigenesis and that heterozygous loss is sufficient to do so in the context of *p16^{Ink4a}* deletion.

To determine whether *Ptprd* was heterozygous in the tumors, tumor cells were sorted from RCAS PDGFB GFP injected *Ptprd* heterozygous mice and PCR genotyped for *Ptprd*. As illustrated in Figure 2.3B, tumors from *Ptprd* heterozygous mice retain one

intact wild-type allele. H&E stained tumors were graded according to criteria set by the World Health Organization (Louis et al. 2007). Interestingly, as shown in Figure 2.3C, there were no significant differences in tumor grade between the genotypes, suggesting that Ptprd may affect other processes that regulate glioma initiation or progression.

Intriguingly, when mice with *Ptprd* loss but wild-type $p16^{Ink4a}$ were injected with RCAS PDGFB virus, the mice had significantly better symptom-free survival than *Ptprd*+/+*p16*+/+ mice (Figure 2.4A). While survival and incidence were affected by *Ptprd* loss, there were no significant differences in tumor grade among the genotypes (Figure 2.4B). In an effort to determine whether increased cell death could explain why *Ptprd*+/-*p16*+/+ and *Ptprd*-/-*p16*+/+ mice had better survival, we stained the tumors for cell death by TUNEL staining. As shown in Figure 2.4C, no significant differences in TUNEL staining were observed between the genotypes. Nevertheless, our data suggest that loss of $p16^{Ink4a}$ is required in the context of *Ptprd* loss for enhanced tumorigenesis. These results may also help explain why *PTPRD* is almost never lost alone but nearly always with *CDKN2A*.

Heterozygous loss of *Ptprd* results in phospho-Stat3 accumulation and activation of Stat3-dependent transcription

Using *in vitro* methods, we previously identified p-STAT3 as a candidate substrate of PTPRD (Veeriah et al. 2009). It is well known that p-STAT3 functions as a transcription factor for genes involved in the tumorigenic process (Brantley et al. 2008, Bournazou et al. 2013). We performed p-Stat3 immunohistochemistry (IHC) on glioma tumors from

Ptprd+/+*p16*-/-, *Ptprd*+/-*p16*-/-, and *Ptprd*-/-*p16*-/- mice. Interestingly, p-Stat3 was significantly elevated in only the *Ptprd*+/-*p16*-/- mice (Figure 2.5A, 2.5B). Total Stat3 levels remained at similar levels between the genotypes, suggesting that the main effect is on the phosphorylation status of Stat3 (Figure 2.5A). To determine if the increased p-Stat3 was inducing transcription of its gene targets, we measured gene expression changes in the *Ptprd*+/+*p16*-/-, *Ptprd*+/-*p16*-/-, and *Ptprd*-/-*p16*-/- tumors. Glioma tumor cells were purified by flow sorting and expression microarray analysis was performed. Consistent with the IHC results, microarray analysis of the tumor cells showed increased expression of known p-Stat3 gene targets in only the *Ptprd*+/-*p16*-/- tumors (Figure 2.5C, Table 2.3). In order to determine whether the changes in the phosphorylation status of STAT3 are also present in human GBM, we determined the relative levels of p-STAT3 in human tumors with varying *PTPRD* status. P-STAT3 / STAT3 protein expression was measured by western blot analysis in *PTPRD*+/+*CDKN2A*-/- and *PTPRD*+/-*CDKN2A*-/- tumors. P-STAT3 was significantly increased in *PTPRD*+/-*CDKN2A*-/- tumors (Figure 2.5D). Due to the low frequency of homozygous deletion of *PTPRD* in human GBM, *PTPRD*-/-*CDKN2A*-/- tumors were not available for quantification. This data shows that heterozygous loss of *PTPRD* and deletion of *CDKN2A*/*p16*^{Ink4a} is sufficient for accumulation of nuclear p-STAT3 and the induction of p-STAT3 gene targets.

Ptprd loss does not increase the rate of cell proliferation or expand the glial progenitor pool

We first evaluated whether *Ptprd* loss affected tumor size by generating a separate cohort of *Ptprd*+/+*p16*-/-, *Ptprd*+/-*p16*-/-, and *Ptprd*-/-*p16*-/- mice that were stereotactically

injected with DF-1 cells expressing RCAS PDGFB virus. Stereotactic injection allows the precise measurement of tumor size. At a defined time-point prior to the development of symptoms, we performed MRI to measure the volume of the gliomas in all genotypes. As expected, there was substantial heterogeneity across the gliomas due to differences in tumor penetrance, as frequently occurs for this cancer type. Interestingly, *Ptprd*+/-*p16*-/- mice showed a strong trend toward having the greatest tumor volume, suggesting that *Ptprd* loss is associated with larger tumor size (Figure 2.6A, 2.6B).

We next determined whether loss of *Ptprd* was increasing the rate of cell proliferation, decreasing the rate of cell death, expanding the glial progenitor pool, or promoting angiogenesis. We used flow cytometry to measure the frequency of Ki67 in GFP positive tumor cells (RCAS-infected cells co-express GFP). Surprisingly, no significant differences in Ki67 were found among the genotypes (Figure 2.6C). We also measured cell death in the tumors by TUNEL immunohistochemistry. As shown in Figure 2.6D, there were no significant differences in the levels of TUNEL staining between the genotypes. In order to determine the differentiation status of the tumor cells, we performed IHC to stain tumors from *Ptprd*+/+*p16*-/-, *Ptprd*+/-*p16*-/-, and *Ptprd*-/-*p16*-/- mice for oligodendrocytes (Olig2), astrocytes (Gfap) and glial progenitors (Nestin). No differences were found in the quantity or intensity of staining between mice of the different genotypes (Figure 2.7A). In order to examine the glial progenitor pool, we also performed side population analysis of the tumors as previously described (Bleau et al. 2009). No differences in the amount of side population cells for each genotype were evident, suggesting that *Ptprd* loss does not expand the glial progenitor pool (Figure

2.7B, 2.7C). Lastly, we performed immunohistochemistry to examine endothelial cells (CD34), and to determine if *Ptprd* loss affects angiogenesis. No differences in the quantity or intensity of staining were evident (Figure 2.7D). Together, this data demonstrates that the effects of *Ptprd* loss and resultant Stat3 activation do not promote tumorigenesis by altering cellular proliferation, cellular death, cellular differentiation, or vascular density.

Ptprd loss activates pathways that regulate the immune response and tumor microenvironment

In order to evaluate the nature of the gene expression changes induced by *Ptprd* loss in our glioma model, we performed gene expression analysis of sorted GFP positive tumor cells from *Ptprd*+/+*p16*-/-, *Ptprd*+/-*p16*-/-, and *Ptprd*-/-*p16*-/- mice. Principal component analysis and hierarchical clustering demonstrated that the transcriptome of *Ptprd*+/-*p16*-/- tumors is significantly different from those of *Ptprd*+/+p16-/- and *Ptprd*-/-*p16*-/- tumors (Figure 2.8A, 2.8B). In order to determine if other tyrosine phosphatases were compensating for loss of *Ptprd* in the tumors at the transcriptional level, we analyzed gene expression of other tyrosine phosphatases. As shown in Figure 2.8C and Table 2.4 no significant differences between the genotypes were observed.

Pathway analysis of the differentially expressed genes in the *Ptprd*+/-*p16*-/- vs. *Ptprd*+/+*p16*-/- tumor cells showed statistically significant enrichment in pathways governing the immune response and macrophage behavior (Figure 2.9A, Table 2.5). A fascinating pattern emerged when we reviewed the expression levels of all known

cytokines and chemokines. Tumor cells from *Ptprd* heterozygotes, but not wild-type or homozygotes, had a concerted and significant increase in the expression of chemokines CCL2, CCL6, CCL12, and CXCL14 (Figure 2.9B). All four chemokines promote M2 pro-tumor polarization of macrophages (Roca et al. 2009, Murray et al. 2011, Gabrusiewicz et al. 2011, and Movahedi et al. 2010). Thus, our gene expression analysis suggests that loss of *Ptprd* in the tumor cells might lead to the activation of genetic programs that affect the immune response, and in particular macrophages.

There is substantial evidence that the immune response (including macrophage activity) influences tumor pathogenicity (da Fonseca et al. 2013, Li et al. 2012, and Hao et al. 2012). Pyonteck et al. (2013) showed that pro-tumor macrophages in RCAS PDGFB gliomas increases tumor aggressiveness. In order to determine whether macrophages were present in the tumors from our mice, we stained *Ptprd*+/+*p16*-/-, *Ptprd*+/-*p16*-/-, and *Ptprd*-/-*p16*-/- tumors with the Iba1 macrophage marker. While the quantity of Iba1 positive-cells was similar for all tumors, we noted that tumors from *Ptprd*+/-*p16*-/- tended to have amoeboid macrophage morphology, which is associated with a pro-tumorigenic phenotype (Gabrusiewicz et al. 2011, Sliwa et al. 2007, and Hanisch et al. 2007) (Figure 2.9C). This was concentrated in the larger tumors. P-Stat3 is a marker of M2 pro-tumor polarized macrophages (Li et al. 2012 and Zhang et al.2009). In order to determine whether macrophages in our tumors might be M2 polarized, we performed immunofluorescence for Iba1 and p-Stat3 and quantified the number of cells that were Iba1 and p-Stat3 positive. Tumors in the *Ptprd*+/-*p16*-/- group had greater numbers of double positive Iba1 and p-Stat3 cells than the other genotypes (Figure 2.9D, 2.9E).

These were again concentrated in the larger tumors. We performed immunofluorescence for Gfap and p-Stat3. Tumors in the *Ptprd+/-p16-/-* group had cells that were both p-Stat3 and Gfap positive as well as cells that were p-Stat3 positive and Gfap negative (Figure 2.10). Together, our data suggest that heterozygous loss of *Ptprd* activates genetic programs regulating immune response and promotes the expression of chemokines that influence immune cell behavior and macrophage biology.

MATERIALS AND METHODS

Mouse Model

P16^{Ink4a}-/-;*Nestin*-tvA mice were kindly provided by Dr. Eric Holland (Memorial Sloan-Kettering Cancer Center, New York, NY) (Uhrbom et al. 1998 and Tchougounaova et al. 2007). *Ptprd+/-* mice were generously provided by Dr. Michael Tremblay (McGill University, Montreal, Canada) (Uetani et al. 2000). Mice experiments were performed with MSKCC Institutional Animal Care and Use Committee approval.

Sorted GFP+ tumor cells from mice injected with RCAS-PDGFB-GFP were extracted using the DNeasy Blood and Tissue kit (Qiagen). PCR was performed with the following *Ptprd* genotyping primers: 5'-GGTGAAGTGTGACCAGTATTGGCC-3', 5'-CTGGAATTGTCTCACTTTCCTC-3', and 5'-GACTGCCTTGGGAAAAGCGCCTCC-3'. Standard PCR procedures were performed with the following reaction buffer: 1M$(NH_4)2SO_4$, 2M Tris, pH 8.8, 1M $MgCl_2$, and 14.4M B-mercaptoethanol.

Cell Culture and RCAS Virus

RCAS retrovirus was propagated in chicken DF-1 cells (ATCC, CRL-12203). The transfection of DF-1 cells with RCAS vectors were performed with Lipofectamine 2000 (Life Technologies). Intracranial injections into neonatal mice were used to introduce DF-1 cells expressing RCAS virus as described previously (Liu et al. 2007). RCAS-PDGFB-HA and RCAS-PDGFB-GFP viral expression plasmids were a gift from Dr. Eric Holland and have been previously described (Dai et al. 2001 and Becher et al. 008). Mice were monitored daily and sacrificed upon demonstration of brain tumor symptoms (hydrocephalus, hunched, or seizure) or at 16 weeks of age.

Stereotactic injections of DF-1 cells propagating RCAS-PDGFB-HA virus was performed in adult mice 7-10 weeks old. Injections into the subventricular zone were performed as described previously (Hambardzumyan et al. 2009). The following coordinates for the subventricular zone were used: Bregma 0mm, lateral right of midline -0.5mm, and depth of 1.5mm from the dural surface. Mice were monitored daily and sacrificed upon demonstration of brain tumor symptoms or at 23 weeks post-injection.

Magnetic Resonance Imaging (MRI)

Brains of injected mice were scanned at 8, 11, 16, and 20 weeks post-injection with a 200MHz Bruker 4.7T Biospec MRI scanner equipped with a 560 mT/m ID 12cm gradient (Bruker Biospin MRI GmbH, Ettlingen, Germany; Resonance Research, Inc., Billerica, MA). For mouse brain imaging, brain coronal T2-weighted images using fast spin-echo RARE sequence (Rapid Acquisition with Relaxation Enhancement) was acquired with

TR 1.5s, TE 50ms, RARE factor of 8, slice thickness of 0.7mm, FOV 30 x 20mm, in-plane resolution of 117 x 125μM, and 24 averages. Tumor volume was calculated by contouring, and measuring the tumor areas and calculating the sum of the areas multiplied by the distance between the centers of two adjacent slices.

Histology and Immunostaining

Brains from mice were collected and fixed with 10% neutral buffered formalin (Sigma). Tissues were embedded in paraffin and 5μM sections were used for analysis. Sections were stained with hematoxylin and eosin (H&E) or used for immunohistochemical analysis.

Immunohistochemistry was performed at the Molecular Cytology Core Facility of Memorial Sloan-Kettering Cancer Center using Discovery XT processor (Ventana Medical Systems). Tissue sections were stained with the following antibodies: p-STAT3 Tyr-705 (Cell Signaling, cat no. 9145, rabbit monoclonal, 0.5μg/mL), STAT3 (Cell Signaling, cat no. 9132, rabbit polyclonal, 0.16μg/mL), Iba1 (Wako Chemicals, cat no. 019-19741, rabbit polyclonal, 0.5μg/mL), GFAP (Dako, cat no. Z033429-2, rabbit polyclonal, 1μg/mL), Olig2 (Millipore, cat no. AB9610, rabbit polyclonal, 2μg/mL), and Nestin (BD Pharmigen, cat no. 556309, mouse monoclonal, 5μg/mL). For rabbit antibodies, tissue sections were blocked in 10% goat serum with 2% BSA in PBS. For the mouse antibody, tissues were blocked with Biotinylated Mouse on Mouse (M.O.M.) anti-Mouse Ig Reagent (Vector Labs, cat no. MKB-2225). Primary antibody incubation was done for 5 hours, followed by a 60 minute incubation with biotinylated goat anti-rabbit

IgG (Vector Labs, cat no. PK6101, 1:200 dilution) or biotinylated anti-mouse IgG (Vector Labs, cat no. BMK-2202) according to the manufacturer's instructions. Detection was performed with Blocker D, Streptavidin-HRP and DAB kit (Ventana Medical Systems) according to the manufacturer's instructions. Slides were counterstained with hematoxylin and coverslipped with Permount (Fisher Scientific).

CD34 staining was performed on the Leica Bond RX (Leica Biosystems) using the Bond Polymer Refine Detection Kit (Leica Biosystems, DS980). Anti-CD34 antibody (Abcam, cat no. ab8158, rat monoclonal, 16μg/mL) was added for 30 minutes followed by a 30 minute incubation of biotinylated anti-rat (Vector Labs, cat no. BA-4001, 1:100 dilution).

TUNEL staining was performed with the following reaction mixture: 0.1M Sodium Cacodylate pH7, 0.1mM DTT, 0.05mg/mL bovine serum albumin, 2u/ul terminal transferase, 0.2nm Biotin-16-dUTP, and 2.5mM Cobalt Chloride for 1 hour at 37 degrees. The reaction was terminated with 300mM sodium chloride and 30mM sodium citrate at room temperature for 15 minutes, incubated in avidin-biotin for 30 minutes, and developed with 3,3'-Diaminobenzidine for 3 minutes.

Dual immunofluorescence of p-Stat3 and Iba1 or Gfap were performed using Discovery XT processor (Ventana Medical Systems). Staining with p-Stat3 Tyr-705 (Cell Signaling, cat. no. 9145, rabbit monoclonal, 0.5μg/mL) followed by Tyramide Alexa Fluor 568 (Invitrogen, cat. no T20914) was performed first. Next, Iba1 (Wako Chemicals, cat. no. 019-19741, rabbit polyclonal, 0.5μg/mL) or Gfap (BD Pharmigen, cat. no. 561483,

mouse monoclonal, 5μg/mL) was added followed by Tyramide-Alexa Fluor 488 (Invitrogen, cat. no. T20922).

Immunostaining Image Analysis

Whole slides were scanned with Pannoramic Flash Scanner (3DHistech, Hungary). Image analysis of tumor areas was performed with Metamorph software (Molecular Devices, PA). For analysis of immunohistochemistry images, color thresholds were set for brown positive staining and for total area (brown staining + blue nuclei). Percent of brown staining to total area was calculated. For analysis of dual immunofluorescence images, a grayscale threshold and standard area was set for green (Iba1), red (p-STAT3), and blue (DAPI). For each sample, the number of DAPI positive nuclei within each stained area, and the number of DAPI within co-localized areas was calculated.

Human Tumor Collection, Tissue Lysates, and Immunoblotting

Fresh human GBM tissue samples were obtained from patients who consented under an Institutional Review Board-approved protocol. Tumor lysates were lysed in CelLytic MT Mammalian Tissue Lysis/Extraction Reagent (Sigma) supplemented with Complete Mini EDTA-free (Roche) and PhosSTOP (Roche) protease inhibitor mixes. Protein lysates were run in SDS/PAGE gels and transferred to nitrocellulose for immunoblotting. The following antibodies were used: p-STAT3 Tyr-705 (Cell Signaling, cat no. 9145, rabbit monoclonal, 1:2000) and STAT3 (Cell Signaling, cat no. 9132, rabbit polyclonal, 1:1000). Quantification of western blot by densitometry analysis was performed using ImageJ software.

Flow Sorting of RCAS PDGFB GFP Tumors

Tumors were dissected from mice injected with RCAS-PDGFB-GFP and enzymatically and mechanically dissociated into single-cell suspensions by treatment with papain and ovomucoid as previously described (Ciznadija et al. 2011). Single cell suspensions were made in PBS with 10%FBS, and GFP+DAPI- cells were sorted on a MoFlo Cell Sorter (Dako Cytomation).

Human Genetic Analysis and Microarray Analysis of Mouse Tumor Cells

The Cancer Genome Atlas (TCGA) data used was previously described (TCGA 2008 and Verhaak et al. 2010). The GBM oncoprint was generated using the cBio Portal as previously described (Cerami et al. 2012).

Sorted GFP+DAPI- tumor cells from mice injected with RCAS-PDGFB-GFP were stored at -80°C in Trizol LS Reagent (Ambion). Samples were processed by the MSKCC Genomics Core. Briefly, RNA was extracted and quality checked using a bioanalyzer. RNA was analyzed using the Affymetrix MOE 430A 2.0 chip following the manufacturer's instructions. Differentially expressed genes were determined using ANOVA. Principal component analysis and hierarchical analysis was performed using the Partek Software Suite. Genes were considered to be differentially expressed if their fold change > 1.8 and p-value < 0.05. Enriched pathways were identified using Ingenuity Pathway Analysis (Ingenuity Systems, Qiagen). Pathways with Benjami-Hochberg multiple testing correction p-value < 0.05 and Bias-corrected z-score > 2 were considered to be significant.

Side Population Assay

Tumors were dissected from mice injected with RCAS-PDGFB-GFP and dissociated into single-cell suspensions as previously described (Cizandaija et al. 2011). Single cell suspensions were made in un-supplemented basal neural stem cell media (Lonza) and counted using a hemocytometer. Side population analysis was performed by Hoechst 33342 exclusion as previously described (Bleau et al. 2009). Cells were incubated with or without verapamil (Sigma) and fumitremorgin c (Sigma) (ABC inhibitors) to set side population gates (Bleau et al. 2009). Flow cytometry was performed with a MoFlo Cell Sorter (Dako Cytomation) and analysis was performed using Flojo software (Treestar Inc.).

Ki67 and GFP Flow Cytometry

Tumors were dissected from mice injected with RCAS-PDGFB-GFP and dissociated into single-cell suspensions as previously described (Ciznadija et al. 2011). Single cell suspensions were made in PBS and counted using a hemocytometer. The following protocol was performed to minimize quenching of native GFP in the tumor cells. 1 million cells were fixed with 1% paraformaldehyde in a buffer made of HBSS and 2% fetal bovine calf serum overnight at 4°C. Cells were permeabilized using 0.5% TritonX-100 in HBSS and 2%FBS for 10 minutes at room temperature. Ki67 antibody conjugated to Alexa 647 (BD Pharmigen, cat no. 561126, mouse monoclonal, 1/60 dilution) was made in HBSS:2% FBS and applied to cells for 1 hour at room temperature. Cells were washed 2 times with HBSS:2% FBS and suspended in PBS:10%FBS for analysis with a

FACSCalibur (BD Biosciences). Analysis was performed using FloJo software (Treestar Inc.).

Flow Cytometry for Nestin

Single cell suspensions of neonatal mouse day 1-3 brains were made using papain digestion as done previously. Staining was performed as described previously using Nestin antibody (BD Pharmigen, mouse monoclonal, cat no. 556309, 1.7µg/mL) and goat anti-mouse Alexa 568 (Life Technologies, cat no. A21124, 33µg/mL) (Ciznadija et al. 2011). Flow cytometry was performed on the FACSCalibur (BD Biosciences), and analysis was performed using FloJo software (Treestar Inc.).

Statistical Analysis

Unless noted, student's t-test was performed for all statistical analysis. Log-rank statistical analysis was performed for Kaplan-Meier curves and Fisher's exact test was performed for the tumor grade analysis.

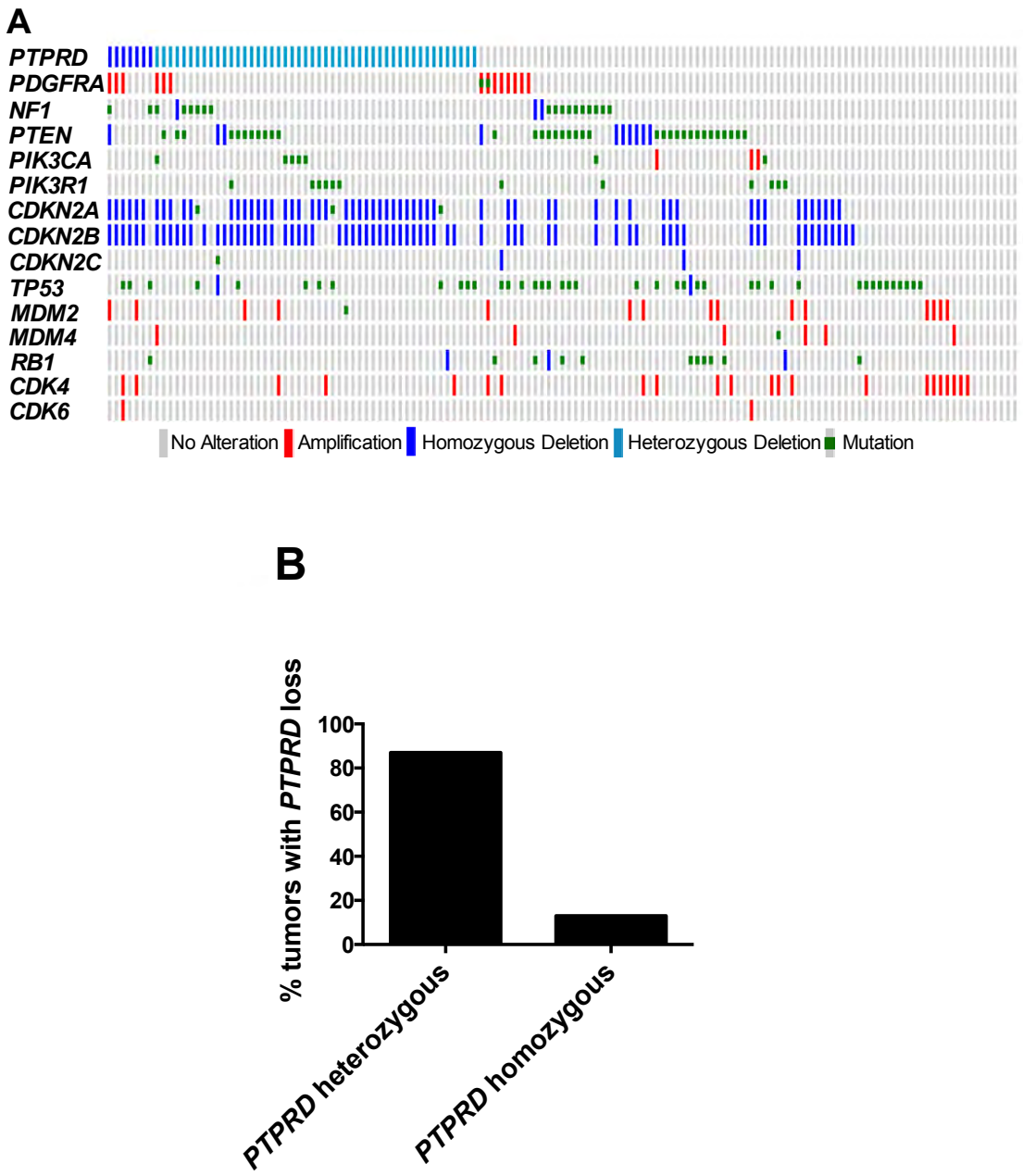

Figure 2.1 Genetic context of *PTPRD* loss in human GBM. (A) *PTPRD* loss co-occurs most frequently with deletion of *CDKN2A* and *CDKN2B*. OncoPrint of *PTPRD* with common GBM alterations (TCGA dataset, The cBio Cancer Genomics Portal). Type of alterations are as labeled in the color legend. (B) Frequency of heterozygous or homozygous loss of *PTPRD* in tumors with *PTPRD* loss.
Ortiz, B., Fabius, A.W., Wu, W.H., Pedraza, A., Brennan, C.W., Schultz, N., Pitter, K.L., Bromberg, J.F., Huse, J.T., Holland, E.C., Chan, T.A. (2014) Loss of the tyrosine phosphatase PTPRD leads to aberrant STAT3 activation and promotes gliomagenesis. *Proc Natl Acad Sci USA*. Jun 3; 111(22): 8149-54

Table 2.1 Concordance of *PTPRD* loss with other common gene alterations in GBM.

Gene	Altered in samples with *PTPRD* loss			Altered in samples with diploid *PTPRD*			Ratio	p-value
PDGFRA	6	55	11%	8	80	10%	1.10	2.20E-01
NF1	9	55	16%	12	80	15%	1.07	1.85E-01
PTEN	14	55	26%	31	80	39%	0.67	4.11E-02
PIK3CA	5	55	9%	5	80	6%	1.50	2.12E-01
PIK3R1	6	55	11%	6	80	8%	1.38	1.88E-01
CDKN2A	**41**	**55**	**75%**	**21**	**80**	**26%**	**2.88**	**2.30E-08**
CDKN2B	**44**	**55**	**80%**	**26**	**80**	**33%**	**2.42**	**3.38E-08**
CDKN2C	1	55	2%	3	80	4%	0.50	3.41E-01
TP53	13	55	24%	30	80	38%	0.63	3.60E-02
MDM2	5	55	9%	11	80	14%	0.64	1.58E-01
MDM4	1	55	2%	6	80	8%	0.25	1.19E-01
RB1	2	55	4%	12	80	15%	0.27	2.35E-02
CDK4	5	55	9%	17	80	21%	0.41	3.29E-02
CDK6	1	55	2%	1	80	1%	2.00	4.86E-01

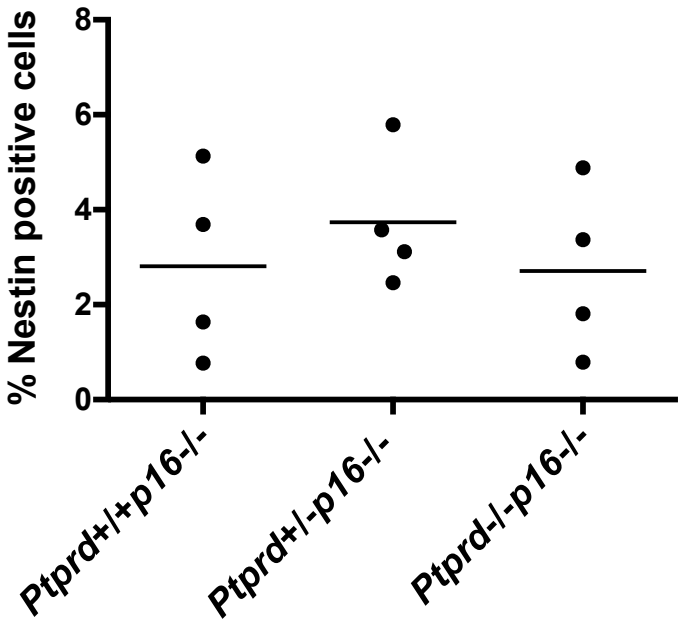

Figure 2.2 *Ptprd* loss does not affect frequency of Nestin-positive cells.
Nestin flow cytometry of neonatal un-injected mice. Bars represent means.

Table 2.2 *PTPRD* loss within GBM transcriptional subtypes

Subtype	Loss	Total loss	Percent loss
Classical	18	54	33%
Neural	14	54	26%
Proneural	11	54	20%
Mesenchymal	11	54	20%

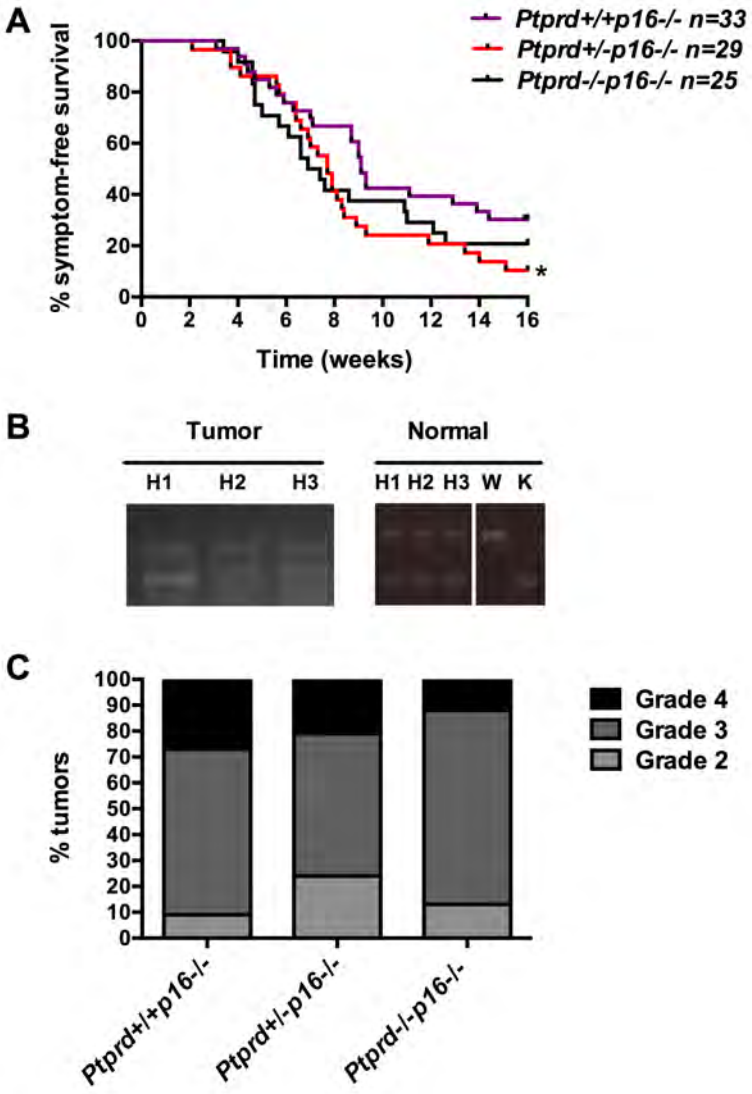

Figure 2.3 *Ptprd* loss cooperates with *Cdkn2a/p16*^{Ink4a} deletion to promote gliomagenesis. (A) Kaplan-Meier survival curve of mice injected intracranially with DF-1 cells expressing RCAS-PDGFB at post-natal day 1-3 and followed for 16 weeks. *Ptprd*+/+*p16*-/- (n=33), *Ptprd*+/-*p16*-/- (n=29), *Ptprd*-/-*p16*-/- (n=25), *Ptprd*+/- (n=19), and *Ptprd*-/- (n=22) mice. ***Ptprd*-/- vs. *Ptprd*-/-p16-/- and *Ptprd*+/- vs. *Ptprd*+/-p16-/- $p<0.01$; **Ptprd*+/-p16-/- vs. *Ptprd*+/+p16-/- $p<0.05$. (B) PCR genotyping of tumor and normal tissue for *Ptprd* demonstrate that tumors from *Ptprd*+/-*p16*-/- mice retain an intact wild-type allele. Mice were injected with RCAS PDGFB-GFP, and DNA was extracted from DAPI- GFP+ tumor cells. Matched ear samples were taken for normal tissue DNA extraction. *Ptprd*+/-*p16*-/- (H), *Ptprd*+/+*p16*-/- (W), *Ptprd*-/-*p16*-/- (K). (C) Tumor grade of gliomas from RCAS mice. H&E stained tumors were graded according to WHO standards. Genotypes of the mice are as indicated.

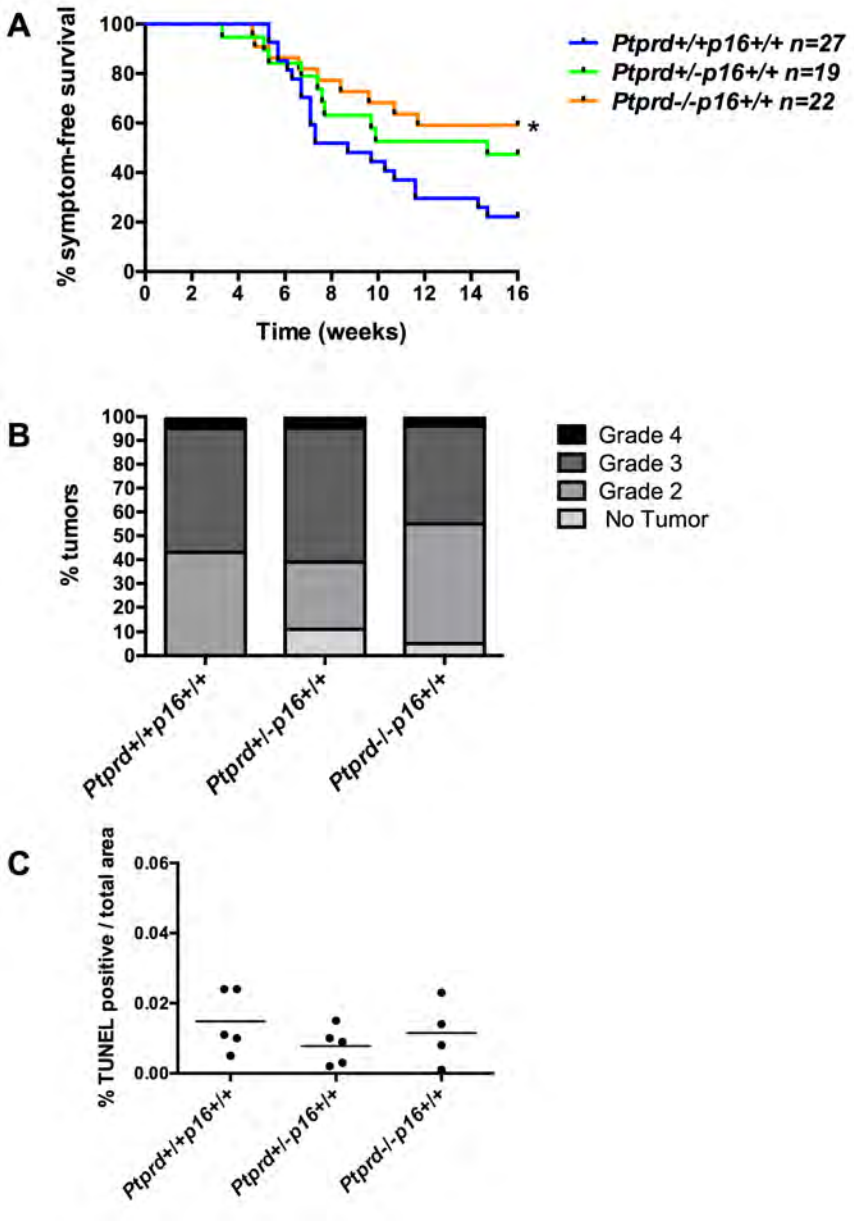

Figure 2.4 Mice with *Ptprd* loss require deletion of *Cdkn2a/p16^{Ink4a}* for tumorigenesis. (A) Kaplan-Meier survival curve of mice infected with RCAS-PDGFB and followed for 16 weeks. *Ptprd*+/+*p16*+/+ (n=27), *Ptprd*+/-*p16*+/+ (n=19) *and Ptprd*-/-*p16*+/+ (n=22). **Ptprd*-/-*p16*+/+ vs. *Ptprd*+/+*p16*+/+ $p<0.05$. (B) Tumors graded according to WHO standards. (C) Metamorph quantification of TUNEL staining on *Ptprd*+/+*p16*+/+ (n=5), *Ptprd*+/-*p16*+/+ (n=5) *and Ptprd*-/-*p16*+/+ (n=4) tumors. No significant differences in cell death were observed.

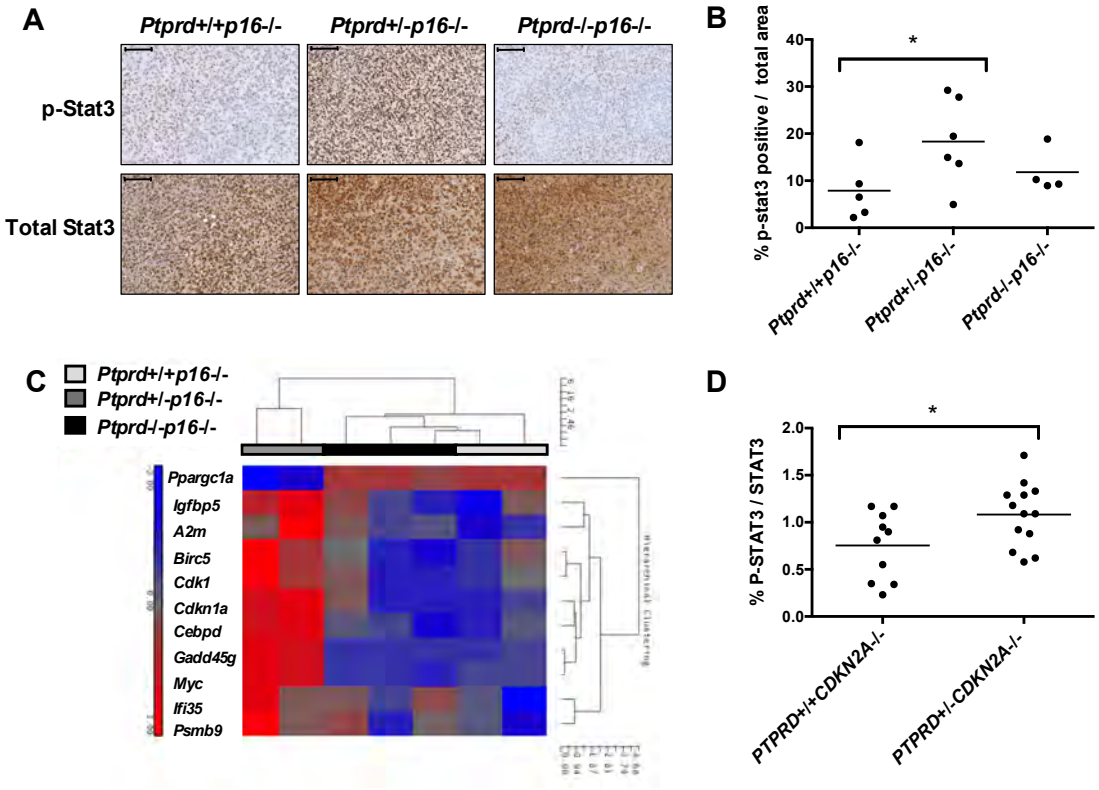

Figure 2.5 Heterozygous loss of *Ptprd* results in increased p-Stat3 and activation of Stat3 gene expression. (A) Representative images of immunohistochemistry for p-Stat3 and Stat3 in RCAS-PDGFB induced tumors from *Ptprd*+/+*p16*-/- (n=5), *Ptprd*+/-*p16*-/- (n=6), and *Ptprd*-/-*p16*-/- (n=4) mice. Scale bars = 100μM. (B) Quantification of immunohistochemistry results showing that levels of p-Stat3 are significantly higher in tumors of *Ptprd*+/-*p16*-/- mice, **Ptprd*+/-*p16*-/- vs. *Ptprd*+/+*p16*-/- p=0.05. (C) Expression of p-Stat3 gene targets are elevated in *Ptprd*+/-*p16*-/- mice. Heat-map of the most variant p-Stat3 target genes across all genotypes from GFP+ sorted tumor cells of RCAS-PDGFB-GFP injected mice. Results from microarray analysis. $p<0.05$, Fold change>1.8, *Ptprd*+/+*p16*-/- (n=2), *Ptprd*+/-*p16*-/- (n=2), *Ptprd*-/-*p16*-/- (n=3). (D) Amount of p-STAT3 protein is increased in PTPRD+/-CDKN2A-/- human GBM tumors. Quantification of western blot analysis for p-STAT3 in GBM tumors *$p<0.05$.

Table 2.3 Stat3 gene targets altered in *Ptprd+/-p16-/-* tumor cells.
Average fold change over *Ptprd+/+p16-/-* tumors.

Gene ID	Fold Change
Timp1	15.27
Gadd45g	7.72
Gbp2	7.46
A2m	6.35
Bcl3	6.20
Vim	5.84
Cdkn1a	5.78
Gfap	5.04
Hk2	4.49
Col3a1	4.39
Cebpd	3.57
Gja1	3.41
Socs3	3.22
Myc	2.93
Tap1	2.75
Col1a2	2.57
Zfp36	2.54
Vegfa	2.05
Ccne1	2.03
Junb	2.01
Ptpn2	1.86
Ppargc1a	-3.38

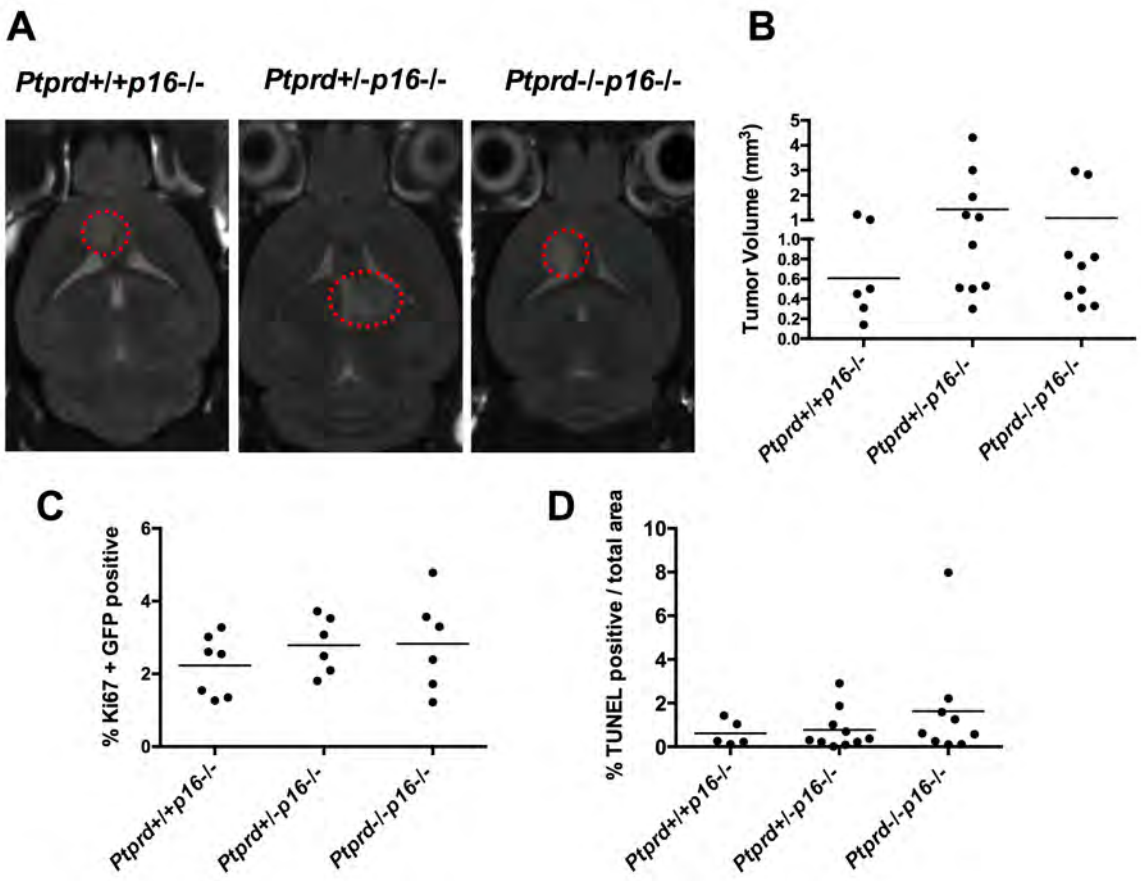

Figure 2.6 *Ptprd* loss does not promote increased cell proliferation. (A) Representative (A) Representative MRI images of *Ptprd+/+p16-/-* (n=6), *Ptprd+/-p16-/-* (n=10), and *Ptprd-/-p16-/-* (n=9) tumors from mice that were stereotactically injected with DF-1 cells expressing RCAS-PDGFB. The presence of a tumor was confirmed by histology. (B) *Ptprd+/-p16-/-* mice show a trend towards having larger tumors (defined as >0.7mm^3). Quantification of tumor size from MRI images. (C) *Ptprd* loss does not increase levels of cell proliferation in gliomas. No significant differences in the levels of Ki67 were observed within the tumor cells of *Ptprd+/+p16-/-* (n=7), *Ptprd+/-p16-/-* (n=6), and *Ptprd-/-p16-/-* (n=6) mice. Ki67 flow cytometry analysis was performed on GFP+ tumor cells from RCAS-PDGFB-GFP tumors. (D) *Ptprd* loss does not alter the levels of cell death in gliomas. Quantification of immunohistochemistry results show that no significant differences in the levels of TUNEL staining were observed in the tumors of stereotactically injected *Ptprd+/+p16-/-* (n=5), *Ptprd+/-p16-/-* (n=10), and *Ptprd-/-p16-/-* (n=9) mice.

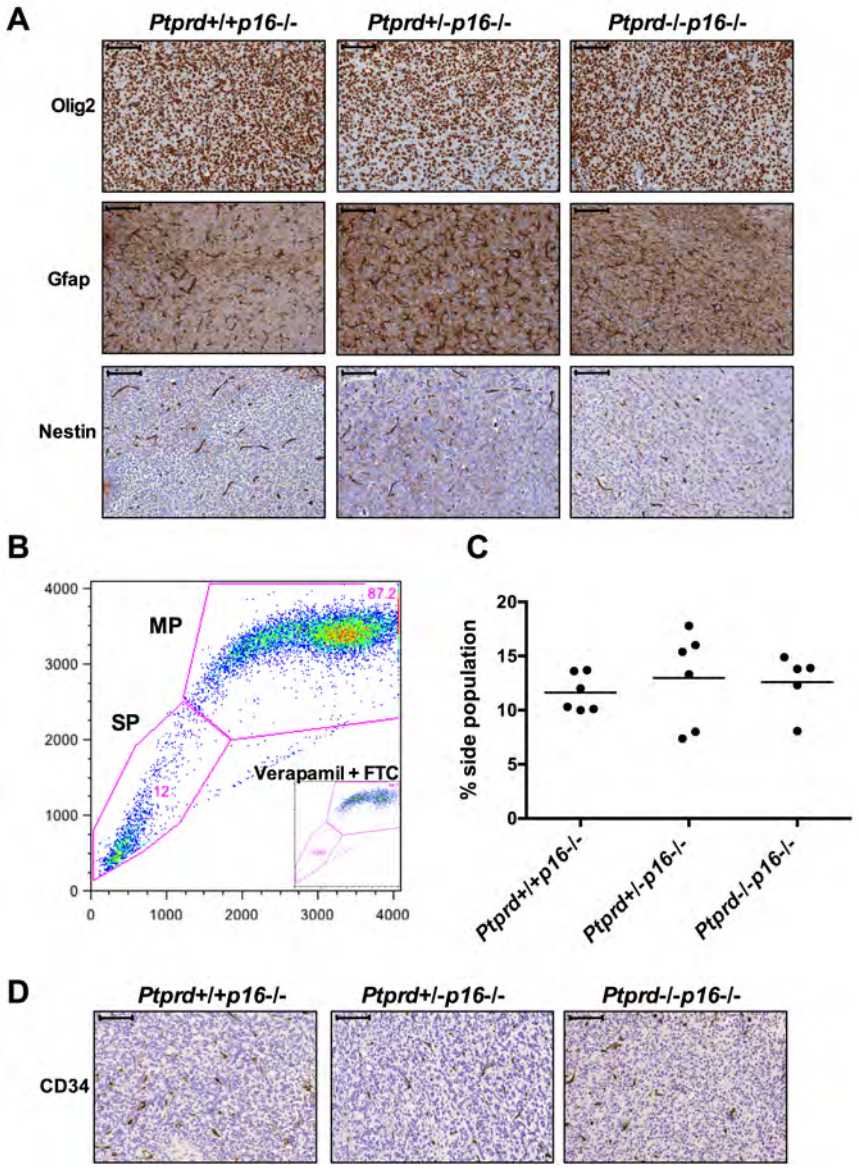

Figure 2.7 *Ptprd* loss does not affect differentiation, the glial stem cell pool, or angiogenesis. (A) Representative images of immunohistochemistry performed on RCAS-PDGFB tumors for Olig2 (oligodendrocytes), GFAP (astrocytes), and Nestin (glial progenitors). Scale bars = 100μM. (B) Representative image of side population analysis (Hoechst 33422 dye exclusion) that was performed on RCAS-PDGFB-GFP tumors. Inset graph, Verapamil and Fumitremorgin c (FTC) ABCG2 transporter inhibitors were applied to the samples tested to set population gates. MP = main population, SP = Side population. (C) Quantification of side population analysis. No differences in the glial stem cell pool were observed. (D) Representative images of immunohistochemistry performed on RCAS PDGFB stereotactically injected tumors for CD34. No differences in vascular density were observed. Scale bars = 100μM.

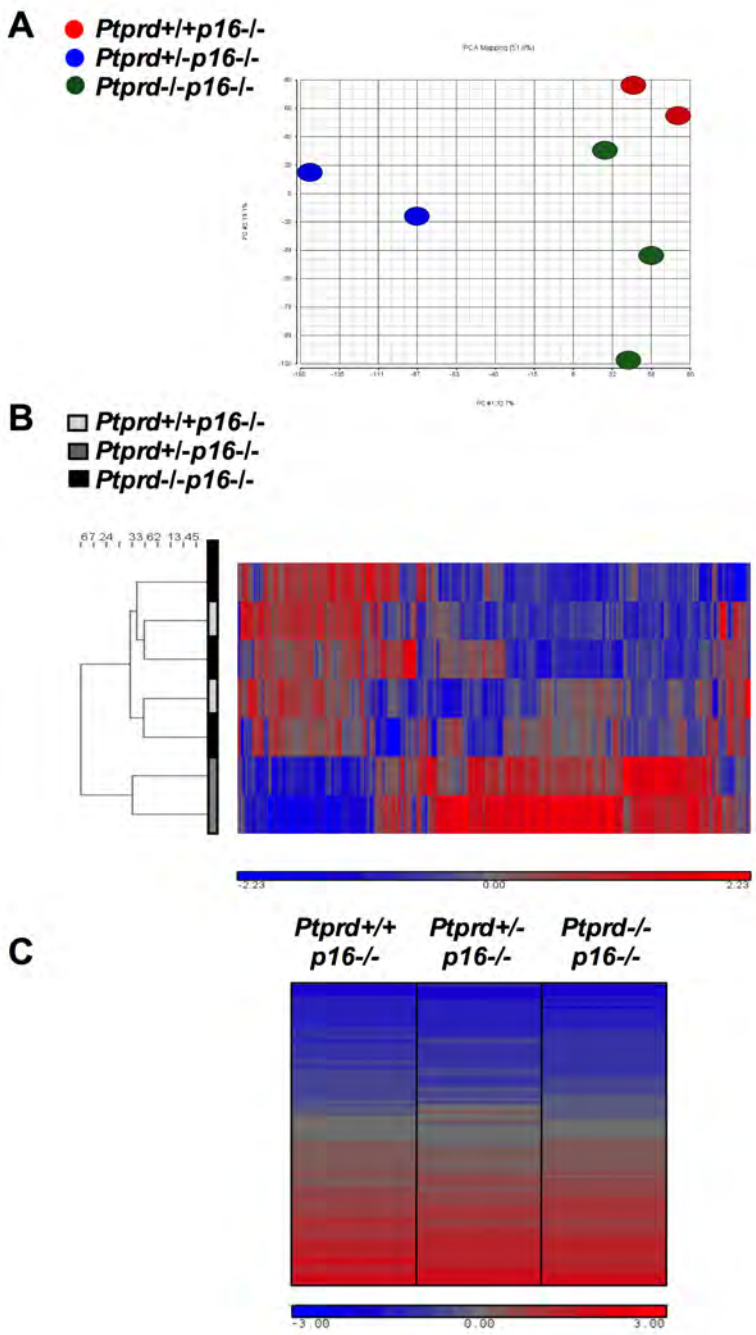

Figure 2.8 Heterozygous *Ptprd* loss leads to distinct gene expression changes. (A) Principal component analysis of expression microarray data from tumors of each genotype. Duplicates represent biological replicates. (B) Hierarchical clustering of expression microarray data from each genotype. Color bar depicts normalized gene expression levels. (C) Heat map of tyrosine phosphatase gene expression from microarray data. Color bar depicts normalized gene expression levels. Average expression of each genotype is shown.

Table 2.4 Tyrosine phosphatase gene expression within *Ptprd*+/+*p16*-/-, *Ptprd*+/-*p16*-/-, and *Ptprd*-/-*p16*-/- tumors.
An average of normalized gene expression values for each genotype are shown.

Gene Symbol	*Ptprd*+/+*p16*-/-	*Ptprd*+/-*p16*-/-	*Ptprd*-/-*p16*-/-
Dusp1	8.98	9.35	9.25
Dusp10	3.60	3.61	3.54
Dusp10	5.97	6.86	6.42
Dusp11	8.63	8.43	8.52
Dusp11	9.31	9.04	9.15
Dusp12	7.24	6.72	7.17
Dusp12	4.77	4.78	4.97
Dusp14	6.24	7.11	6.44
Dusp15	7.65	6.85	7.68
Dusp16	8.32	7.68	8.49
Dusp18	6.82	7.08	6.67
Dusp19	7.78	8.07	8.15
Dusp19	6.90	6.73	7.11
Dusp2	5.03	5.06	5.01
Dusp22	7.16	6.98	7.31
Dusp26	9.51	9.22	9.32
Dusp3	5.87	5.57	5.60
Dusp3	8.46	8.46	8.46
Dusp6	11.13	10.50	11.27
Dusp7	7.73	7.30	7.67
Dusp7	7.39	6.97	7.27
Dusp7	5.35	5.22	5.34
Dusp8	7.09	6.47	7.01
Dusp9	4.03	4.11	4.20
Dusp9	3.69	3.74	3.46
Dusp9	3.40	3.49	3.44
Eya1	5.51	4.75	5.44
Pten	9.16	9.16	9.07
Pten	9.24	8.96	8.96
Pten	10.20	9.97	10.11
Ptpn1	8.62	8.89	8.78

Ptpn1	7.76	7.88	7.82
Ptpn11	4.26	4.30	4.13
Ptpn11	7.27	7.69	7.28
Ptpn11	9.62	9.62	9.43
Ptpn12	10.88	10.59	10.73
Ptpn12	8.10	7.82	7.76
Ptpn12	9.10	8.94	8.85
Ptpn12	10.16	9.89	9.95
Ptpn13	3.58	3.42	3.63
Ptpn13	5.59	6.55	6.32
Ptpn14	4.87	4.87	4.85
Ptpn14	4.42	4.34	4.21
Ptpn18	4.98	5.34	5.09
Ptpn2	8.46	8.90	8.49
Ptpn2	5.19	5.38	5.03
Ptpn2	3.05	3.64	3.28
Ptpn2	8.61	8.84	8.67
Ptpn20	5.29	5.11	5.50
Ptpn21	6.89	6.42	6.85
Ptpn21	6.73	6.54	6.86
Ptpn21	5.47	4.86	5.24
Ptpn22	3.22	3.36	3.41
Ptpn23	6.86	6.69	6.86
Ptpn4	5.20	4.85	4.87
Ptpn5	7.41	7.05	7.44
Ptpn5	4.48	4.21	4.55
Ptpn5	5.81	5.76	5.95
Ptpn6	5.88	6.09	6.10
Ptpn6	3.63	4.06	3.67
Ptpn9	8.51	8.23	8.49
Ptpra	9.81	9.41	9.84
Ptprb	5.24	5.50	4.74
Ptprc	4.08	5.50	4.41
Ptprd	10.68	9.27	9.23
Ptprd	10.83	9.24	9.58
Ptprd	9.64	8.05	8.27

Ptpre	10.19	9.73	9.91
Ptpre	10.56	10.00	10.38
Ptprf	6.72	6.70	6.50
Ptprf	9.43	9.44	9.36
Ptprf	9.47	9.29	9.30
Ptprg	8.18	7.79	8.04
Ptprj	3.34	3.14	3.28
Ptprj	4.16	3.94	4.04
Ptprj	3.97	3.71	3.90
Ptprj	7.50	6.99	7.31
Ptprk	7.29	7.04	7.27
Ptprk	8.61	7.84	8.53
Ptprk	5.14	4.86	4.62
Ptprm	7.76	7.00	7.67
Ptprn	7.43	7.83	7.79
Ptprn2	4.31	4.20	4.39
Ptpro	9.79	9.17	9.72
Ptpro	6.43	5.75	6.04
Ptprr	7.64	6.44	7.46
Ptprs	11.07	10.69	11.05
Ptprs	3.74	3.73	3.91
Ptprs	5.09	4.48	4.96
Ptprt	4.92	4.80	4.84
Ptprt	8.24	7.56	7.81
Ptpru	7.89	7.26	7.82
Ptprv	4.45	4.92	5.04
Rngtt	6.41	6.64	6.43
Rngtt	6.90	6.61	6.76
Styx	3.55	3.65	3.47
Tenc1	5.50	5.97	5.24
Tpte	4.48	4.49	4.51

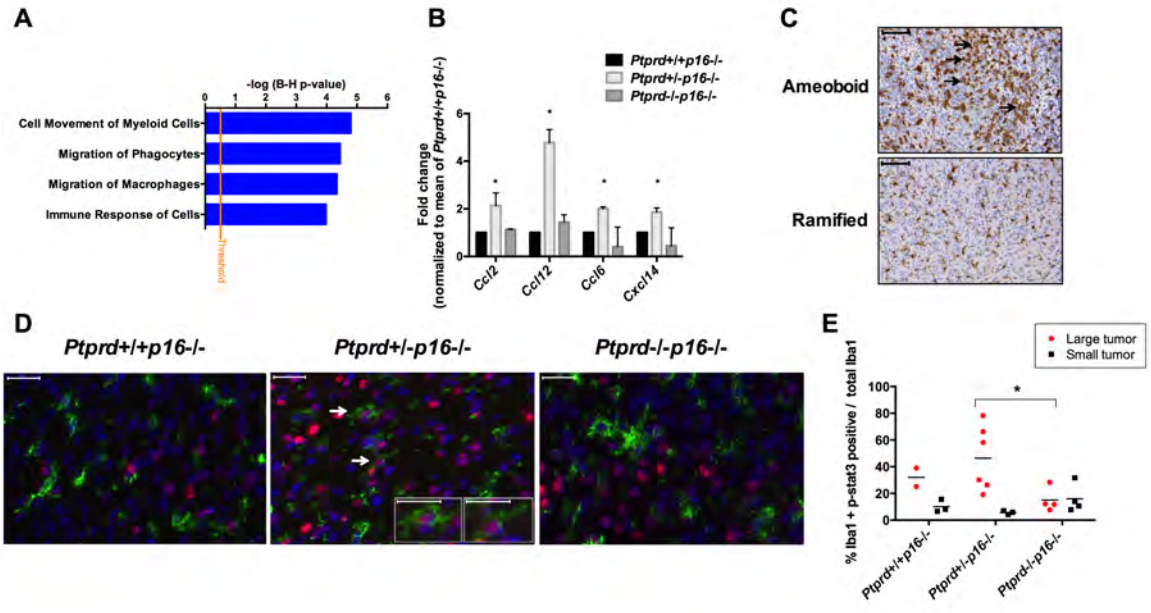

Figure 2.9 Heterozygous loss of *Ptprd* activates immune programs and influences the macrophage response. (A) Immune response gene expression pathways are activated in *Ptprd*+/-*p16*-/- tumors. Gene expression microarray analysis was performed on GFP+ tumor cells from *Ptprd*+/+*p16*-/- (n=2), *Ptprd*+/-*p16*-/- (n=2), and *Ptprd*-/-*p16*-/- (n=3) mice. A selection of the top activated pathways enriched in the differentially expressed genes of *Ptprd*+/-*p16*-/- vs. *Ptprd*+/+*p16*-/- tumors are shown, FDR $p<0.05$. (B) Expression of chemokines that promote M2 polarization of macrophages is increased in *Ptprd*+/-*p16*-/- tumors. Fold change of chemokine expression normalized to mean of *Ptprd*+/+*p16*-/- expression from microarray analysis. Error bars=1 standard deviation. *Ptprd*+/+*p16*-/- (n=2), *Ptprd*+/-*p16*-/- (n=2), and *Ptprd*-/-*p16*-/- (n=3). **Ptprd*+/-*p16*-/- vs. *Ptprd*+/+*p16*-/- $p< 0.05$. (C) Examples of tumors stained with the Iba1 macrophage marker. Arrows indicate locations of amoeboid macrophages. Amoeboid morphology is enriched in large tumors and ramified macrophages mainly occur in smaller tumors (large tumors defined as $>0.7mm^3$ tumor volume). Examples from *Ptprd*+/-*p16*-/- mice (amoeboid) and *Ptprd*+/+*p16*-/- mice (ramified). Scale bars = 100µm. (D) Representative images of Iba1 and p-Stat3 immunofluorescence on tumors from indicated genotypes. Green=Iba1, blue=DAPI, red=p-Stat3. Large image scale bars = 20µm. White arrows indicate cells with nuclear p-Stat3 and cytoplasmic Iba1 and are enlarged in the insets, scale bars = 10µm. (E) *Ptprd*+/-*p16*-/- large tumors have greater p-Stat3 expression in Iba1 positive macrophages. Metamorph quantification of Iba1 and p-Stat3 positive cells, **Ptprd*+/-*p16*-/- *vs. Ptprd*-/-*p16*-/- (large tumors) $p<0.05$.

Table 2.5 Ingenuity Pathway Analysis of *Ptprd+/-p16-/-* tumors.

Category	Predicted Activation State	p-Value	Bias corrected Z-score	Number of Molecules
Immune Cell Trafficking				
migration of macrophages	Increased	4.59E-05	2.8	13
migration of antigen presenting cells	Increased	8.61E-05	2.8	19
migration of phagocytes	Increased	3.60E-05	2.5	27
cell movement of myeloid cells	Increased	1.59E-05	2.0	44
Inflammatory Response				
migration of macrophages	Increased	4.59E-05	2.8	13
migration of phagocytes	Increased	3.60E-05	2.5	27
phagocytosis	Increased	2.11E-05	2.5	28
phagocytosis of cells	Increased	2.70E-05	2.2	26
immune response of cells	Increased	1.05E-04	2.2	29
phagocytosis of tumor cell lines	Increased	3.55E-04	2.0	10
Cell Movement				
migration of macrophages	Increased	4.59E-05	2.8	13
migration of antigen presenting cells	Increased	8.61E-05	2.8	19
migration of phagocytes	Increased	3.60E-05	2.5	27
migration of cells	Increased	8.86E-19	2.3	155
cell movement	Increased	5.32E-20	2.1	170
migration of blood cells	Increased	3.89E-09	2.1	75
invasion of tumor cell lines	Increased	2.06E-15	2.0	68
cell movement of myeloid cells	Increased	1.59E-05	2.0	44

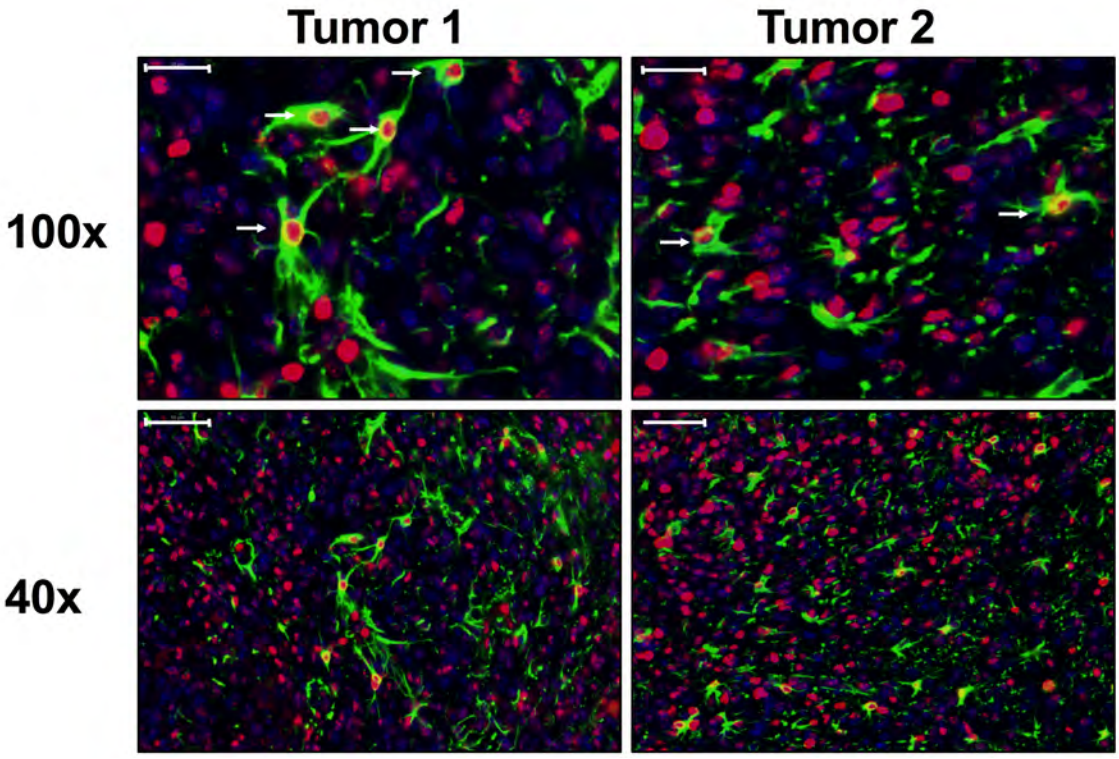

Figure 2.10 Glial cells within *Ptprd+/-p16-/-* tumors express p-Stat3. Co-immunofluorescence of Gfap and p-Stat3 was performed on *Ptprd*+/-*p16*-/- tumors. White arrows point to cells with cytoplasmic Gfap and nuclear p-Stat3. Representative images from two tumors are shown. Top images scale bars = 20μm, lower images scale bars = 50μm.

CHAPTER THREE

Deletion of Ptprd and Cdkn2a cooperate to accelerate tumorigenesis

ABSTRACT

PTPRD encodes the protein tyrosine phosphatase receptor delta and is frequently inactivated across many human cancers. Despite its frequent inactivation, it is unknown whether loss of *PTPRD* promotes tumorigenesis *in vivo*. *PTPRD* is located on chromosome 9p, as is *CDKN2A*, and the two loci are frequently deleted together. Here, we show that co-deletion of *Ptprd* and *Cdkn2a* cooperate to accelerate tumorigenesis. Interestingly, heterozygous loss of *Ptprd* was sufficient to promote tumorigenesis in our model, suggesting that *Ptprd* may be a haploinsufficient tumor suppressor. The loss of *Ptprd* resulted in changes to the tumor spectrum in mice and increased the frequency of lymphomas. In total, we reveal that *Ptprd* is a tumor suppressor that can promote tumorigenesis in concert with *Cdkn2a* loss.

INTRODUCTION

Protein tyrosine phosphatase receptor delta (*PTPRD*) is a tumor suppressor gene on chromosome 9p. *PTPRD* inactivation is common in human malignancies and occurs in a number of cancer types including colorectal, esophageal adenocarcinoma, neuroblastoma, renal cell carcinoma, Ewing sarcoma, chronic myeloid leukemia, squamous cell carcinoma of the vulva, breast, lung cancer, melanoma, and glioblastoma (Brim et al. 2014, Frankel et al. 2014, Boeva et al. 2013, Du et al. 2013, Jiang et al. 2013,

Gerber et al. 2013, Micci et al. 2013, TCGA 2012, Kohno et al. 2010, Solomon et al. 2009, and Veeriah et al. 2009). Despite the high prevalence of *PTPRD* inactivation in human tumors, it is not known whether loss of *PTPRD* directly promotes tumorigenesis *in vivo*.

In humans, *PTPRD* is located on 9p23-24.3 and is telomeric to *CDKN2A*. The *CDKN2A* gene produces the $p16^{Ink4a}$ and $p14/p19^{Arf}$ tumor suppressors (Scherr et al. 2001). We and others have shown that selective pressure exists for inactivation of both genes on chromosome 9p, by deletion or mutation (TCGA 2012, Solomon et al. 2009, Veeriah et al. 2009, and Beroukhim et al. 2010). Despite the potential role of *PTPRD* loss in cancer, *Ptprd* deficient mice do not spontaneously develop tumors (Uetani et al. 2000). In contrast, 69% of *Cdkn2a-/-* mice develop tumors at an average age of 29 weeks (Serrano et al. 1996). We generated *Ptprd/Cdkn2a* co-deleted mice to determine if *Ptprd* loss contributes to tumorigenesis.

Here, we report that in the absence of *Cdkn2a*, *Ptprd* loss results in accelerated tumor development compared to mice lacking *Cdkn2a* alone. Both heterozygous and homozygous deletion of *Ptprd* accelerated tumorigenesis suggesting that loss of one copy of *Ptprd* is sufficient to act on tumor initiation or growth. Furthermore, loss of *Ptprd* changed the tumor spectrum, resulting in greater frequencies of aggressive lymphomas and histiocytic sarcomas. Our data show that *Ptprd* loss contributes to tumorigenesis in the setting of *Cdkn2a* deletion.

RESULTS

Genetic patterns of *PTPRD* loss in cancer

We reviewed several genomic studies to define patterns of *PTPRD* loss in cancer. As shown in Figure 3.1A, *PTPRD* inactivation via deletion or mutation occurs frequently. In tumors with *PTPRD* copy number loss, loss of one copy of *PTPRD* occurs most commonly (Figure 3.1A). Moreover, co-deletion of *PTPRD* and *CDKN2A* occurs across a number of cancer types (Figure 3.1B). Co-occurrence of *PTPRD* and *CDKN2A* loss is significant across cancers (Figure 3.1B, $p<0.05$, $5 >$ Odds Ratio < 707, Table 3.1).

Ptprd loss cooperates with *Cdkn2a* deletion to promote tumorigenesis.

To investigate the role of *Ptprd* loss in tumorigenesis, we generated mice with loss of *Ptprd* alone, *Cdkn2a*, or both, and determined disease-free survival in each genotype (Figure 3.2A). Mice were euthanized and necropsied at the time of onset of clinical signs (hunched, sick, showing a swollen abdomen, or palpable lumps) or at a pre-determined endpoint. In accordance with Uetani et al. (2000), we did not observe tumor development in *Ptprd*+/- and *Ptprd*-/- mice (Figure 3.2A). However interestingly, *Ptprd*+/-*Cdkn2a*-/- and *Ptprd*-/-*Cdkn2a*-/- had significantly worse survival times than *Ptprd*+/+*Cdkn2a*-/- mice (Figure 3.2A, $p<0.0001$). These data suggest that *Ptprd* loss alone is not sufficient to initiate tumorigenesis but that in the context of *Cdkn2a* loss, *Ptprd* loss can cooperate to accelerate tumor development.

The results in Figure 3.2A suggest that loss of only one allele of *Ptprd* is sufficient to produce a phenotypic effect. In order to determine whether *Ptprd*+/- tumors retained an

intact wild-type allele, we extracted DNA from tumors (histiocytic sarcoma) in *Ptprd*+/-*Cdkn2a*-/- mice and characterrized *Ptprd* gene status using PCR. As shown in Figure 3.2B, tumors from *Ptprd*+/-*Cdkn2a*-/- mice retain an intact wild-type allele. As a control we extracted matched normal DNA (Figure 3.2C). Our results demonstrate that *Ptprd* loss and *Cdkn2a* deletion cooperate to promote tumorigenesis, and that heterozygous loss of *Ptprd* is sufficient to achieve this effect.

Deletion of *Ptprd* and *Cdkn2a* alters the tumor spectrum

In order to determine why mice with *Ptprd* loss had a faster onset of clinical signs, we first examined whether mice with *Ptprd* and *Cdkn2a* deletion had a greater number of tumor types compared to mice with *Cdkn2a* deletion alone. As shown in Figure 3.3A, no significant increases in the number of tumor types were observed in mice with *Ptprd* loss. In fact, mice with *Ptprd* loss tended to have fewer types of tumors.

We next determined whether *Ptprd* and *Cdkn2a* deletion altered the resultant tumor spectrum. Interestingly, *Ptprd*-/-*Cdkn2a*-/- mice developed significantly more lymphomas than *Ptprd*+/+*Cdkn2a*-/- mice (Figure 3.3B, $p<0.05$). In addition, *Ptprd*+/-*Cdkn2a*-/- mice showed a trend toward developing more lymphomas than *Ptprd*+/+*Cdkn2a*-/- mice (Figure 3.3B). Figure 3.4A and 3.4B shows examples of hematoxylin and eosin stained lymphomas in the mesenteric lymph node and small intestine, respectively. These tumors were composed of sheets of discrete round cells with scant basophilic cytoplasm and large round to polygonal nuclei. The neoplastic infiltrates often effaced normal tissue architecture, particularly within the lymph nodes

(Figure 3.4A). In order to determine the cell origin of the lymphomas, we stained the tumors for B220, a B-cell marker, and CD3, a T-cell marker (Figure 3.4A, 3.4B). As listed in Table 3.2, all *Ptprd+/-Cdkn2a-/-* lymphomas were of a B-cell origin. Interestingly, 2/3 of the *Ptprd-/-Cdkn2a-/-* tumors were of T-cell origin (Table 3.2, Figure 3.4B). In order to quantitate the proliferative index of lymphoma cells, mesenteric lymph nodes from age-matched (28-39 weeks old) mice with or without lymphoma were stained for Ki67. Lymphomas from *Ptprd+/-Cdkn2a-/-* mice and *Ptprd-/-Cdkn2a-/-* mice had increased Ki67 staining, confirming the proliferative nature of the lymphomas (Figure 3.4C). Lymphomas from *Ptprd+/-Cdkn2a-/-* and *Ptprd-/-Cdkn2a-/-* mice had similar levels of Ki67 staining. Our results indicate that loss of *Ptprd* in *Cdkn2a* null mice promotes the development of lymphomas.

We observed that mice also developed either histiocytic sarcomas or soft tissue sarcomas (Table 3.2). Histiocytic sarcomas were composed of sheets of discrete round cells with moderate amounts of amphophilic cytoplasm and large round to polygonal nuclei. Within the liver, these cells frequently dissected between hepatic cords and regionally effaced normal tissue architecture (Figure 3.5A, *left*). Neoplastic cells were also frequently found within hepatic blood vessels (Figure 3.5A, *middle*). The cells stained positively with Mac2 consistent with histiocytic cell origin (Figure 3.5A, *right*). Soft tissue sarcomas (fibrosarcomas) were composed of streams, broad interlacing bundles, and frequent herringbone displays of spindle-shaped cells having moderate amounts of eosinophilic, fine fibrillar cytoplasm, poorly demarcated cell margins, and large oval to elongate nuclei. Within the skeletal muscle, these cells dissected between and frequently effaced

myocytes (figure 3.5B). While mice of all genotypes developed a similar frequency of sarcoma, it was interesting that *Ptprd-/-Cdkn2a-/-* mice developed significantly more histiocytic sarcomas than soft tissue sarcomas, suggesting that loss of both copies of *Ptprd* can preferentially promote the development of cancers with hematopoietic origin. (Figure 3.3B, $p<0.05$).

We assessed levels of proliferation, apoptosis, and angiogenesis in the histiocytic and soft tissue sarcomas in *Cdkn2a*-/- mice with varying *Ptprd* genotype. All genotypes displayed positive staining for Ki67, TUNEL, and CD34, suggesting that loss of a single copy of *Ptprd* is sufficient to achieve tumor proliferation, apoptosis, and angiogenesis respectively (Figure 3.5C). No significant differences in the intensity or quantity of staining of Ki67, TUNEL, or CD34 were observed (Figure 3.5C, Table 3.3). Since it was previously shown that p-Stat3 is a substrate of PTPRD, we measured the levels of p-Stat3 by immunohistochemistry. No significant differences in the levels of p-Stat3 were observed, suggesting that Ptprd may have other substrates that mediate its tumor suppressive function in these tumor types (Figure 3.5C, Table 3.3).

MATERIALS AND METHODS

Genetic Analysis of Human Tumors

The frequency of *PTPRD* inactivation and the co-occurrence of *PTPRD* and *CDKN2A* deletion were identified using genomic data in the cBio Portal (Cerami et al. 2012).

Generation of Mice

Ptprd heterozygous mice (Uetani et al. 2000) were crossed to *Cdkn2a* knockout mice (Serrano et al. 1996). Mice were in a C57/Bl6 background. Mice were monitored twice a week and had complete necropsy performed if hunched, sick, or showing a swollen abdomen or palpable lumps. Mice with *Cdkn2a* deletion were monitored until 52 weeks. Wild-type and mice with *Ptprd* loss alone were monitored for 104 weeks. Mice experiments were performed with MSKCC Institutional Animal Care and Use Committee approval.

Histology and Pathology

The following tissues were dissected, fixed in 10% formalin (Sigma), and embedded in paraffin: heart, thymus, lung, tracheal/mandibular/mesenteric lymph nodes, kidneys, liver, pancreas, spleen, gall bladder, intestines, stomach, skin, urinary bladder, uterus/cervix/vagina/ovaries or testes/epdididymis/prostate/seminal vesicles, bone marrow, vertebral column, femur/tibia/surrounding muscles, sternum, eyes, tongue, teeth, salivary glands, adrenals, thyroid, esophagus, trachea, oral-nasal cavity, olfactory bulbs, brain, ear, pituitary, and thalamus. 5μM sections were stained with hematoxylin and eosin (H&E) and reviewed by a board-certified veterinary pathologist.

Tumor Genotyping

Liver histiocytic sarcoma was macrodissected and DNA was extracted using the DNeasy Blood and Tissue kit (Qiagen). Tumors were confirmed by histological analysis. DNA from ear tissue was extracted as a normal tissue control. PCR was performed with the

following *Ptprd* genotyping primers: 5'GGTGAAGTGTGACCAGTATTGGCC3', 5'CTGGAATTGTCTCACTTTCCTC3', 5'GACTGCCTTGGGAAAAGCGCCTCC3'. Standard PCR procedures were performed with the following reaction buffer: 1M$(NH_4)_2SO_4$, 2M Tris, pH 8.8, 1M $MgCl_2$, and 14.4M B-mercaptoethanol.

Immunohistochemistry

Dissected tissues were fixed in 10% formalin and embedded in paraffin. 5μM sections were used for immunohistochemical analysis. The Leica Bond RX automated system (Leica Biosystems) was used with the Polymer Refine Detection System (Leica Biosystems) for the following antibodies: B220 (BD Biosciences cat. no. 550286, mouse monoclonal, 1:200), CD3 (Vector, cat. no. VP-RM01, rabbit monoclonal, 1:100), Ki67 (Abcam, cat. no. ab16667, rabbit monoclonal, 1:100), and CD34 (Abcam, cat. no. ab8158, rat monoclonal, 16μg/mL). The Mac-2 (Cedarlane, cat.no. CL8942B, mouse monoclonal biotinylated) staining was performed manually with 10mM citrate retrieval for 30 minutes and the standard avidin/biotin immunoperoxidase protocol. For p-Stat3 immunohistochemistry, tissue sections were blocked in 10% goat serum with 2% BSA in PBS. Primary p-Stat3 Tyr-705 (Cell Signaling, cat no. 9145, rabbit monoclonal, 0.5μg/mL) antibody was incubated for 5 hours, followed by a 60 minute incubation with biotinylated goat anti-rabbit IgG (Vector Labs, cat. no. PK6101, 1:200 dilution) according to the manufacturer's instructions. Detection was performed with Blocker D, Streptavidin-HRP and DAB kit (Ventana Medical Systems) according to the manufacturer's instructions. Slides were counterstained with hematoxylin and coverslipped with Permount (Fisher Scientific). TUNEL staining was performed with the

following reaction mixture: 0.1M Sodium Cacodylate pH7, 0.1mM DTT, 0.05mg/mL bovine serum albumin, 2u/ul terminal transferase, 0.2nm Biotin-16-dUTP, and 2.5mM Cobalt Chloride for 1 hour at 37 degrees. The reaction was terminated with 300mM sodium chloride and 30mM sodium citrate at room temperature for 15 minutes, incubated in avidin-biotin for 30 minutes, and developed with 3,3'-Diaminobenzidine for 3 minutes.

Immunostaining Image Analysis

Whole slides were scanned with Pannoramic Flash Scanner (3DHistech, Hungary). Image analysis of tumor areas was performed with Metamorph software (Molecular Devices, PA). For analysis of immunohistochemistry images, color thresholds were set for brown positive staining and for total area (brown staining + blue nuclei).

Statistical Analysis

Unless noted, student's t-test was performed for all statistical analysis. Log-rank statistical analysis was performed for Kaplan-Meier curves. Fisher's exact test was performed for the tumor spectrum analysis.

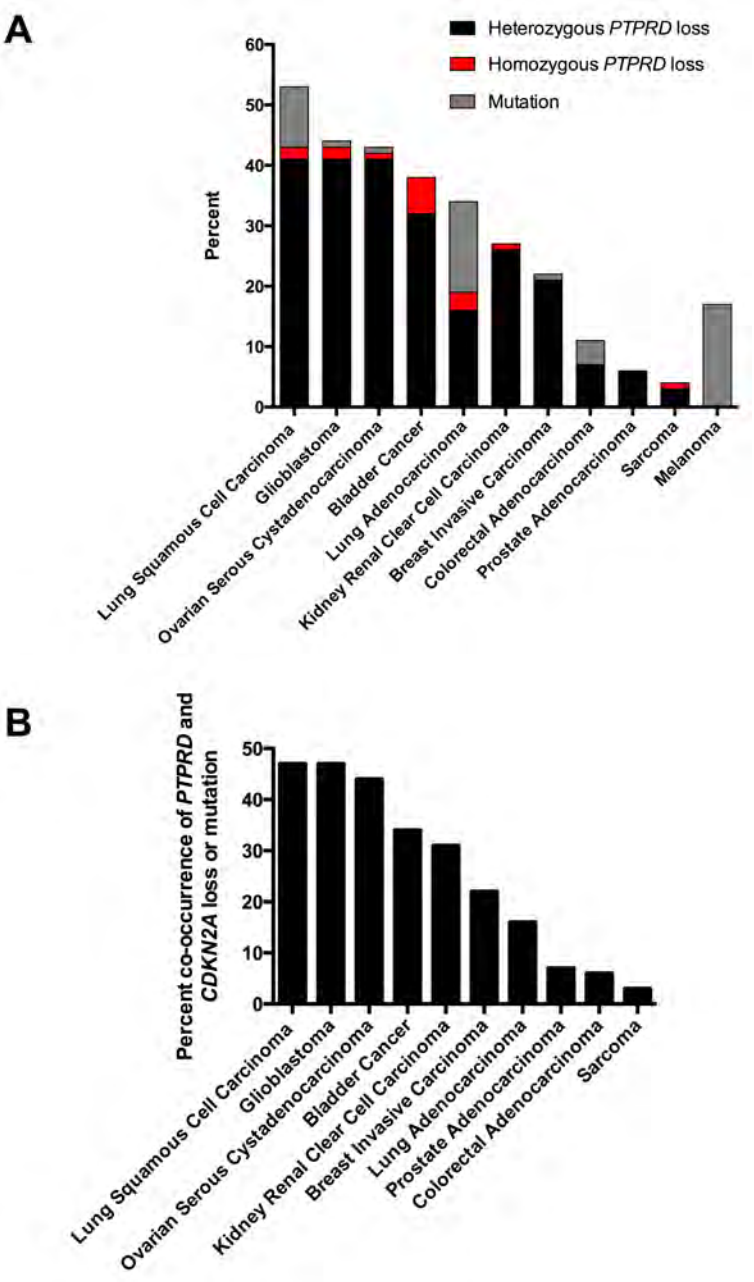

Figure 3.1 Genetic patterns of *PTPRD* loss in human cancers. (A) Histogram of the frequency of mutation and copy number loss of *PTPRD* in human cancers. Point mutations, heterozygous loss, and homozygous deletions are presented. Data from the cBio Portal. (B) Histogram of the frequency of *PTPRD* and *CDKN2A* inactivation (mutation and deletion) in human cancers. Data from the cBio Portal.
Ortiz, B., White, J.R., Wu, W.H., Chan T.A. (2014) Deletion of *Ptprd* and *Cdkn2a* cooperate to accelerate tumorigenesis. *Oncotarget*. In press.

Table 3.1 Co-occurrence of *PTPRD* and *CDKN2A* inactivation in human cancers

	PTPRD and CDKN2A inactivation	Total # Samples	Percent co-occurance	Odds Ratio	95% confidence interval	p-value	Study
Clear Cell Renal Cell Carcinoma	129	418	31	707	236.8-2110.5	0	TCGA 2013
Ovarian Serous Cystadenocarcinoma	139	316	44	119	53.2-264.2	0	TCGA 2011
Glioblastoma	127	273	47	92	12.5-678.2	0	Brennan et al. 2013
Breast	105	482	22	88	45.1-170.4	0	TCGA 2012
Prostate	7	103	7	51	8.7-303.1	0.000003	Taylor et al. 2010
Colorectal Adenocarcinoma	12	212	6	34	9.7-116.8	0	TCGA 2012
Bladder	33	97	34	29	9.1-89.8	0	Iyer et al. 2013
Lung squamous Cell Carcinoma	84	178	47	23	8.3-61	0	TCGA 2012
Sarcoma	7	207	3	16	3.9-66.2	0.0001	Barretina et. al 2010
Lung adenocarcinoma	30	182	16	5	2.4-9.3	0.000007	Imielinski et al. 2012

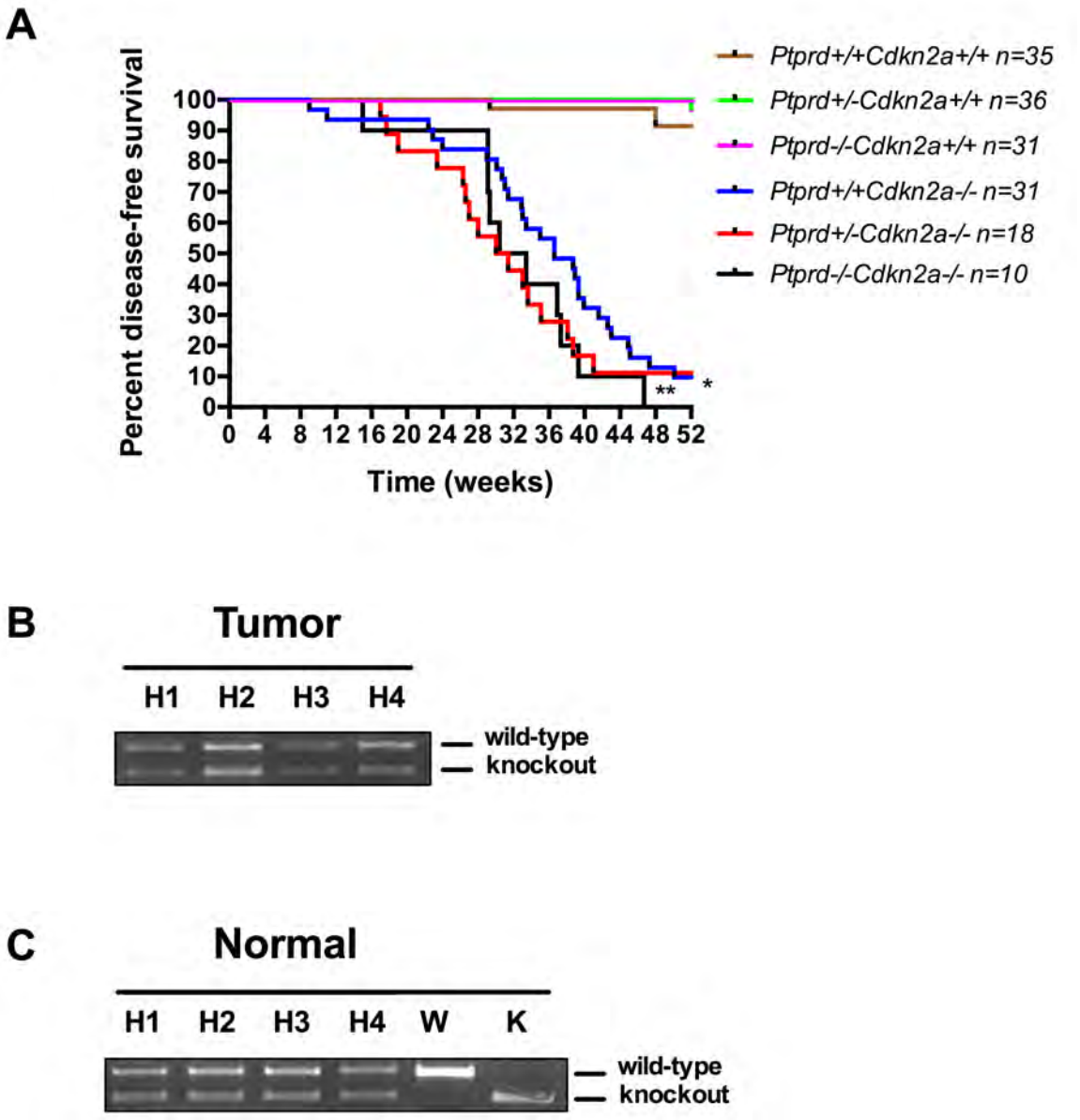

Figure 3.2 *Ptprd* loss cooperates with *Cdkn2a* deletion to promote tumorigenesis. (A) Kaplan-Meier survival curve of *Ptprd+/+Cdkn2a+/+* (n=35), *Ptprd+/-Cdkn2a+/+* (n=36), *Ptprd-/-Cdkn2a+/+* (n=31), *Ptprd+/+Cdkn2a-/-* (n=31), *Ptprd+/-Cdkn2a-/-* (n=18), *and Ptprd-/-Cdkn2a-/-* (n=10) mice followed for 52 weeks. **Ptprd+/-Cdkn2a-/-* vs. *Ptprd+/+Cdkn2a-/-* and ** *Ptprd-/-Cdkn2a-/-* vs. *Ptprd+/+Cdkn2a-/-,* p-value < 0.0001. (B) PCR genotyping of tumor tissue (histiocytic sarcoma) and (C) normal tissue for *Ptprd.* Tumors from *Ptprd+/-Cdkn2a-/-* mice retain an intact wild-type *Ptprd* allele. H = *Ptprd+/-Cdkn2a-/-*, W = *Ptprd+/+* control, K = *Ptprd-/-* control.

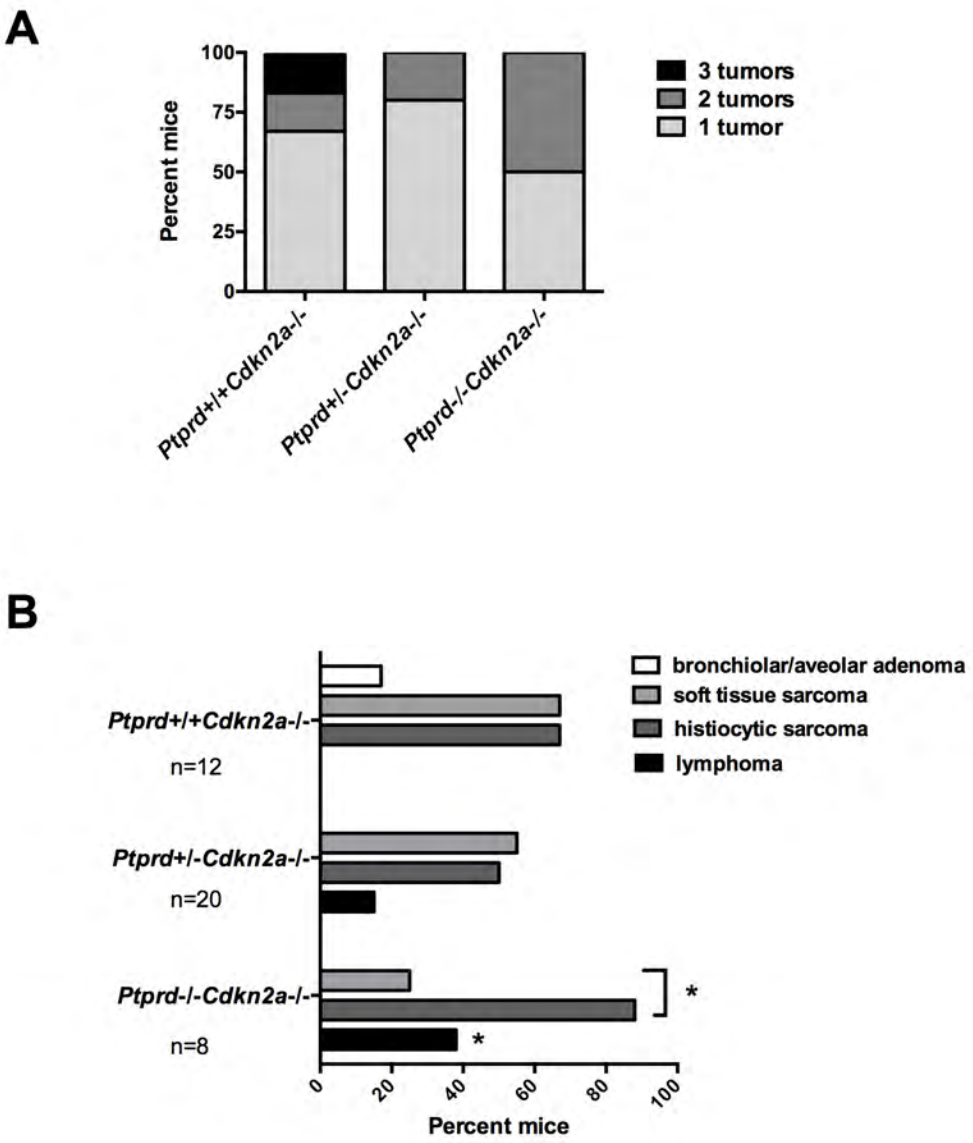

Figure 3.3 Mice with *Ptprd* loss and *Cdkn2a* deletion develop lymphomas, histiocytic sarcomas, and soft tissue sarcomas. (A) Number of tumor types (lymphoma, histiocytic sarcoma, soft tissue sarcoma, or bronchiolar/alveolar carcinoma) per mouse of each genotype. (B) Frequency of tumor types by genotype. *Ptprd+/+Cdkn2a-/-* (n= 12), *Ptprd+/-Cdkn2a-/-* (n=20), and *Ptprd-/-Cdkn2a-/-* (n=8) mice. **Ptprd-/-Cdkn2a-/-* vs. *Ptprd+/+Cdkn2a9-/-* lymphomas $p<0.05$; * with bracket, *Ptprd-/-Cdkn2a-/-* histiocytic sarcomas vs. soft tissue sarcoma $p<0.05$.

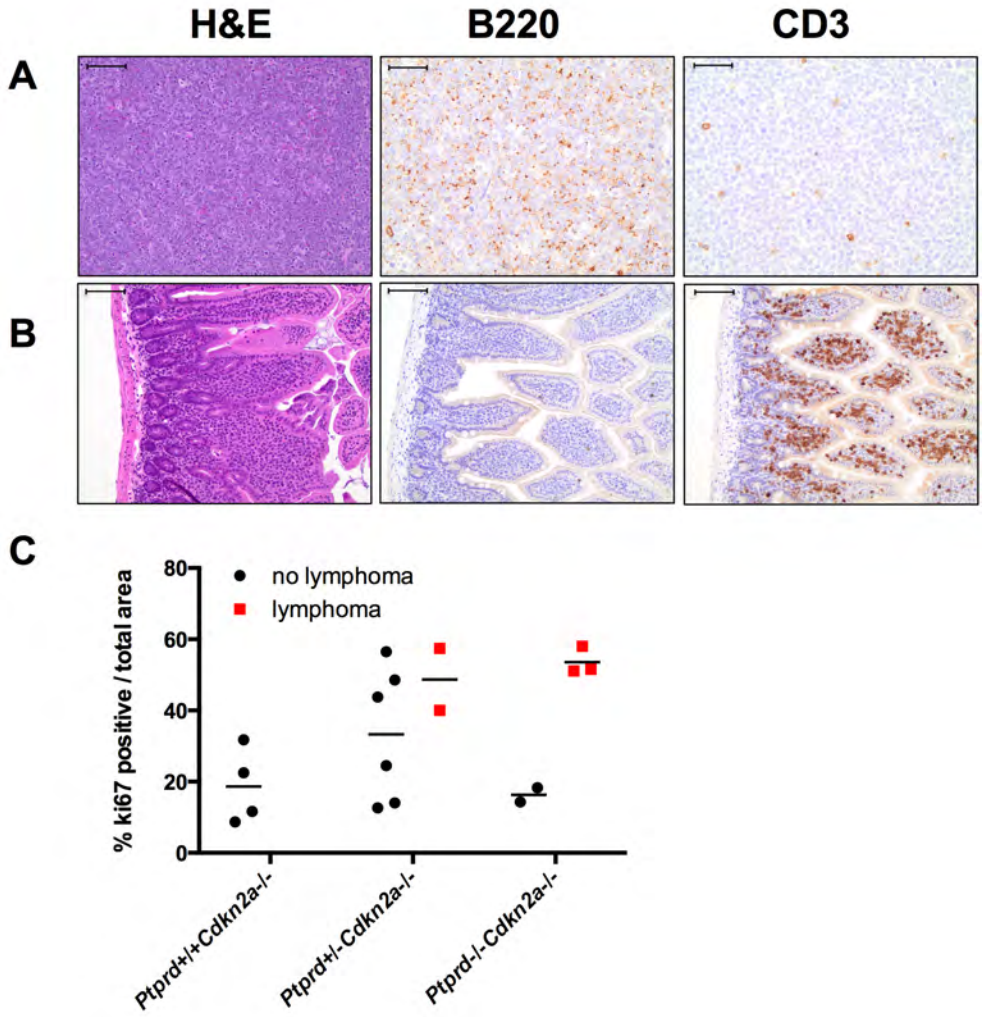

Figure 3.4 Lymphomas in mice with *Ptprd* and *Cdkn2a* loss. (A) Representative images of *Ptprd*+/-*Cdkn2a*-/- B-cell lymphoma in a mesenteric lymph node. Left, scale bar = 100μm; Middle, B220 staining is used to identify B-cells, scale bar = 50μm, Right, CD3 staining is used to identify T-cells, scale bar = 50μm. (B) Representative images of *Ptprd*-/-*Cdkn2a*-/- T-cell lymphoma in the small intestine. Left, scale bar = 100μm; Middle, B220 staining, scale bar = 100μm, Right, CD3 staining, scale bar = 100μm. (C) Lymphomas in *Ptprd*+/- or *Ptprd*-/- mice have similar proliferative indices. Age-matched mesenteric lymph nodes with and without lymphoma were stained with Ki67 by immunohistochemistry.

Table 3.2 Tumors in mice with *Ptprd* loss and *Cdkn2a* deletion.

***Ptprd*+/+*Cdkn2a*-/-**				
Mouse ID	**Sex**	**Age**	**Diagnosis**	**Sites**
1	F	33	Soft Tissue Sarcoma	abdominal mass
2	F	43	Histiocytic Sarcoma	bone marrow, liver, lymph nodes (mesenteric), mesentery, ovaries, pancreas, small intestine, spleen, uterus
3	M	37	Histiocytic Sarcoma	bone marrow, liver, spleen
4	M	11	Histiocytic Sarcoma Soft Tissue Sarcoma Bronchiolar/alveolar adenoma	spleen, lung perirectal mass lung
5	M	45	Histiocytic Sarcoma Soft Tissue Sarcoma Bronchiolar/alveolar carcinoma	bone marrow, brown fat, kidney, liver, lung, lymph nodes (mandibular, mesenteric, tracheobronchial), spleen, stomach, urinary bladder liver lung
6	F	43	Histiocytic Sarcoma	duodenum, liver, lungs, lymph nodes, ovaries, oviduct, spleen, uterus
7	M	30	Histiocytic Sarcoma	bone marrow, kidney, liver, lung, lymph nodes (mandibular, mesenteric), spleen, thymus
8	F	31	Soft Tissue Sarcoma	flank skin
9	M	39	Histiocytic Sarcoma Soft Tissue Sarcoma	blood vessels (renal, meningeal, and brain), liver, lungs, lymph nodes (mandibular, mediastinal, mesenteric), spleen, thymus soft tissues of right head and neck
10	F	33	Histiocytic Sarcoma	bone marrow, cecum, colon, connective tissue (mesenteric and paraovarian), lymph nodes (submandibular), ovaries,

			Soft tissue Sarcoma	oviduct, thymus, uterus axillary subcutis, connective tissue, lymph nodes (axillary), mammary gland, skeletal muscle, spinal cord/dura, vertebrae
11	M	22	Soft Tissue Sarcoma	subcutis dorsal neck
12	M	33	Soft Tissue Sarcoma	haired skin
Ptprd+/-Cdkn2a-/-				
13	F	27	Histiocytic Sarcoma Soft Tissue Sarcoma	bone marrow, liver, lymph node (mesenteric), oviducts lower back mass
14	M	28	Histiocytic Sarcoma Soft Tissue Sarcoma	bone marrow, liver vertebra, lungs, liver
15	F	33	Histiocytic Sarcoma	lymph nodes (mandibular, mesenteric), spleen, thymus
16	M	17	Soft Tissue Sarcoma	left flank mass
17	M	19	B-cell Lymphoma	adipose tissue (perivertebral, periadrenal), eye, haired skin, kidney, liver, lungs, lymph nodes, parotid salivary gland, prostate gland, spleen, stomach, thymus
18	M	41	Histiocytic Sarcoma	bone marrow, kidney, liver, lymph nodes (mesenteric), skin, spleen
19	M	28	B-cell Lymphoma	liver, lymph nodes (mandibular, mediastinal, mesenteric) pancreas, spleen, subcutaneous tissues
20	F	34	Histiocytic Sarcoma B-cell Lymphoma	oviduct, uterus lymph nodes (mandibular, mediastinal, mesenteric), oviduct, pancreas, spleen
21	M	18	Soft Tisssue Sarcoma	kidney, lumbar, lymph nodes (renal), pelvic mass

22	M	38	Histiocytic sarcoma	bone marrow, liver, lymph nodes, spleen
23	F	28	Soft Tissue Sarcoma	leg mass
24	M	21	Soft Tissue Sarcoma	left shoulder mass, lymph nodes
25	M	31	Histiocytic Sarcoma Soft Tissue Sarcoma	adipose tissue (parasternal), kidneys, liver, lungs, lymph nodes (mandibular, mesenteric), spleen left thigh mass
26	F	39	Histiocytic Sarcoma	bone marrow, cervix, liver, lymph nodes (mesenteric), ovaries, thymus, uterus, vagina
27	M	30	Histiocytic Sarcoma	bone marrow, liver, lung, lymph nodes (mandibular, mesenteric), spleen, thymus
28	M	30	Histiocytic sarcoma	liver, lung, lymph nodes (tracheobronchial), spleen, thymus
29	M	28	Soft Tissue Sarcoma	subcutaneous abdominal mass
30	M	6	Soft Tissue Sarcoma	retobullar/subcutaneous mass
31	M	19	Soft Tissue Sarcoma	left flank mass
32	M	31	Soft Tissue Sarcoma	sublumbar soft tissues
Ptprd-/-Cdkn2a-/-				
33	F	37	Histiocytic Sarcoma T-cell Lymphoma	liver, lymph nodes (mesenteric, pancreatic), ovaries, pancreas, stomach, uterus muzzle (skeletal muscle, bone, subcutis)
34	F	39	Histiocytic Sarcoma	bone marrow, blood vessels, liver, lungs, lymph nodes (mandibular, mesenteric, tracheobronchial, mesovarium, ovary, spleen, uterus
35	M	37	Histiocytic Sarcoma	adipose tissue (brain, pervetrebral), blood vessels of kidneys, liver, lungs, mediastinal tissue/thymis

36	F	33	Histiocytic Sarcoma	broad ligament of mesovarium and uterus, kidney, liver, lymph nodes (pancreatic and renal), ovaries, pancreas, spleen
37	F	39	Histiocytic Sarcoma T-cell Lymphoma	bone marrow, kidneys, liver, lungs, lymph nodes (inguinal, mandibular, mesenteric), ovaries, small intestine, sternum, stomach, uterus small intestine, spleen
38	M	29.1	Soft Tissue Sarcoma	thoracic mass
39	F	29.3	Histiocytic Sarcoma B-cell Lymphoma	adipose tissue (mesenteric), adrenal glands, bone marrow, kidneys, liver, ovaries, pancreas, small intestine, spleen, stomach, uterus lungs, lymph nodes (axillary, inguinal, mandibular), thymus
40	F	46.7	Histiocytic Sarcoma Soft Tissue Sarcoma	bone marrow, intestines, liver, mesentery, ovaries, pancreas, urinary bladder, uterus right stifle

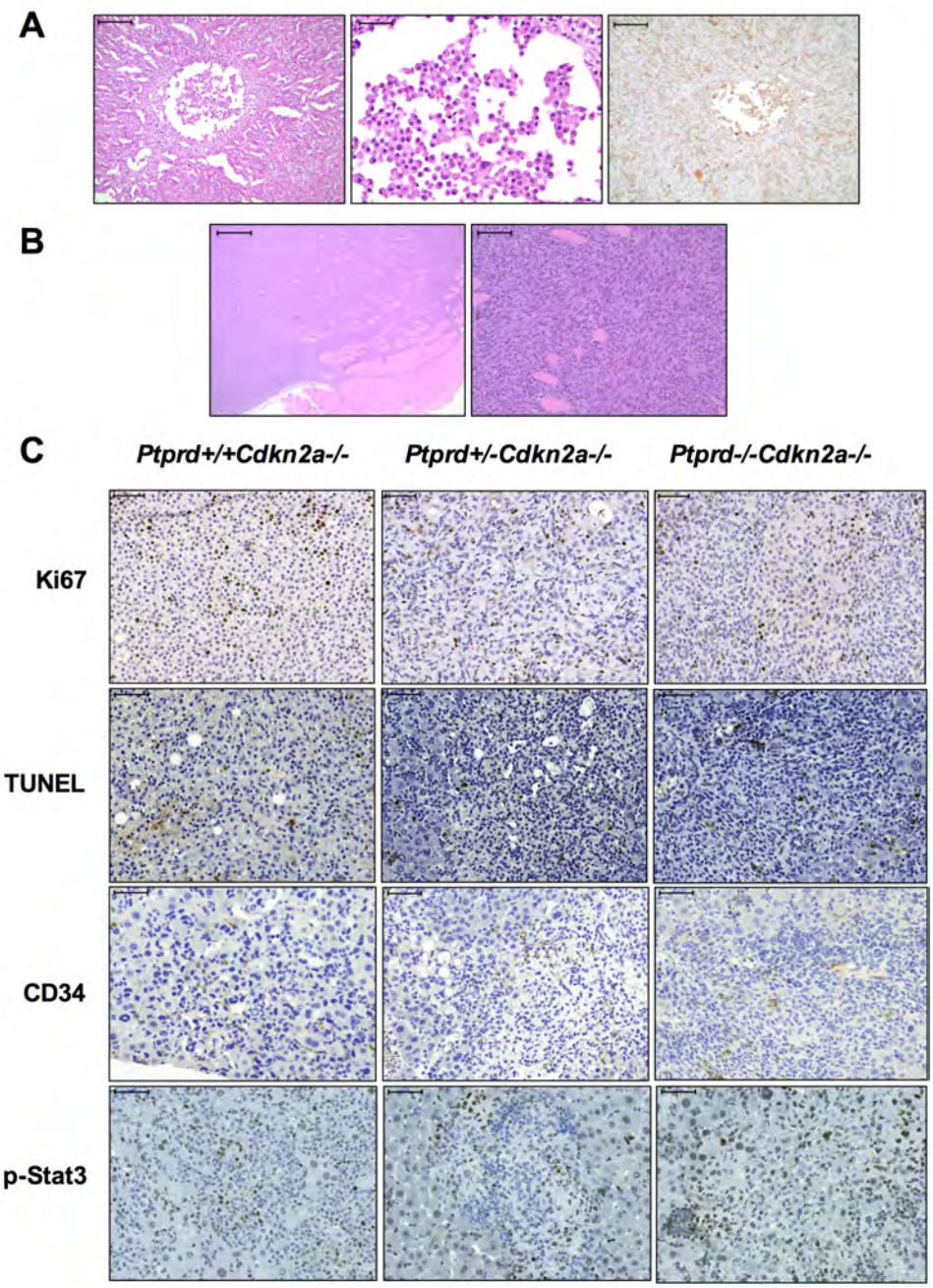

Figure 3.5 Histiocytic sarcomas and soft tissue sarcomas from mice with *Ptprd* and *Cdkn2a* deletion (A) Representative images of histiocytic sarcoma. Left, H&E staining of *Ptprd+/+Cdkn2a-/-* liver histiocytic sarcoma. Left, scale bar = 200μm. Middle, higher magnification of left image with scale bar = 50μm. Right, Mac-2 staining of *Ptprd+/+Cdkn2a-/-* liver histiocytic sarcoma with scale bar = 200μm. (B) Representative images of soft tissue sarcoma. Left, H&E staining of *Ptprd+/-Cdkn2a-/-* fibrosarcoma with scale bar = 500μm. Right, higher magnification of left image with scale bar = 100μm. (C) Representative images of *Ptprd+/+Cdkn2a-/-, Ptprd+/-Cdkn2a-/-,* and *Ptprd-/-Cdkn2a-/-* histiocytic sarcomas stained with Ki67, TUNEL, CD34, and p-Stat3. Scale bars = 50μm.

Table 3.3 Quantification of immunohistochemistry analysis of histiocytic sarcoma tumors in mice with *Ptprd* loss and *Cdkn2a* deletion

IHC Marker	*Ptprd+/+Cdkn2a-/-*	*Ptprd+/-Cdkn2a-/-*	*Ptprd-/-Cdkn2a-/-*
Ki67	32.7 ± 4.7	38.3 ± 4.7	34.2 ± 5.3
CD34	6.0 ± 5.1	6.1 ± 1.7	7.3 ± 0.9
TUNEL	2.6 ± 1.4	4.5 ± 1.5	8.4 ± 8.6
p-Stat3	29.4 ± 2.3	29.8 ± 26.2	23.5 ± 7.4

Values shown are % positive / total area ± standard deviation. No significant differences were observed between genotypes.

CHAPTER FOUR

Prohibitin is a potential substrate of PTPRD

ABSTRACT

PTPRD is a tumor suppressor that is frequently inactivated in several cancers. Our lab previously showed that p-Stat3 is de-phosphorylated by PTPRD, however other molecular mechanisms that could underlie the tumor suppressive effect of PTPRD remain to be discovered. We hypothesized that additional novel substrates of PTPRD may help mediate its tumor suppressive function. To identify them, we generated a GST-tagged substrate-trapping mutant (PTPRD-TRAP), performed a pull-down of PTPRD interactors, and identified interacting proteins by quantitative mass spectrometry. Candidate hits were prioritized as peptides that are more abundant in the PTPRD-TRAP pull-down versus the GST pull-down. From our list of potential interactors, we validated that PTPRD interacts with Prohibitin (PHB1). Future work will determine the ability of PTPRD to de-phosphorylate PHB1, as well as investigate its biological significance. These experiments will shed light on the molecular mechanisms underlying the tumor suppressive role of PTPRD.

INTRODUCTION

PTPRD interacting proteins

Protein tyrosine phosphatases have been implicated in the regulation of receptor tyrosine kinases, cell adhesion, cell migration, angiogenesis, tumor suppression, and oncogenesis (Ostman et al. 2006). Our lab previously showed that the *in vitro* role of PTPRD in GBM

is to suppress growth and that PTPRD de-phosphorylates Stat3 (Veeriah et al. 2009). Moreover, proteins that interact with PTPRD in other contexts have also been reported. Meehan et al. (2012) demonstrated that PTPRD dephosphorylates aurora kinase A, which causes downstream destabilization of MYCN within Neuroblastoma. Woodings et al. (2003) reported that MIM-B, a putative metastasis suppressor protein that binds to actin and regulates its assembly, binds to the cytoplasmic domain of PTPRD in a yeast two-hybrid assay with a human brain library. PTPRD has also been implicated as a neurite-promoting and cell adhesion molecule via homophilic binding of the ectodomain of PTPRD (Wang et al. 1999). In this study we use a high-throughput approach to systematically identify PTPRD interacting proteins in glioma cells.

Mass spectrometry with stable isotope labeling of amino acids in cell culture

One way to identify interaction partners for a protein of interest is to prepare a pull-down (a biochemical purification of the protein from an appropriate biological sample) and perform mass spectrometry analysis. One of the biggest challenges in determining interaction partners by mass spectrometry is to identify and eliminate non-specific contaminants. Currently, the best way to distinguish true interaction partners from contaminants is to use quantitative proteomics (Paul et al. 2011). This strategy involves comparing the abundance of proteins identified in a protein of interest pull-down with a suitable control pull-down. True interaction partners are more abundant in the protein of interest pull-down as compared to the control. In contrast, non-specific contaminants are equally abundant in both pull-downs.

One of the most precise quantitative methods to identify interactors, is to perform mass spectrometry on cell lines with stable isotope labeling of amino acids in cell culture (SILAC) (Paul et al. 2011). SILAC is achieved by supplementing media lacking "light" arginine and lysine with "heavy" $^{13}C6^{15}N4$ L-arginine (R10) and $^{13}C6^{15}N2$ L-lysine (K8). Since heavy and light peptides can be distinguished by a shift in their mass peak, the protein of interest pull-down and the control pull-down mass spectrometry can be run together, and peptide abundance can be compared directly.

Substrate-trapping for the identification of protein tyrosine phosphatase substrates

Receptor tyrosine phosphatases like PTPRD have an ectodomain consisting of fibronectin and immunoglobulin subunits, and an endodomain made up of two phosphatase domains, of which only the first phosphatase domain is catalytically active (Ostman et al. 2006). In order to uncover a phosphatase's substrates, substrate-trapping mutants are often used, in which catalysis is blocked and the substrate is trapped in the catalytic pocket of the phosphatase domain.

The most widely used mutations replace the signature motif cysteine with serine (C/S) and/or the WPD loop aspartate to alanine (D/A) (Blanchetot et al. 2005). A C/S mutation allows binding of the substrate to the mutant phosphatase and blocks catalysis, leading to the stable formation of a PTP-Ser-PO_3-substrate complex. Following binding of the substrate into the catalytic pocket, the tip of the WPD loop flips over the phospho-tyrosine residue of the substrate holding the substrate in place and bringing the aspartate (WPD) residue close. The aspartate serves as a general base by reacting with a water

molecule to attack the cys-PO_3 intermediate and releasing a free phosphate and the substrate. The D/A mutation traps the substrate by blocking it into the catalytic pocket through the flipping of the WPD loop and blocking the catalytic process (Blanchetot et al. 2005). A double C/S and D/A substrate-trapping mutant was used to demonstrate that p-Stat3 is a substrate of PTPRT (Zhang et al. 2007).

We identified proteins that interact with our substrate-trapping mutant of PTPRD using SILAC mass spectrometry of two GBM cell lines. As shown in Figure 4.1, heavy (K8/R10) SILAC lysate was combined with a recombinant GST tagged substrate-trapping mutant of PTPRD (PTPRD-TRAP-GST), and light (K0/R0) SILAC lysate was combined with recombinant GST only. Both pull-downs were pooled and submitted for mass spectrometry analysis. Peptides that were more abundant in the PTPRD substrate trapping pull-down with heavy lysate in comparison to the GST only pull-down with light lysate were considered potential interactors of PTPRD. Non-specific interactors were identified as peptides that were present in equal or more quantities in the GST only pull-down. In this study, we validated PHB1 as an interacting partner of PTPRD. Confirmation of the ability of PTPRD to de-phosphorylate PHB1 and exploration of its biological significance will shed light on the tumor suppressive role of PTPRD and provide the field with possible molecular targets for therapeutic intervention or diagnostics.

RESULTS

PTPRD suppresses growth in SKMG3 and SF539 GBM cell lines

In order to verify that PTPRD can suppress growth in the SKMG3 and SF539 GBM cell lines, PTPRD was stably expressed and growth curve analysis was performed. PTPRD protein and mRNA expression were higher in the cells overexpressing PTPRD than in cells expressing empty vector, confirming that over-expression of PTPRD was achieved. (Figure 4.2A, 4.2B). Growth curve analysis of SKMG3 and SF539 cells expressing PTPRD demonstrated that PTPRD significantly suppresses growth as compared to cells expressing empty vector (Figure 4.2C, $p<0.05$).

SKMG3 and SF539 incorporation of K8/R10

Since the growth of the SKMG3 and SF539 GBM cell lines were sensitive to overexpression of PTPRD, they were chosen for identification of PTPRD substrates by SILAC mass spectrometry analysis. Stable isotope labeling of the SKMG3 and SF539 cells was achieved by passaging in light (K0/R0) and heavy (K8/R10) media. The amount of heavy SILAC incorporation was determined by mass spectrometry analysis of heavy and light labeled SKMG3 and SF539 cells. As shown in Figure 4.3, the median percent incorporation of heavy K8/R10 was 99% in both cell lines.

Validation of the PTPRD substrate-trapping mutant

A PTPRD substrate-trapping mutant was generated by site-directed mutagenesis of C1540S and D1508A (PTPRD-TRAP-GST) (Figure 4.4A). These mutations were previously shown to be capable of identifying physiological substrates of PTP1B (Flint et

al. 1997). Substrate-trapping was performed with recombinant PTPRD-TRAP-GST on lysate from the SKMG3 cell line as previously described (Zhang et al. 2007). As a control for non-specific interactions, substrate-trapping was conducted with GST only recombinant protein. In order to verify our experimental procedure, we confirmed that Stat3 is an interaction partner of PTPRD-TRAP-GST. Stat3 was present when substrate-trapping was performed with the PTPRD-TRAP-GST mutant but not with GST only (Figure 4.4B). This suggested that the PTPRD-TRAP-GST mutant could be used to pull-down novel substrates of PTPRD.

Prohibitin is a potential substrate of PTPRD

Substrate-trapping was performed with SILAC labeled SKMG3 and SF539 lysate. Heavy and light labeled pull-downs were pooled and submitted for mass spectrometry analysis. "Forward" pull-downs were performed with GST only and light lysate while "reverse" pull-downs combined GST only with heavy lysate. Peptides with greater than a two fold difference in peptide counts from the PTPRD-TRAP-GST pull-downs to peptide counts in the GST only pull-downs were considered potential substrates (Figure 4.5). As listed in Table 4.1, 18 potential PTPRD interactions were found by this method.

Prohibitin (PHB1) was the most significant hit with tyrosine phosphorylation sites cited in literature (Ande et al. 2009a, Ande et al. 2009b, Kim do et al. 2013, and Chiu et al. 2013). In order to confirm that PHB1 interacts with PTPRD, a PTPRD-TRAP-GST pull-down was performed followed by immunoblot analysis of PHB1. PHB1 was present in the PTPRD-TRAP-GST pull-down and not with GST only, verifying that PTPRD

interacts with PHB1 (Figure 4.6).

MATERIALS AND METHODS

Stable Isotope Labeling of Amino Acids in Cell Culture (SILAC)

SKMG3 and SF539 GBM cells were grown in DMEM supplemented with 10% FBS. SILAC medium was prepared by supplementing DMEM lacking arginine and lysine (Thermo scientific) with 28mg/mL $^{13}C_6{}^{15}N_4$ L-arginine (Cambridge Isotopes) and 49mg/mL $^{13}C_6{}^{15}N_2$ L-lysine (Cambridge Isotopes). Light SILAC medium was prepared by adding the corresponding non-labeled amino acids. SKMG3 and SF539 cell lines were labeled for 10 cell divisions in SILAC media.

Viral Infection for Overexpression of PTPRD

A PTPRD construct in pCDF1 (Solomon et al. 2009) was expressed in 293T cells using Fugene 6 (Promega). Viral supernatant was harvested, mixed with 1x polybrene (Sigma), aliquoted, and stored at -80^{o}C. A 0.5mL aliquot was used to infect 150,000 cells. Overexpression of PTPRD was confirmed by qPCR and western blot analysis. For qPCR, RNA was extracted using the RNEasy mini prep kit (Qiagen), cDNA was synthesized with an OligodT RNA to cDNA premix (Clontech). qPCR was performed with FastStart Universal SYBR Green Master mix (Roche). The following *PTPRD* primer sequences: 5'-GTGTGGCCTCAAATAATGTGGG-3' and 5'-TGTGAGTCTGGTGGATACACTT3-' and GAPDH primer sequences: 5'-AAGGTGAAGGTCGGAGTCAA-3' and 5'-AATGAAGGGGTCATTGATGG-3' were used. For western blot analysis, cells were harvested by scraping in PBS, lysed with Cell

Lytic (Sigma) and 1X protease inhibitor (Sigma) by sonication. Protein was transferred to Immobilon PVDF (Millipore) and blotted with a PTPRD antibody (C-18, Santa Cruz).

Growth Curve Analysis

Growth curve analysis was performed on the xCELLigence System (Roche) following the manufacturer's instructions. 2,500 cells were seeded / well in triplicate, and electrical impedence was measured every 12 hours for 48 hours.

SILAC Incorporation

SILAC labeled SKMG3 and SF539 cells at passage five were lysed with Cell Lytic Buffer (Sigma) and protease inhibitor (Sigma). 1 ug of protein was loaded onto 10% Bis-Tris gel (Invitrogen) and run until 1 cm below stack. A 1cm box of gel was cut, trypsinized, and analyzed by mass spectrometry using Orbitrap HPLC/MS/MS. The median percent incorporation (heavy/lightX100) was calculated for 200 matched peptides.

Pervanadate Treatment

Pervanadate was made as previously described by Huyer G et al. (1997). Briefly, 30% hydrogen peroxide (Sigma) was diluted to 3% with 20mM Hepes pH 7.3 (Sigma). Fresh 100mM sodium orthvanadate was added to the 3% hydrogen peroxide. After 5 minutes a scoop of bovine liver catalase (Sigma) was added. The 1mM fresh pervanadate was added to cell media to a final concentration of 125uM pervanadate. Cells were incubated in pervanadate for 30 minutes in 37 degree CO_2 incubator.

Cell Lysis for Pull-down

Pervanadate treated cells were harvested by scraping in PBS. Cell lysis was performed as previously described by Zhang et al. (2007). Briefly the cell pellet of 10, 15cm plates was lysed in 500ul of the following cell lysis buffer: 25mM Hepes pH7.4, 150mM NaCl, 1% Nonidet P-40, 1mM EDTA, 1mM Benzimidine, 1X protease inhibitor (Sigma). After a vigorous vortex, lysate was treated with 5mM iodoacetic acid on ice for 5 minutes, neutralized with 10mM DTT on ice for 15 minutes, and cleared by 16,000 x g centrifugation for 10 minutes.

Substrate-Trapping Mutants Cloning

PTPRD was cloned into the pGex4T3 (GE Healthcare) vector from the pCDNA plasmid created by Veeriah et al. (2009). C1540S and D1508A mutations were generated by site directed mutagenesis (Invitrogen) following the manufacturer's instructions with the following primers for the a4523c mutation: 5'-caccgcctggcctgctcatggtgttccag-3' and 5'-ctggaacaccatgagcaggccaggcggtg-3' and the following primers for the g4619c mutation 5'-gatggttgtgcactccagtgcgggagttg-3' and 5'-caactcccgcactggagtgcacaaccatc-3'.

GST Recombinant Protein Expression

GST and PTPRD-TRAP-GST plasmids were transformed in DH10B E.coli. LacZ promoter driven induction of protein expression was achieved with 0.2mM IPTG in a 25 degree shaker for 24 hours. The bacterial pellet was lysed in PBS + 1% Triton-X 100 + 1X protease inhibitor (Sigma), sonicated for 5 minutes on ice, and rotated at 4 degrees for

30 minutes. Lysate was cleared with 10,000 x g centrifugation for 20 minutes at 4 degrees.

GST Protein Purification and Crosslinking to Sepharose

To purify GST proteins, equilibrated Glutathione Hi-Cap Matrix (Qiagen) was added to lysate and rotated overnight at 4 degrees. Beads were washed four times with PBS. GST and GST-PTPRD-TRAP proteins were eluted with the following elution buffer prepared fresh: 50mM reduced glutathione (Sigma), 0.4M NaCl, 50mM Tris pH 8.0, 0.1 TritonX-100, 1mM DTT at pH 8 with NaOH. Beads were incubated with elution buffer for 30 minutes in a 4 degree rotation. Five elutions were pooled and concentrated in 30K MWCO Centrifugal Filter Units (Millipore) with 5,000 x g swinging bucket rotation for 30 minutes at 4 degrees. 150ug of GST protein was crosslinked to NHS Sepharose (GE) as previously described (Paul et al. 2011).

Substrate-Trapping Immunoprecipitation

Cross-linked beads were combined with 500ul (10, 15cm plates) of lysate and rotated at 4 degrees for 2 hours. Beads were washed three times in Nonidet P-40 cell lysis buffer described above, three times in a stringency wash buffer: 20mM Tris pH 7.6, 300 mM NaCl, 5mM MgCl2, 0.5% Nonidet P-40, and one time in PBS. Proteins were eluted off the beads with 2X B-mercaptoethanol sample buffer and boil for 5 minutes at 95 degrees.

Mass Spectrometry

The GST only and PTPRD-TRAP-GST pull-downs were pooled 1:1 and run on a 10% Bis-Tris pre-cast gel (Invitrogen). The gel was stained with Colloidal Blue (Simply Blue Safe Stain, Invitrogen) for 1 hour at room temperature and rinsed with distilled H_2O for 1 hour room temperature. The Microchemistry and Proteomics Core Facility at Memorial Sloan-Kettering Cancer Center performed the mass spectrometry using the Orbitrap LS/MS/MS followed by MaxQuant quantification analysis (de Godoy et al. 2008).

Statistical Analysis

Student's t-test was used to determine statistical significance.

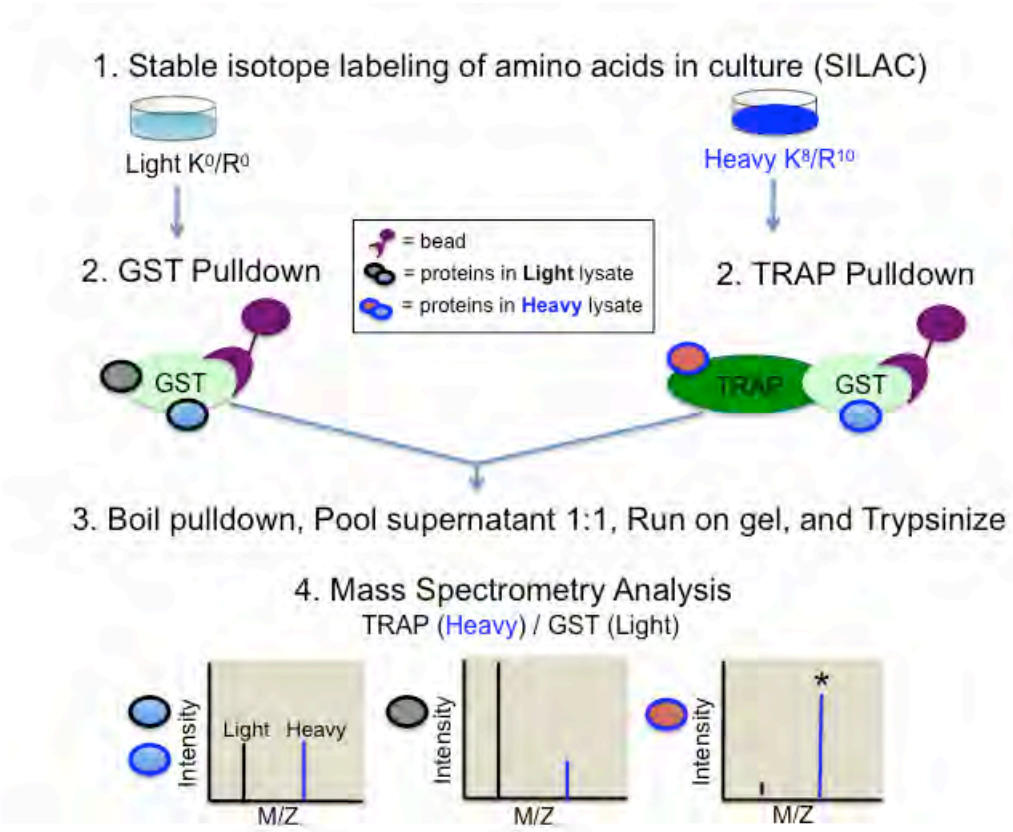

Figure 4.1 Experimental design for the identification of potential substrates by quantitative mass spectrometry. Each cell line (SKMG3 and SF539) were labeled with light (K0/R0) or heavy (K8/R10) SILAC. The GST pull-down was performed with light lysate and the TRAP pull-down was performed with heavy lysate. Mass spectrometry analysis of the pull-down shows non-specific peptides as having equal intensity in both the GST/light and TRAP/heavy pull-down. Peptides that are more abundant in the TRAP/heavy pull-down are potential substrates of PTPRD.

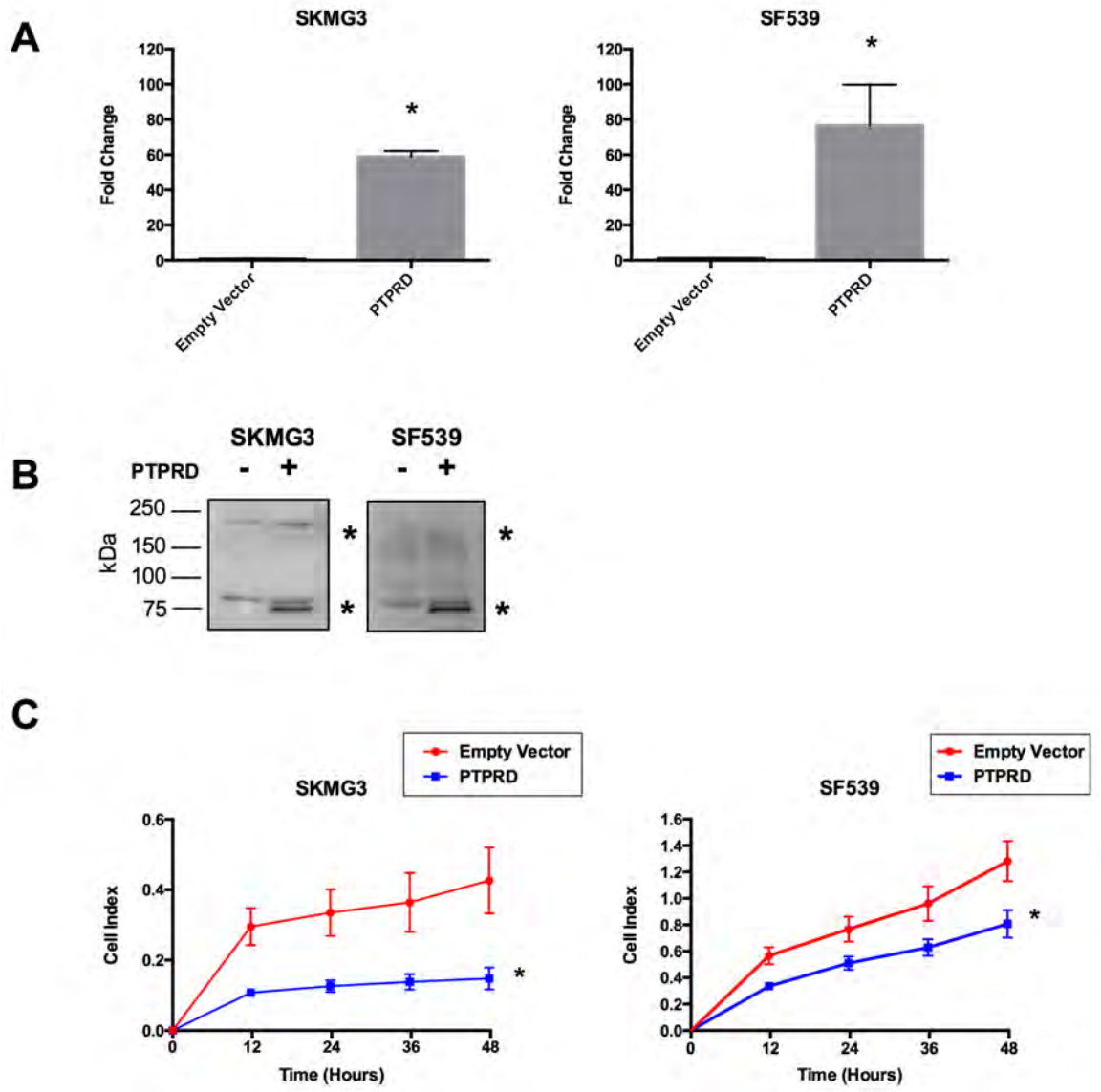

Figure 4.2 PTPRD overexpression in SKMG3 and SF539 cell lines suppresses growth. (A) mRNA expression of PTPRD was measured by qPCR. Cells were transduced with empty vector or PTPRD *p<0.05. (B) Western blot analysis of cells in A. Full length PTPRD is ~175kDa and is cleaved producing ~75kDa cleavage product. * indicates slightly smaller PTPRD overexpression bands. Top bands are endogenous PTPRD. (C) Growth curve analysis was performed. Cell index = electrical impedence *p<0.05 at 48 hour time point.

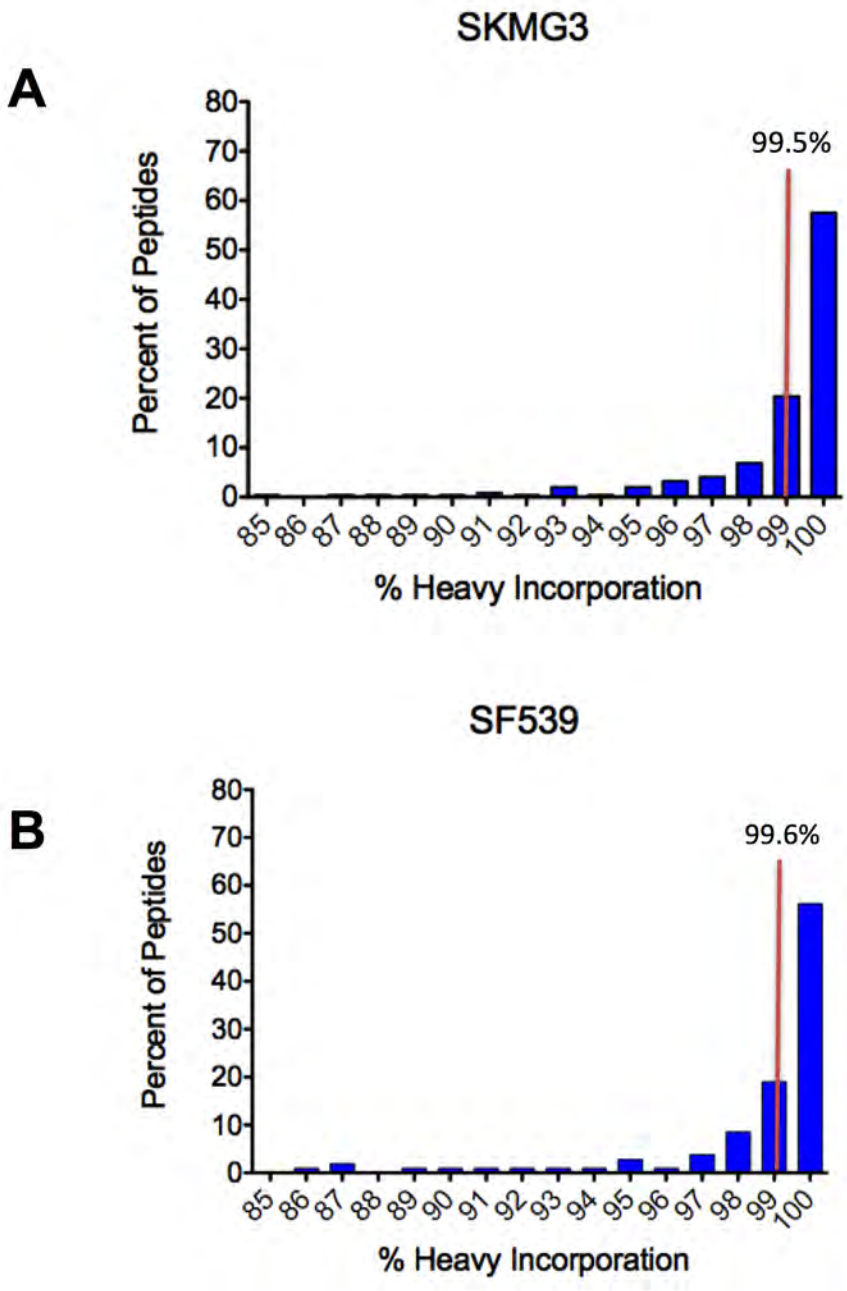

Figure 4.3 K8/R10 incorporation in SKMG3 and SF539 cell lines. Median incorporation of K8/R10 was 99% in both cell lines. Mass spectrometry analysis of peptides from K0/R0 labeled lysate was compared to K8/R10 labeled lysate.

Figure 4.4 Substrate- trapping mutant of PTPRD interacts with Stat3. (A) Structure of wild-type PTPRD and the GST-tagged PTPRD substrate-trapping mutant with D1508A and C1540S mutations. (B) SKMG3 lysate was combined with GST only, wild-type PTPRD, or PTPRD-TRAP-GST. Stat3 binds more efficiently to PTPRD-TRAP-GST than to wild-type PTPRD.

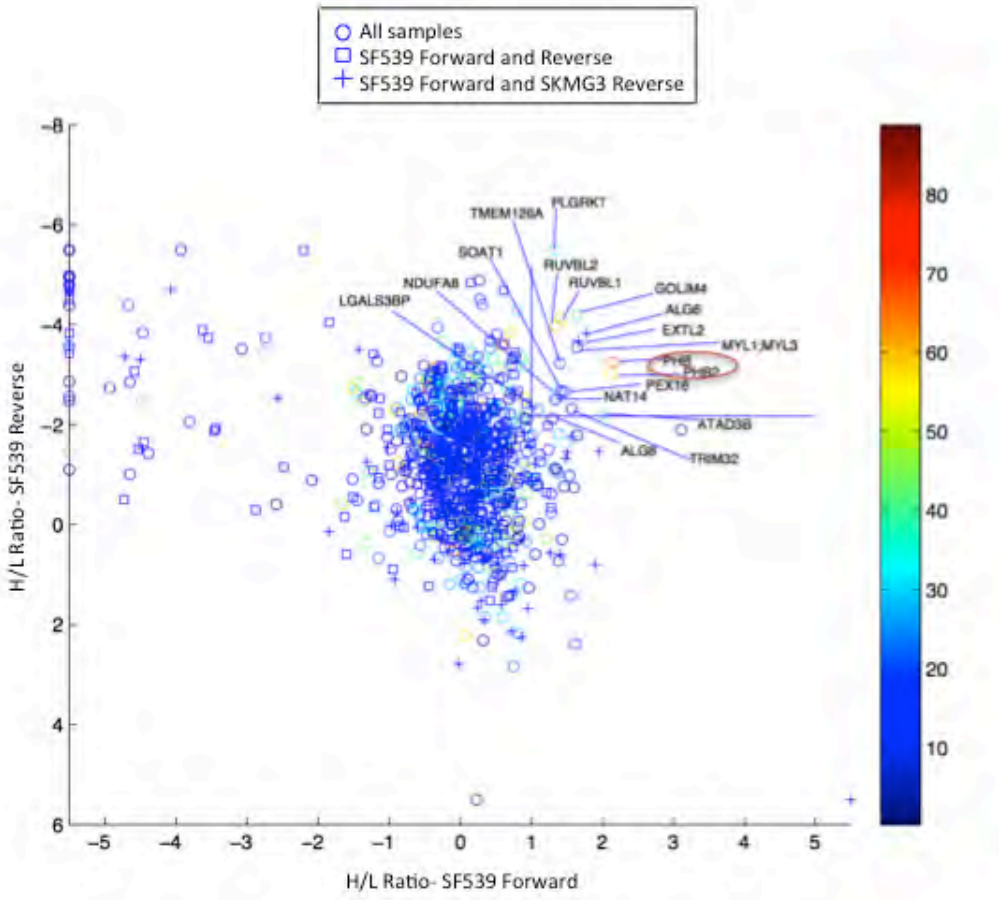

Figure 4.5 PTPRD interacting proteins identified by mass spectrometry. SF539 Forward sample = PTPRD-TRAP with heavy lysate and GST only with light lysate. SF539 and SKMG3 Reverse sample = GST only with light lysate and PTPRD-TRAP-GST with heavy lysate. Color bar represents percent sequence coverage of the protein identified in SF539 Reverse sample.

Table 4.1 PTPRD interacting proteins

Protein ID	Protein name	SF539 Forward Ratio (H/L)	SF539 Reverse Ratio (H/L)	SKMG3 Reverse Ratio (H/L)	Function	Phospho-Tyr sites?
PHB1	Prohibitin	4.4317	0.10528	0.19216	DNA biosynthesis process, negative regulation of transcription from RNA polymerase II promoter	114, 249, 259
PHB2	Prohibitin-2	4.3426	0.1231	0.22029	negative regulation of transcription	128, 248
ATAD3B	ATPase family AAA domain-containing protein 3B	4.049	0.21526	0.60598	ATP binding	unknown
ALG6	Dolichyl pyrophosphate Man9GlcNAc2 alpha-1,3-glucosyltransferase	3.4183	ND	0.070611	N-linked glycosylation	yes
EXTL2	Exostosin-like 2;Processed exostosin-like 2	3.159	ND	0.078685	N-acetylglucaosamine metabolic process	yes
MYL1;MYL3	Myosin light chain 1/3, skeletal muscle isoform;Myosin light chain 3	3.1181	0.08567	1.1713	motor protein	yes
GOLIM4	Golgi integral membrane protein 4	3.1181	0.054535	0.14111	endosome to Golgi traffiking	yes
TRIM32	E3 ubiquitin-protein ligase TRIM32	2.956	0.20087	0.35503	ubiquitin ligase, positive regulation of proliferation, migration, negative regulation of apoptosis	yes
SOAT1	Sterol O-acyltransferase 1	2.7663	0.15844	0.093068	cholesterol and lipid metabolism	unknown
PEX16	Peroxisomal membrane protein PEX16	2.6753	0.15748	0.93421	peroxisome biogenesis	unknown
RUVBL1	RuvB-like 1, also called pontin	2.6484	0.057544	0.053975	DNA duplex unwinding, DNA recombination, DNA repair, mitosis	yes
TMEM126A	Transmembrane protein 126A	2.6356	0.10693	0.2619	optic nerve development in brain	yes
NDUFA8	NADH dehydrogenase [ubiquinone] 1 alpha subcomplex subunit 8	2.5851	0.15895	0.26556	electron transport respiratory chain	yes
NAT14	N-acetyltransferase 14	2.5291	0.17615	0.29973	N-acetyl transferase, postitive regulation of transcription,	unknown
RUVBL2	RuvB-like 2, also called reptin	2.5103	0.063261	0.046091	DNA replicaton and repair, regulation of growth	yes
PLGRKT	Plasminogen receptor (KT)	2.4909	0.017526	0.10055	regulation of immune response	yes
ALG8	Probable dolichyl pyrophosphate Glc1Man9GlcNAc2 alpha-1,3-glucosyltransferase	2.4558	0.23024	0.17857	N-linked glycosylation	yes
LGALS3bp	Galectin-3-binding protein	2.1317	0.20271	0.0090354	cell adhesion	yes

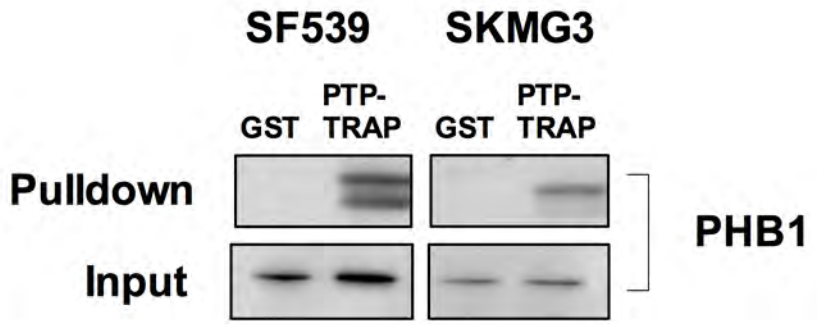

Figure 4.6 PTPRD interacts with PHB1. A GST pull-down with PTPRD-TRAP-GST was performed and PHB1 were detected by western blot analysis. Cell lines used were as labeled in the figure.

CHAPTER FIVE

Discussion and Future Directions

The scope and frequency of PTPRD inactivation in human cancers highlights its importance in tumorigenesis (Brim et al. 2014, Frankel et al. 2014, Boeva et al. 2013, Du et al. 2013, Jiang et al 2013, Gerber et al. 2013, Micci et al. 2013, TCGA 2012, Kohno et al. 2010, Solomon et al. 2009 and Veeriah et al. 2009, and Beroukhim et al. 2010). Efforts to investigate the contribution of PTPRD to disease progression have only been studied *in vitro*, and show that PTPRD can suppress growth, induce apoptosis, and reduce migration (Veeriah et al. 2009, Solomon et al. 2009, and Funato et al. 2009). Here, our studies in chapter two and three demonstrate the *in vivo* role of PTPRD in tumorigenesis, while chapter four discusses the identification of potential substrates of PTPRD. In this chapter, I discuss some of the biological implications of these findings.

Loss of PTPRD leads to aberrant Stat3 activation and promotes gliomagenesis

Discussion

In chapter two, our results describe a number of important, novel observations. First, to our knowledge, we provide the first evidence that *Ptprd* loss, in the setting of *Cdkn2a/p16*^{Ink4a} deletion and PDGFB overexpression, can promote growth of tumors *in vivo*. Second, we show that *Ptprd* heterozygous loss and *Cdkn2a/p16*^{Ink4a} deletion accelerates tumorigenesis, which supports a rationale for the patterns of *PTPRD* loss observed in human GBM and other tumor types. Third, our data indicates that

heterozygous loss of *Ptprd*, a phosphatase targeting Stat3, causes p-Stat3 accumulation and Stat3 activation in murine tumors, a finding that was validated in human GBMs. This places PTPRD in the growing list of tumor suppressors, which display haploinsufficiency. Lastly, we showed that *Ptprd* loss can promote tumor growth via a non-canonical means, perhaps by altering the immune response.

Our findings show that heterozygous loss of *PTPRD* most commonly co-occurs with deletion of *CDKN2A/p16*^{INK4A} in human GBM. We generated an *in vivo* glioma model of *Ptprd* and *Cdkn2a/p16*^{Ink4a} deletion in order to study the contribution of each chromosome 9p gene to gliomagenesis. Importantly, mice with *Ptprd* loss and *p16*^{Ink4a} deletion had worse survival than mice with *p16*^{Ink4a} deletion alone. These observations demonstrate that loss of these two 9p tumor suppressors cooperate and influence tumorigenesis in a context-dependent fashion. Interestingly, *Ptprd* loss in the context of wild-type *p16*^{Ink4a} demonstrated better survival. Staining for TUNEL, a marker for cell death, showed that increased cell death does not explain the better survival. Nevertheless, it is clear that in the context of our mouse model, *p16*^{Ink4a} loss is required for enhancing tumorigenesis. These results are consistent with the high level of concordance between genetic events targeting the two genes in human GBM.

Perhaps most interesting were our observations pertaining to *Ptprd* gene dosage - poorer survival, altered gene expression, increased p-Stat3, and increased production of chemokines all occurred to a greater extent when *Ptprd* was heterozygous. This suggests that heterozygous loss of *PTPRD* is sufficient to promote tumorigenesis, in the setting of

CDKN2A deletion. However, our findings were somewhat unexpected as a classical haploinsufficient tumor suppressor typically produces at least equivalent (or more severe) functional impact in the homozygous setting. In contrast, complete abrogation of Ptprd resulted in a paradoxical decrease in intensity of observable phenotypes. This suggests that PTPRD dosage is critical. It is possible that complete abrogation of PTPRD ultimately leads to activation of a negative feedback loop in STAT3 signaling, what down-regulates the pathway. Indeed, negative feedback is well established in STAT3 signaling and can exist at many levels. In our mouse models, we may be observing the consequences of negative feedback inhibition when tonic Stat3 hyperactivation exceeds a threshold, as previously observed (Ernst et al. 2009, Trilling et al. 2013, and Nichane et al. 2010). Furthermore, STAT3 signaling pathways are subject to significant crosstalk. It is possible that when both alleles of *PTPRD* are deleted, other partially redundant phosphatases are induced and bring p-STAT3 levels down to below that in *PTPRD* heterozygous tumors (Zhang et al. 2007). However, we measured the gene expression levels of other tyrosine phosphatases by microarray to determine if these changes were occurring at the transcriptional level. No significant differences were observed between the genotypes suggesting that compensation by other tyrosine phosphatases may be occurring at the post-translational level. Additional work will need to be done to elucidate the intricacies of these signaling pathways. Nevertheless, our data provides one potential explanation of why the vast majority of *PTPRD* genetic alterations (both somatic mutation and copy number loss) in human cancers are heterozygous.

Another intriguing and novel aspect of our study was that *PTPRD* loss appears to act not by promoting cell division or blocking differentiation, but by altering the tumor

microenvironment. Our gene expression analysis of the tumor cells demonstrated that activation of genetic programs governing immune response and macrophage response were at play. More specifically, *Ptprd*+/-*p16*-/- tumors had activated genes involved in up-regulation of several chemokines, all of which promote M2 polarization (Roca et al. 2009, Murray et al. 2011, Gabrusiewicz et al. 2011, and Movahedi et al. 2010). Macrophages can enhance tumor cell survival by promoting tumor growth, invasion, or immunosuppression (da Fonseca et al. 2013, Li et al. 2012, and Hao et al. 2012). In addition, recent work by Pyonteck et al. (2013) showed that RCAS PDGFB gliomas have tumor-associated macrophages, and that inhibiting their polarization state can significantly improve survival. Several studies demonstrate that p-Stat3 within macrophages polarizes them to a M2 tumor promoting state (Li et al. 2012 and Zhang et al. 2009). We show that *Ptprd*+/-*p16*-/- tumors had higher levels of p-Stat3 in macrophages, demonstrating that *Ptprd* loss can affect p-Stat3 accumulation in the macrophages and may alter the macrophage state.

In summary, we show that *Ptprd* loss with *Cdkn2a/p16*^{Ink4a} deletion can promote gliomagenesis. These findings have substantial implications for our understanding of a commonly mutated tumor suppressor gene as well as for our comprehension of the novel mechanisms that can be employed to promote gliomagenesis.

Future Directions

Is Stat3 negative feedback induced in tumors with homozygous loss of *Ptprd*?

In our studies, it was intriguing that mice with homozygous deletion of *Ptprd* had a less dramatic phenotype than *Ptprd* heterozygous mice. We took a close look at our

microarray data for potential compensation by other phosphatases when both copies of *Ptprd* are lost. We did not see compensation by other phosphatases suggesting that compensation may be occurring at the post-transcriptional level. One approach to determine the cause of negative feedback in tumors with homozygous deletion of *Ptprd* is to explore in depth signaling crosstalk and the activity of regulators of Stat3 signaling like SOCS proteins, PIAS proteins, and PTPRT (Starr et al. 1999, Chung et al. 1997, and Zhang et al. 2007).

Is loss of *Ptprd* in tumor cells sufficient for polarization of macrophages?

In our studies we found that both GFP-positive tumor cells and Iba-positive macrophages had increased p-Stat3 with heterozygous loss of *Ptprd*. Knowing that *Ptprd* loss can affect the tumor microenvironment, it would be interesting to determine the individual contribution of the tumor cells and of the tumor-associated macrophages by removing *Ptprd* from only the tumor cells using an inducible mouse model. One could cross *Nestin*-cre and *Nestin*-tvA to *Ptprd* flox/flox mice. In these mice, *Ptprd* loss and infection with RCAS PDGFB would only occur in the *Nestin*-positive tumor cells. Previous studies have shown that tumor cells expressing p-Stat3 can secrete chemokines that recruit macrophages and polarize them (Wu et al. 2010 and da Fonseca et al. 2013). By inducing deletion of *Ptprd* in only *Nestin*-positive cells, one could determine if loss of *Ptprd* and activation of Stat3 in only the tumor cells is sufficient to polarize macrophages and promote tumorigenesis.

Deletion of *Ptprd* and *Cdkn2a* cooperate to accelerate tumorigenesis

Discussion

In chapter three, our results highlight several important observations. First, we show that *Ptprd* loss promotes tumorigenesis in the setting of *Cdkn2a* deletion. Second, we show that heterozygous loss of *Ptprd* is sufficient to promote tumorigenesis. This is consistent with the hypothesis that the frequently observed heterozygous loss of *PTPRD* in human cancers contributes to tumor development. Third, our data suggests that loss of *Ptprd* plays a role in determining which types of tumors form.

We generated a mouse model with *Ptprd* and *Cdkn2a* in order to study the role of *Ptprd* in tumorigenesis. While mice with *Ptprd* loss alone did not show increased tumorigenesis, mice with *Ptprd* and *Cdkn2a* deletion had significantly shorter survival times than mice with *Cdkn2a* deletion alone. These results support the hypothesis that there is selective pressure for co-deletion of these two chromosome 9p tumor suppressors in human malignancies, and supports a rationale for the patterns of *PTPRD* loss observed in human cancers.

In humans, loss of chromosome 9p occurs in B-cell lymphomas (Berglund et al. 2002). Intriguingly, in our study, mice with *Ptprd* loss developed more lymphomas. It was also interesting that we observed a shift in the spectrum of sarcomas to a greater number of histiocytic sarcomas in *Ptprd-/-Cdkn2a-/-* mice. Histiocytes, or macrophages of the liver, are the cell of origin for hisitiocytic sarcomas. Again, here, it would appear that in mice loss of *Ptprd* in addition to *Cdkn2a* increases the propensity to develop tumors of hematopoietic origin.

In summary, we show that *Ptprd* copy number loss and *Cdkn2a* cooperate to promote tumorigenesis. These findings have substantial implications for our understanding of a commonly inactivated tumor suppressor.

Future Directions

Why do mice with *Ptprd* loss have higher incidence of lymphomas?

We show that mice with *Ptprd* loss have higher incidence of lymphomas, suggesting that *Ptprd* loss may affect the developmental stages of B-lymphocytes. In order to test this hypothesis, one can examine the differentiation states of B-cells in the bone marrow of *Ptprd+/+Cdkn2a-/-, Ptprd+/-Cdkn2a-/-, Ptprd-/-Cdkn2a-/-* mice. Isolated bone marrow cells can be stained with B220, IgM, and IgD. B220 is a marker of B-cells, and IgM and IgD are developmental markers of B cells. We expect that *Ptprd+/-Cdkn2a-/-* and *Ptprd-/-Cdkn2a-/-* mice will have a greater IgM^- IgD^- fraction, suggesting that *Ptprd* loss promotes an accumulation of immature B-cells.

Prohibitin is a potential substrate of PTPRD

Discussion

In Chapter Four, we identified proteins that interact with PTPRD by quantitative mass spectrometry and validated that Prohibitin (PHB1) interacts with PTPRD. The Prohibitin protein sequence includes three tyrosines, and phosphorylation has been reported at Tyr 114 and Tyr 259 (Ande et al. 2009a, Ande et al. 2009b, Kim do et al. 2013, and Chiu et al. 2013). Prohibitin has been shown to localize in the mitochondria, plasma membrane, cytoplasm, and nucleus (Thaud et al. 2013). Furthermore, Prohibitin can protect cells

from oxidative stress in the mitochondria and affects metabolism, transcription, apoptosis/survival, cytoskeleton reorganization, and differentiation (Thaud et al. 2013 and Sievers et al. 2010). Future experiments will determine which PHB tyrosine phosphorylation site is altered by the PTPRD phosphatase. We will also determine the biological significance of the interaction.

Future Directions

Does PTPRD de-phosphorylate PHB1?

In order to confirm that PTPRD is de-phosphorylating PHB1, we have decided to take a mass spectrometry approach. We will immunoprecipitate PHB1 from cells expressing PTPRD and empty vector and submit the PHB protein band for post-translational mass spectrometry analysis. We will use SILAC labeled lysate with this approach, in order to quantitatively compare the phosphorylation of PHB1 with and without PTPRD. We hypothesize that we will see a reduction in phosphorylation at a particular PHB1 tyrosine site in lysate from cells with PTPRD overexpression.

What is the biological significance of the PTPRD and PHB1 interaction?

It has previously been shown that phosphorylation of Tyr 259 of Prohibitin can promote migration via the RAS/MAPK pathway. It has also been described that PTPRD suppresses migration of colon cancer cells (Funato et al. 2011). If we find that PTPRD de-phosphorylates Tyr-259, one hypothesis is that PTPRD alters the ability of cells to migrate. In order to test this hypothesis, we would first have to determine if migration of cells in the SKMG3 and SF539 cell lines is reduced by PTPRD overexpression. Next, we

can create a phospho-negative mutant of PHB1 by mutating Tyrosine 259 to Phenalanine, and express the mutant in the context of PTPRD knockdown. The phospho-negative mutant should suppress migration that is induced by knockdown of PTPRD.

In Chapter Four, we have shown that PTPRD overexpression suppresses survival and growth of the SKMG3 and SF539 cells. Interestingly, it has previously been described that PHB1 reduces mitochondrial reactive oxygen species and protects brain cells (Zhou et al. 2012). Another hypothesis for the biological significance of the PTPRD and PHB interaction is that loss of *PTPRD* induces p-PHB, which promotes cell survival by reducing reactive oxygen species in the cell. To test this, one can overexpress PTPRD and measure reactive oxygen species and cell survival. We hypothesize that overexpression of PTPRD would reduce p-PHB and increase reactive oxygen species. It is known that radiation can induce reactive oxygen species (Mikkelsen et al. 2003). In particular, it would be interesting to test whether PTPRD alters the ability of cells to recover from radiation induced reactive oxygen species. One could knockdown PTPRD and determine if cells have less radiation induced reactive oxygen species and increased survival.

Ultimately, the identification of a novel PTPRD substrate will allow us to understand the molecular basis for the suppression of growth by a tumor suppressor that is inactivated in several cancers.

BIBLIOGRAPHY

Ande, S. R., Y. Gu, et al. (2009). "Insulin induced phosphorylation of prohibitin at tyrosine 114 recruits Shp1." Biochimica et biophysica acta **1793**(8): 1372-1378.

Ande, S. R., S. Moulik, et al. (2009). "Interaction between O-GlcNAc modification and tyrosine phosphorylation of prohibitin: implication for a novel binary switch." PloS one **4**(2): e4586.

Barbieri, C. E., S. C. Baca, et al. (2012). "Exome sequencing identifies recurrent SPOP, FOXA1 and MED12 mutations in prostate cancer." Nature genetics **44**(6): 685-689.

Barretina, J., B. S. Taylor, et al. (2010). "Subtype-specific genomic alterations define new targets for soft-tissue sarcoma therapy." Nature genetics **42**(8): 715-721.

Becher, O. J., D. Hambardzumyan, et al. (2008). "Gli activity correlates with tumor grade in platelet-derived growth factor-induced gliomas." Cancer research **68**(7): 2241-2249.

Berglund, M., G. Enblad, et al. (2002). "Chromosomal imbalances in diffuse large B-cell lymphoma detected by comparative genomic hybridization." Modern pathology : an official journal of the United States and Canadian Academy of Pathology, Inc **15**(8): 807-816.

Beroukhim, R., C. H. Mermel, et al. (2010). "The landscape of somatic copy-number alteration across human cancers." Nature **463**(7283): 899-905.

Blanchetot, C., L. G. Tertoolen, et al. (2002). "Intra- and intermolecular interactions between intracellular domains of receptor protein-tyrosine phosphatases." The Journal of biological chemistry **277**(49): 47263-47269.

Bleau, A. M., D. Hambardzumyan, et al. (2009). "PTEN/PI3K/Akt pathway regulates the side population phenotype and ABCG2 activity in glioma tumor stem-like cells." Cell stem cell **4**(3): 226-235.

Boeva, V., S. Jouannet, et al. (2013). "Breakpoint features of genomic rearrangements in neuroblastoma with unbalanced translocations and chromothripsis." PloS one **8**(8): e72182.

Bournazou, E. and J. Bromberg (2013). "Targeting the tumor microenvironment: JAK-STAT3 signaling." JAK-STAT **2**(2): e23828.

Brantley, E. C. and E. N. Benveniste (2008). "Signal transducer and activator of transcription-3: a molecular hub for signaling pathways in gliomas." Molecular cancer research : MCR **6**(5): 675-684.

Brennan, C. W., R. G. Verhaak, et al. (2013). "The somatic genomic landscape of glioblastoma." Cell **155**(2): 462-477.

Brim, H., M. S. Abu-Asab, et al. (2014). "An Integrative CGH, MSI and Candidate Genes Methylation Analysis of Colorectal Tumors." PloS one **9**(1): e82185.

Carro, M. S., W. K. Lim, et al. (2010). "The transcriptional network for mesenchymal transformation of brain tumours." Nature **463**(7279): 318-325.

Cerami, E., J. Gao, et al. (2012). "The cBio cancer genomics portal: an open platform for exploring multidimensional cancer genomics data." Cancer discovery **2**(5): 401-404.

Charles, N., T. Ozawa, et al. (2010). "Perivascular nitric oxide activates notch signaling and promotes stem-like character in PDGF-induced glioma cells." Cell stem cell **6**(2): 141-152.

Chiu, C. F., M. Y. Ho, et al. (2013). "Raf activation by Ras and promotion of cellular metastasis require phosphorylation of prohibitin in the raft domain of the plasma membrane." Oncogene **32**(6): 777-787.

Chung, C. D., J. Liao, et al. (1997). "Specific inhibition of Stat3 signal transduction by PIAS3." Science **278**(5344): 1803-1805.

Ciznadija, D., Y. Liu, et al. (2011). "Cyclin D1 and cdk4 mediate development of neurologically destructive oligodendroglioma." Cancer research **71**(19): 6174-6183.

da Fonseca, A. C. and B. Badie (2013). "Microglia and macrophages in malignant gliomas: recent discoveries and implications for promising therapies." Clinical & developmental immunology **2013**: 264124.

Dai, C., J. C. Celestino, et al. (2001). "PDGF autocrine stimulation dedifferentiates cultured astrocytes and induces oligodendrogliomas and oligoastrocytomas from neural progenitors and astrocytes in vivo." Genes & development **15**(15): 1913-1925.

Dai, C., Y. Lyustikman, et al. (2005). "The characteristics of astrocytomas and oligodendrogliomas are caused by two distinct and interchangeable signaling formats." Neoplasia **7**(4): 397-406.

de Godoy, L. M., J. V. Olsen, et al. (2008). "Comprehensive mass-spectrometry-based proteome quantification of haploid versus diploid yeast." Nature **455**(7217): 1251-1254.

Du, Y., T. Su, et al. (2013). "Polymorphism in protein tyrosine phosphatase receptor delta is associated with the risk of clear cell renal cell carcinoma." Gene **512**(1): 64-69.

Dulak, A. M., P. Stojanov, et al. (2013). "Exome and whole-genome sequencing of esophageal adenocarcinoma identifies recurrent driver events and mutational complexity." Nature genetics **45**(5): 478-486.

Ernst, M. B., C. M. Wunderlich, et al. (2009). "Enhanced Stat3 activation in POMC neurons provokes negative feedback inhibition of leptin and insulin signaling in obesity." The Journal of neuroscience : the official journal of the Society for Neuroscience **29**(37): 11582-11593.

Flint, A. J., T. Tiganis, et al. (1997). "Development of "substrate-trapping" mutants to identify physiological substrates of protein tyrosine phosphatases." Proceedings of

the National Academy of Sciences of the United States of America **94**(5): 1680-1685.

Frankel, A., N. Armour, et al. (2014). "Genome-wide analysis of esophageal adenocarcinoma yields specific copy number aberrations that correlate with prognosis." Genes, chromosomes & cancer **53**(4): 324-338.

Funato, K., Y. Yamazumi, et al. (2011). "Tyrosine phosphatase PTPRD suppresses colon cancer cell migration in coordination with CD44." Experimental and therapeutic medicine **2**(3): 457-463.

Gabrusiewicz, K., A. Ellert-Miklaszewska, et al. (2011). "Characteristics of the alternative phenotype of microglia/macrophages and its modulation in experimental gliomas." PloS one **6**(8): e23902.

Gerber, J. M., J. L. Gucwa, et al. (2013). "Genome-wide comparison of the transcriptomes of highly enriched normal and chronic myeloid leukemia stem and progenitor cell populations." Oncotarget **4**(5): 715-728.

Hambardzumyan, D., N. M. Amankulor, et al. (2009). "Modeling Adult Gliomas Using RCAS/t-va Technology." Translational oncology **2**(2): 89-95.

Hanahan, D. and R. A. Weinberg (2011). "Hallmarks of cancer: the next generation." Cell **144**(5): 646-674.

Hanisch, U. K. and H. Kettenmann (2007). "Microglia: active sensor and versatile effector cells in the normal and pathologic brain." Nature neuroscience **10**(11): 1387-1394.

Hao, N. B., M. H. Lu, et al. (2012). "Macrophages in tumor microenvironments and the progression of tumors." Clinical & developmental immunology **2012**: 948098.

Ho, A. S., K. Kannan, et al. (2013). "The mutational landscape of adenoid cystic carcinoma." Nature genetics **45**(7): 791-798.

Holland, E. C., W. P. Hively, et al. (1998). "A constitutively active epidermal growth factor receptor cooperates with disruption of G1 cell-cycle arrest pathways to induce glioma-like lesions in mice." Genes & development **12**(23): 3675-3685.

Huyer, G., S. Liu, et al. (1997). "Mechanism of inhibition of protein-tyrosine phosphatases by vanadate and pervanadate." The Journal of biological chemistry **272**(2): 843-851.

Imielinski, M., A. H. Berger, et al. (2012). "Mapping the hallmarks of lung adenocarcinoma with massively parallel sequencing." Cell **150**(6): 1107-1120.

Iyer, G., H. Al-Ahmadie, et al. (2013). "Prevalence and co-occurrence of actionable genomic alterations in high-grade bladder cancer." Journal of clinical oncology : official journal of the American Society of Clinical Oncology **31**(25): 3133-3140.

Jiang, Y., F. Janku, et al. (2013). "Germline PTPRD mutations in Ewing sarcoma: biologic and clinical implications." Oncotarget **4**(6): 884-889.

Kamijo, T., F. Zindy, et al. (1997). "Tumor suppression at the mouse INK4a locus mediated by the alternative reading frame product p19ARF." Cell **91**(5): 649-659.

Kandoth, C., N. Schultz, et al. (2013). "Integrated genomic characterization of endometrial carcinoma." Nature **497**(7447): 67-73.

Katz, A. M., N. M. Amankulor, et al. (2012). "Astrocyte-specific expression patterns associated with the PDGF-induced glioma microenvironment." PloS one **7**(2): e32453.

Kennedy, B. C., C. R. Showers, et al. (2013). "Tumor-associated macrophages in glioma: friend or foe?" Journal of oncology **2013**: 486912.

Kim do, K., H. S. Kim, et al. (2013). "The scaffold protein prohibitin is required for antigen-stimulated signaling in mast cells." Science signaling **6**(292): ra80.

Kohno, T., A. Otsuka, et al. (2010). "A catalog of genes homozygously deleted in human lung cancer and the candidacy of PTPRD as a tumor suppressor gene." Genes, chromosomes & cancer **49**(4): 342-352.

Krauthammer, M., Y. Kong, et al. (2012). "Exome sequencing identifies recurrent somatic RAC1 mutations in melanoma." Nature genetics **44**(9): 1006-1014.

LaFleur, A. M., N. W. Lukacs, et al. (2004). "Role of CC chemokine CCL6/C10 as a monocyte chemoattractant in a murine acute peritonitis." Mediators of inflammation **13**(5-6): 349-355.

Li, W. and M. B. Graeber (2012). "The molecular profile of microglia under the influence of glioma." Neuro-oncology **14**(8): 958-978.

Liu, Y., N. Yeh, et al. (2007). "Somatic cell type specific gene transfer reveals a tumor-promoting function for p21(Waf1/Cip1)." The EMBO journal **26**(22): 4683-4693.

Louis, D. N., H. Ohgaki, et al. (2007). "The 2007 WHO classification of tumours of the central nervous system." Acta neuropathologica **114**(2): 97-109.

Lui, V. W., N. D. Peyser, et al. (2014). "Frequent mutation of receptor protein tyrosine phosphatases provides a mechanism for STAT3 hyperactivation in head and neck cancer." Proceedings of the National Academy of Sciences of the United States of America.

Mauro, L. J. and J. E. Dixon (1994). "'Zip codes' direct intracellular protein tyrosine phosphatases to the correct cellular 'address'." Trends in biochemical sciences **19**(4): 151-155.

Meehan, M., L. Parthasarathi, et al. (2012). "Protein tyrosine phosphatase receptor delta acts as a neuroblastoma tumor suppressor by destabilizing the aurora kinase A oncogene." Molecular cancer **11**: 6.

Micci, F., I. Panagopoulos, et al. (2013). "Genomic aberration patterns and expression profiles of squamous cell carcinomas of the vulva." Genes, chromosomes & cancer **52**(6): 551-563.

Molenaar, J. J., J. Koster, et al. (2012). "Sequencing of neuroblastoma identifies chromothripsis and defects in neuritogenesis genes." Nature **483**(7391): 589-593.

Movahedi, K., D. Laoui, et al. (2010). "Different tumor microenvironments contain functionally distinct subsets of macrophages derived from Ly6C(high) monocytes." Cancer research **70**(14): 5728-5739.

Murray, P. J. and T. A. Wynn (2011). "Protective and pathogenic functions of macrophage subsets." Nature reviews. Immunology **11**(11): 723-737.

Navis, A. C., M. van den Eijnden, et al. (2010). "Protein tyrosine phosphatases in glioma biology." Acta neuropathologica **119**(2): 157-175.

Nichane, M., X. Ren, et al. (2010). "Self-regulation of Stat3 activity coordinates cell-cycle progression and neural crest specification." The EMBO journal **29**(1): 55-67.

Noushmehr, H., D. J. Weisenberger, et al. (2010). "Identification of a CpG island methylator phenotype that defines a distinct subgroup of glioma." Cancer cell **17**(5): 510-522.

Orsulic, S. (2002). "An RCAS-TVA-based approach to designer mouse models." Mammalian genome : official journal of the International Mammalian Genome Society **13**(10): 543-547.

Ostman, A., C. Hellberg, et al. (2006). "Protein-tyrosine phosphatases and cancer." Nature reviews. Cancer **6**(4): 307-320.

Parsons, D. W., S. Jones, et al. (2008). "An integrated genomic analysis of human glioblastoma multiforme." Science **321**(5897): 1807-1812.

Paul, F. E., F. Hosp, et al. (2011). "Analyzing protein-protein interactions by quantitative mass spectrometry." Methods **54**(4): 387-395.

Pyonteck, S. M., L. Akkari, et al. (2013). "CSF-1R inhibition alters macrophage polarization and blocks glioma progression." Nature medicine **19**(10): 1264-1272.

Roca, H., Z. S. Varsos, et al. (2009). "CCL2 and interleukin-6 promote survival of human CD11b+ peripheral blood mononuclear cells and induce M2-type macrophage polarization." The Journal of biological chemistry **284**(49): 34342-34354.

Sarafi, M. N., E. A. Garcia-Zepeda, et al. (1997). "Murine monocyte chemoattractant protein (MCP)-5: a novel CC chemokine that is a structural and functional homologue of human MCP-1." The Journal of experimental medicine **185**(1): 99-109.

Serrano, M., H. Lee, et al. (1996). "Role of the INK4a locus in tumor suppression and cell mortality." Cell **85**(1): 27-37.

Sharpless, N. E., M. R. Ramsey, et al. (2004). "The differential impact of p16(INK4a) or p19(ARF) deficiency on cell growth and tumorigenesis." Oncogene **23**(2): 379-385.

Sherr, C. J. (2001). "The INK4a/ARF network in tumour suppression." Nature reviews. Molecular cell biology **2**(10): 731-737.

Shurin, G. V., R. L. Ferris, et al. (2005). "Loss of new chemokine CXCL14 in tumor tissue is associated with low infiltration by dendritic cells (DC), while restoration

of human CXCL14 expression in tumor cells causes attraction of DC both in vitro and in vivo." Journal of immunology **174**(9): 5490-5498.

Sievers, C., G. Billig, et al. (2010). "Prohibitins are required for cancer cell proliferation and adhesion." PloS one **5**(9): e12735.

Sliwa, M., D. Markovic, et al. (2007). "The invasion promoting effect of microglia on glioblastoma cells is inhibited by cyclosporin A." Brain : a journal of neurology **130**(Pt 2): 476-489.

Solomon, D. A., J. S. Kim, et al. (2008). "Mutational inactivation of PTPRD in glioblastoma multiforme and malignant melanoma." Cancer research **68**(24): 10300-10306.

Solomon, D. A., J. S. Kim, et al. (2009). "Lack of inherited mutations of PTPRD in familial melanoma and melanoma-astrocytoma syndrome." Pigment cell & melanoma research **22**(4): 489-491.

Starr, R., T. A. Willson, et al. (1997). "A family of cytokine-inducible inhibitors of signalling." Nature **387**(6636): 917-921.

Stupp, R., W. P. Mason, et al. (2005). "Radiotherapy plus concomitant and adjuvant temozolomide for glioblastoma." N Engl J Med **352**(10): 987-996.

Taylor, B. S., N. Schultz, et al. (2010). "Integrative genomic profiling of human prostate cancer." Cancer cell **18**(1): 11-22.

TCGA (2008). "Comprehensive genomic characterization defines human glioblastoma genes and core pathways." Nature **455**(7216): 1061-1068.

TCGA (2011). "Integrated genomic analyses of ovarian carcinoma." Nature **474**(7353): 609-615.

TCGA (2012). "Comprehensive genomic characterization of squamous cell lung cancers." Nature **489**(7417): 519-525.

TCGA (2012). "Comprehensive molecular characterization of human colon and rectal cancer." Nature **487**(7407): 330-337.

TCGA (2012). "Comprehensive molecular portraits of human breast tumours." Nature **490**(7418): 61-70.

TCGA (2013). "Comprehensive molecular characterization of clear cell renal cell carcinoma." Nature **499**(7456): 43-49.

TCGA (2014). "Comprehensive molecular characterization of urothelial bladder carcinoma." Nature.

Tchougounova, E., M. Kastemar, et al. (2007). "Loss of Arf causes tumor progression of PDGFB-induced oligodendroglioma." Oncogene **26**(43): 6289-6296.

Thuaud, F., N. Ribeiro, et al. (2013). "Prohibitin ligands in cell death and survival: mode of action and therapeutic potential." Chemistry & biology **20**(3): 316-331.

Tonks, N. K. (2006). "Protein tyrosine phosphatases: from genes, to function, to disease." Nature reviews. Molecular cell biology **7**(11): 833-846.

Trilling, M., V. T. Le, et al. (2014). ""Activated" STAT Proteins: A Paradoxical Consequence of Inhibited JAK-STAT Signaling in Cytomegalovirus-Infected Cells." Journal of immunology **192**(1): 447-458.

Uetani, N., K. Kato, et al. (2000). "Impaired learning with enhanced hippocampal long-term potentiation in PTPdelta-deficient mice." The EMBO journal **19**(12): 2775-2785.

Uhrbom, L., G. Hesselager, et al. (1998). "Induction of brain tumors in mice using a recombinant platelet-derived growth factor B-chain retrovirus." Cancer research **58**(23): 5275-5279.

Uhrbom, L. and E. C. Holland (2001). "Modeling gliomagenesis with somatic cell gene transfer using retroviral vectors." Journal of neuro-oncology **53**(3): 297-305.

Veeriah, S., C. Brennan, et al. (2009). "The tyrosine phosphatase PTPRD is a tumor suppressor that is frequently inactivated and mutated in glioblastoma and other human cancers." Proceedings of the National Academy of Sciences of the United States of America **106**(23): 9435-9440.

Verhaak, R. G., K. A. Hoadley, et al. (2010). "Integrated genomic analysis identifies clinically relevant subtypes of glioblastoma characterized by abnormalities in PDGFRA, IDH1, EGFR, and NF1." Cancer cell **17**(1): 98-110.

Wallace, M. J., C. Fladd, et al. (1998). "The second catalytic domain of protein tyrosine phosphatase delta (PTP delta) binds to and inhibits the first catalytic domain of PTP sigma." Molecular and cellular biology **18**(5): 2608-2616.

Wang, J. and J. L. Bixby (1999). "Receptor tyrosine phosphatase-delta is a homophilic, neurite-promoting cell adhesion molecular for CNS neurons." Molecular and cellular neurosciences **14**(4-5): 370-384.

Woodings, J. A., S. J. Sharp, et al. (2003). "MIM-B, a putative metastasis suppressor protein, binds to actin and to protein tyrosine phosphatase delta." The Biochemical journal **371**(Pt 2): 463-471.

Wu, A., J. Wei, et al. (2010). "Glioma cancer stem cells induce immunosuppressive macrophages/microglia." Neuro-oncology **12**(11): 1113-1125.

Zhang, L., D. Alizadeh, et al. (2009). "Stat3 inhibition activates tumor macrophages and abrogates glioma growth in mice." Glia **57**(13): 1458-1467.

Zhang, X., A. Guo, et al. (2007). "Identification of STAT3 as a substrate of receptor protein tyrosine phosphatase T." Proceedings of the National Academy of Sciences of the United States of America **104**(10): 4060-4064.